Universidad de Oviedo

ESCUELA POLITÉCNICA DE INGENIERÍA DE GIJÓN

GRADO EN INGENIERÍA DE TECNOLOGÍAS INDUSTRIALES

THERMAL MACHINES AND ENGINES AREA

Optimization of the efficiency of a combined cycle

D. PEÓN GARCÍA, Rogelio Amado
TUTOR: D. MEANA FERNANDEZ, Andrés

DATE: June, 2024

Table of Contents

LIST OF FIGURES

LIST OF TABLES

LIST OF ABBREVIATIONS

CCPP - Combined Cycle Power Plant

NGCC - Natural Gas Combined Cycle

HRSG - Heat Recovery Steam Generator

LNG - Liquefied Natural Gas

ORVs - Open Rack Vaporizers

STP - Standard temperature and pressure

LMTD - Logarithmic Mean Temperature Difference

CT - Cooling Tower

RH - Relative Humidity

NO_x - Nitrous Oxide

NPV - Net Present Value

LCOH - Levelized Cost Of Hydrogen

LP - Levels of Pressure

EER - Energy Efficiency Ratio

TMY - Typical Meteorological Year

SCR - Selective Catalytic Reductor

TET - Turbine Exhaust Temperature

LFL - Lower Flammability Limit

Abstract.

This final degree project investigates three innovative methods to enhance the efficiency and sustainability of combined cycle power plants. Using an advanced thermodynamic software program, the performance of each optimization strategy will be evaluated.

The first optimization strategy includes integrating a chiller, which cools down the intake air of the gas turbine, potentially generating more power.

The second approach involves the design of the heating circuit for liquified natural gas, to find its most suitable location.

The third study is the addition of hydrogen to the methane gas to allow existing combined cycles to operate with a more sustainable fuel.

The findings of this project could be relevant to the design of existing and future combined cycles, paving the way for more sustainable and efficient combined cycle operation.

Resumen.

En este proyecto de fin de grado se analizan tres métodos innovadores para mejorar la eficiencia e impacto medioambiental de unas plantas de producción energética, los ciclos combinados. Se utilizará un programa informático avanzado de análisis termodinámico con el que se evaluará el impacto de cada estrategia de optimización.

La primera se basa en la integración de un enfriador, conocido como “chiller”, que baja la temperatura del aire de entrada a la turbina de gas, potencialmente aumentando la potencia neta del ciclo.

El segundo objeto de estudio es el diseño del circuito de calentamiento de gas natural licuado, para encontrar su ubicación idónea.

El tercero trata de la mezcla de hidrógeno con gas metano para permitir que los ciclos actuales puedan emplear combustibles más sostenibles.

Los resultados de este proyecto pueden ser relevantes en el diseño de ciclos combinados, pudiendo ofrecer una operación más sostenible y eficiente.

1. Introduction.

In recent years, there has been an important concern among people regarding the environmental impact of society and industry. The increasing number of pollutants produced accumulate over time and pose a serious risk for public health. Perhaps the most studied pollutants are greenhouse gases, whose concentration in the last hundred years has made a notorious impact on world climate. From 1950: [1]

- Atmospheric carbon dioxide measured at Mauna Loa Observatory rose more than 30%.
- Global average temperatures rose 1.2ºC.
- The frequency and intensity of 10-year extreme hot temperature events have increased by 2.8 times.
- The frequency and intensity of 50-year extreme hot temperature events have increased by 4.8 times.
- The frequency and intensity of 10-year extreme drought events have increased by 1.7 times.

And the list goes on, with an increasing number of heavy precipitation events, smaller Arctic Sea ice area, increasing ocean acidity and sea level… In addition, the proportion of CO_2 emissions captured by land and ocean carbon sinks is smaller in scenarios with higher cumulative CO_2 emissions, as their ability to absorb this gas is reduced [2]. With an increasing global population and consumption of natural resources, if no action is taken, the Earth will transform into a harsh environment no one would like to live in.

Fossil fuels account for more than 60% of all energy produced in the world. [3] But the share is not evenly distributed across the world. In fact, some European countries have a 90% share of non-fossil generation, while most parts of Africa and Asia rely heavily on fossil fuels. [4]

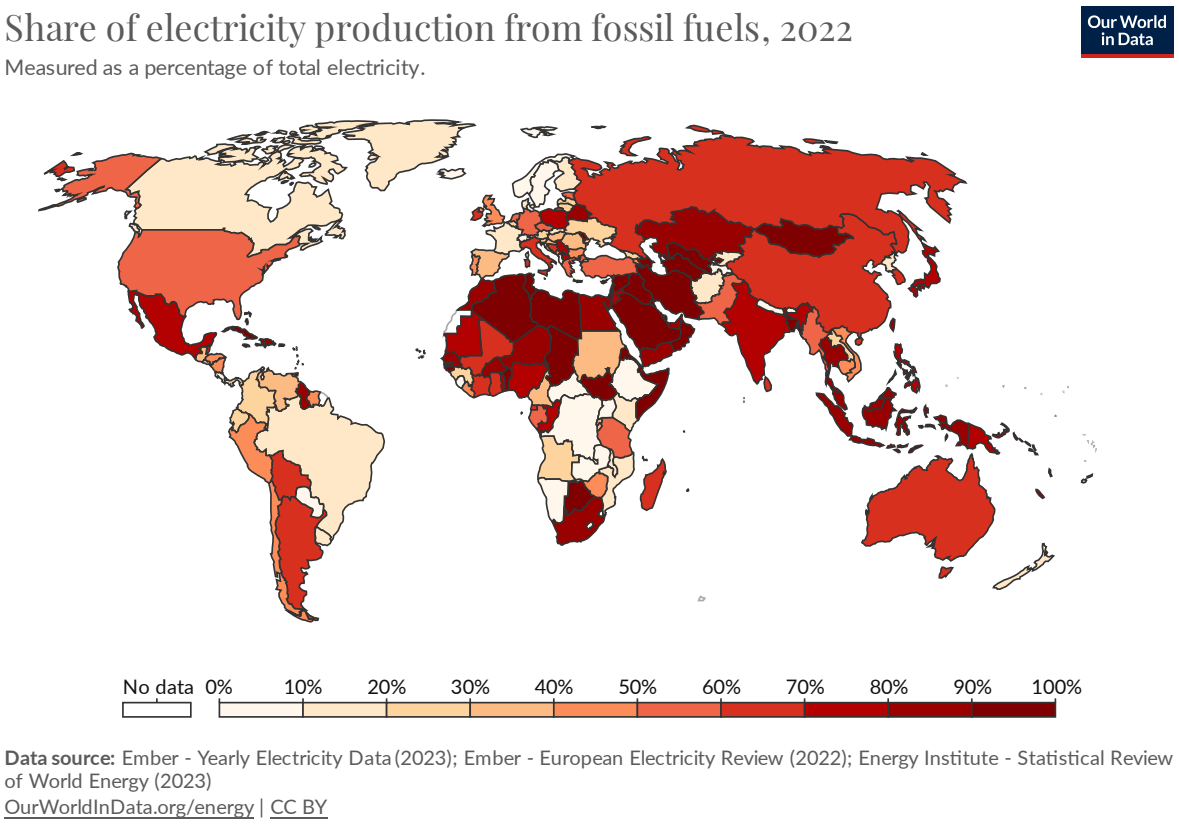

Figure 1.1 Share of fossil fuel electricity production in 2022 (Source: [4])

Even though the best alternative, from an occidental point of view, is to switch to renewable energy, most countries in the world are far from achieving the same generation capacity of fossil fuels using renewables. In order to reduce global emissions of carbon dioxide and other greenhouse gases, the most sensible strategy is using the same energy sources with higher-efficiency systems until renewables can enter the market appropriately.

There is not an ideal energy source, as renewable sources are highly dependent on natural phenomena such as wind, rain and sun, which requires energy storage solutions, increasing installation costs. Nuclear energy creates radioactive waste and can become dangerous if not operated correctly. Considering fossil fuels, gas cycles pollute almost 50% and 20% less than coal or fuel power plants, respectively [5].

The transition to clean energy sources must be made as smoothly as possible; otherwise, developing countries will not be able to fulfill the carbon dioxide emission requirements and economic sanctions would harm them instead of encouraging this energy transition.

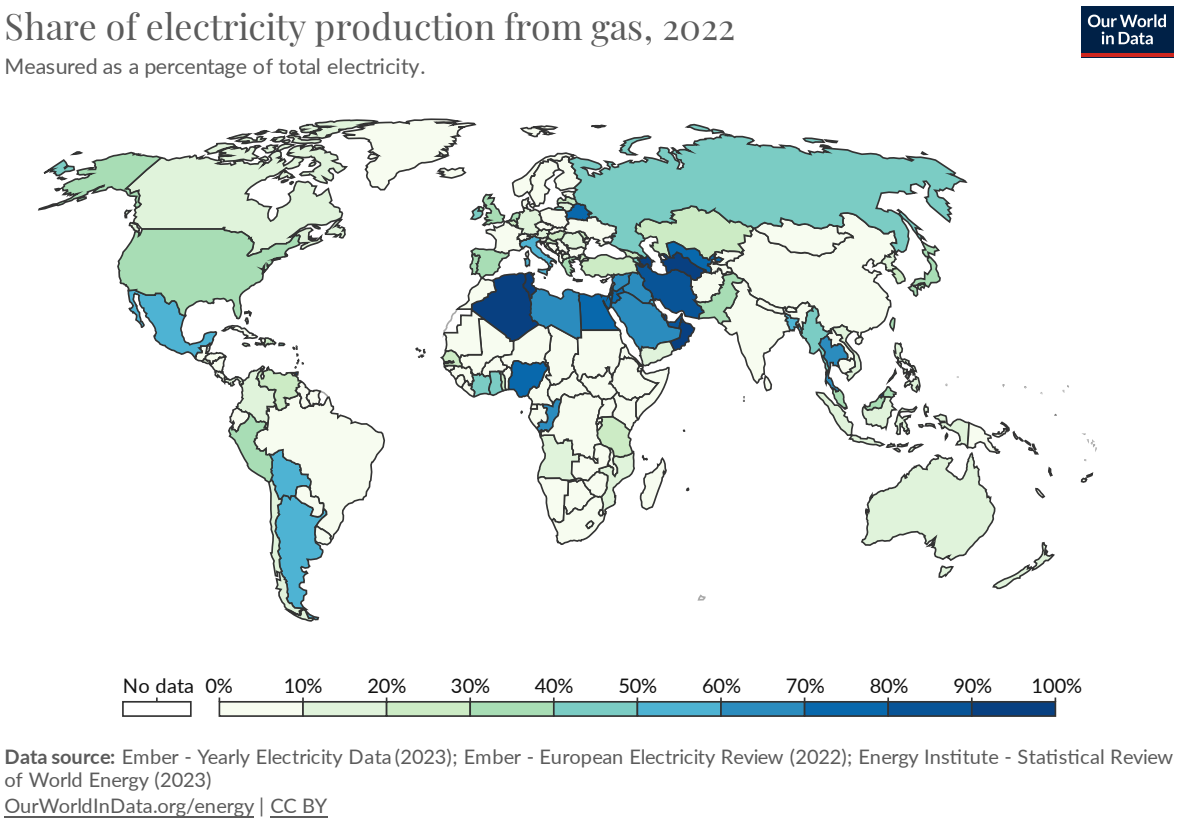

Figure 1.2 Global electricity production from gas in 2022. (Source: [4])

In order to check where combined cycles are used, the International Energy Agency published Figure 1.2 showing where energy production from gas is taking place. It can be deduced that on North America, South America, the middle East, the north of Africa and Russia, combined cycles are a relevant electricity source. By optimizing these cycles, even slightly, the improvement of energy efficiency and reduction in carbon emissions is multiplied.

According to the International Energy Agency, electricity generated from gas accounted for 6489 TWh in 2021, around 23% of all energy generated worldwide. Gas electricity production is expected to reach 6522 TWh in 2025, mainly in Africa and the Middle East, whose increase of gas generation is expected to rise 1.01% and 1.15% respectively.[6]

In Dominican Republic, 7421 GWh were produced in 2023 from coal, 31.03% of all power generated while natural gas produced 9255 GWh, 38.70% of the total power generated. [7] Natural gas is the main source of energy for Dominican Republic, and improving combined cycle performance can lower carbon emissions, avoiding the use of coal power generation and reducing costs.

In the context of regions where the transition to a renewable energy system in a short timeline is not an option, this project is focused on studying strategies for reducing the emissions from the fossil fuels used for energy generation. In Chapter 2, the background and objectives of the work will be introduced. The methodology used to evaluate the alternatives proposed will be shown in Chapter 3 and in Chapter 4, the results of the simulations will be displayed.

2. Background and objectives.

2.1.-Background.

In 1940, the first Combined Cycle Power Plant (CCPP) came online in Switzerland, producing 4 MW of power from gas. A year later, the Natural Gas Combined Cycle (NGCC) was invented, and it was claimed to be “the most efficient and low-cost route

to electricity production" [8] Nowadays, active research is still performed to adapt and improve combined cycles. Only in the US, 20 new NGCC are expected to come online between 2024 and 2025, with a total capacity of 7.7 GW[9].

Natural Gas Combined cycles consist of two coupled Brayton and Rankine cycles, as depicted in the top Brayton cycle, atmospheric air is compressed and mixed with natural gas in a combustion chamber, being expanded afterwards in a gas turbine. Then, the exhaust hot gases enter a Heat Recovery Steam Generator (HRSG) which is composed of a series of heat exchangers that are used to generate steam for the bottom Rankine cycle.

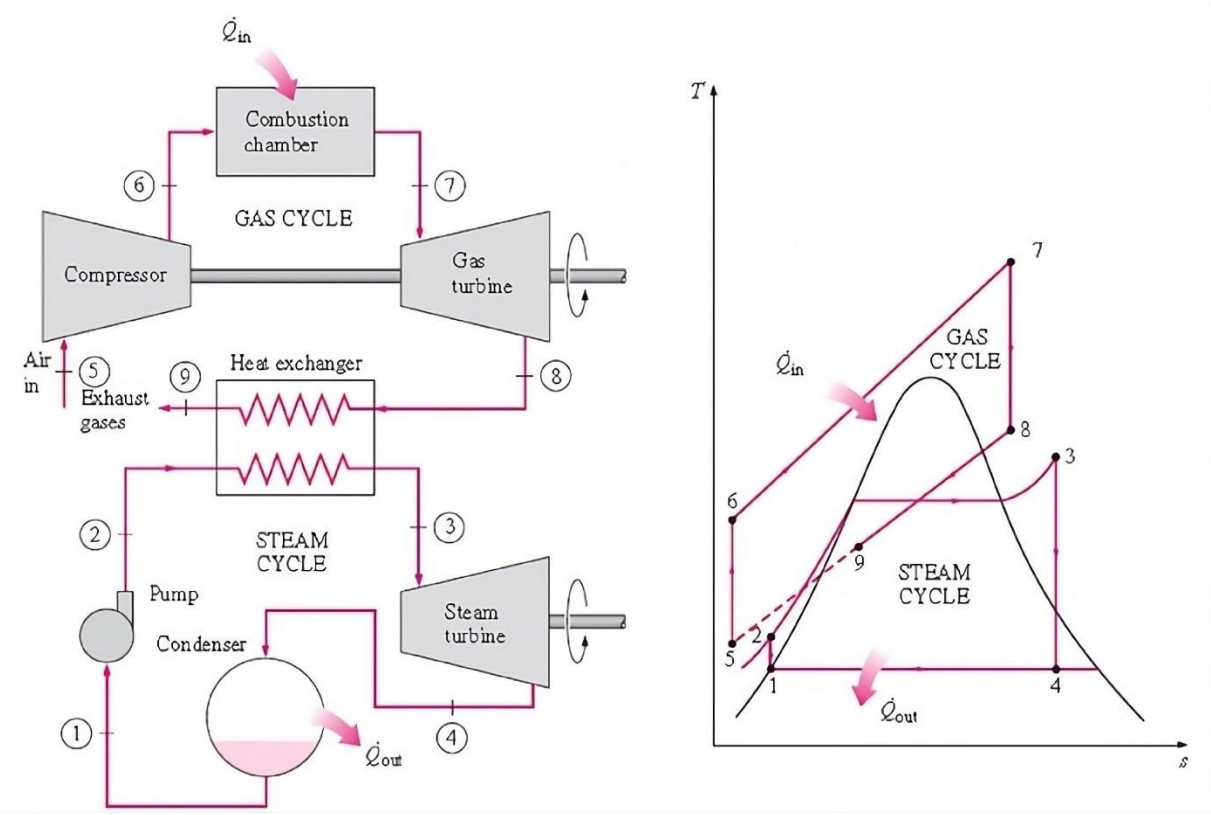

Figure 2.1 Brayton (gas) and Rankine (steam) cycles. (Source: [10])

In the Rankine cycle, inside the HRSG, evaporators at different pressure levels are used to generate steam for powering the turbines. Economizers and superheaters are

used to heat up liquid water before the evaporators and superheat the steam after them. The superheated steam is then expanded in the steam turbines, generating power. The turbine exhaust steam is driven to a condenser, becoming liquid water again thanks to a refrigeration circuit with a cooling tower. Finally, water is pumped back into the HRSG.

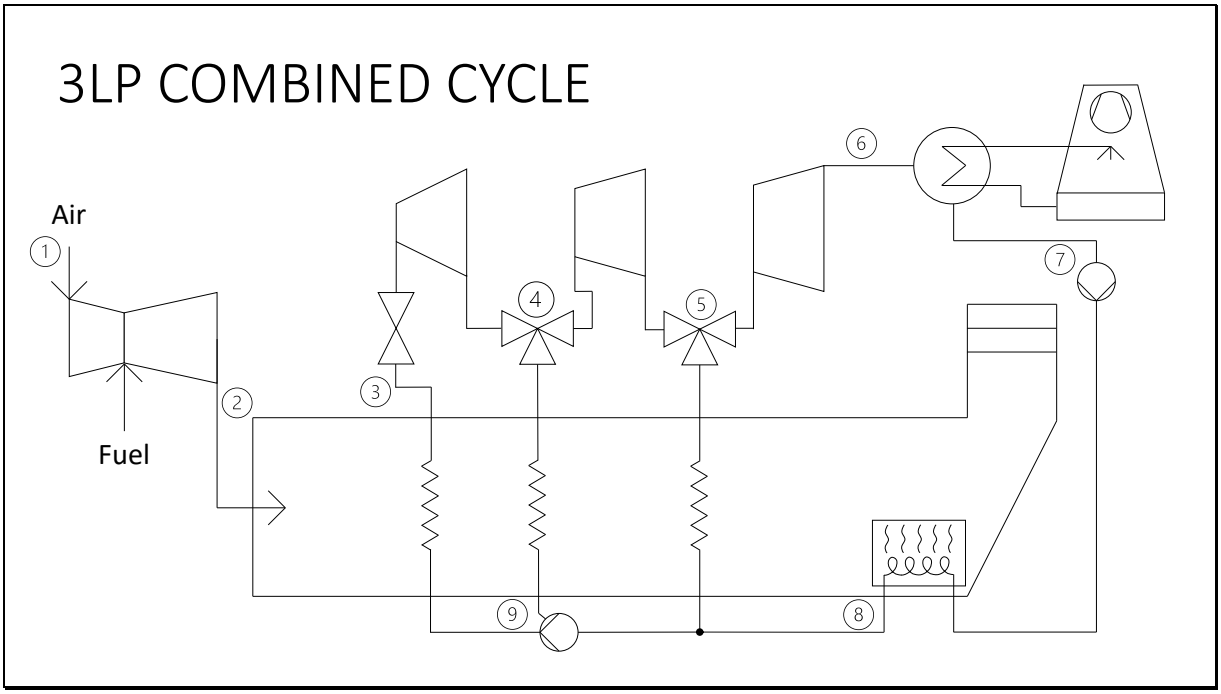

Figure 2.2 Combined cycle with three pressure levels (3LP).

Combined cycles can be adapted to various scenarios, a popular one is offshore production, mainly used by the oil and gas industry to power machinery, and Flatebø proved that it is possible to build a 53 MW plant with 50.3% efficiency, with the limitations of weight and volume offshore production sets. [11]

Recent research has been made towards the reduction of carbon emissions, using post-combustion carbon capture systems, integrating combined cycles with solar power plants, to improve energy efficiency. [12], [13]

In recent years, some researchers have investigated the use of LNG (Liquefied Natural Gas) as fuel [14], but to the author´s knowledge, performance and cost analyses for

using the cooling power of LNG in different cooling circuit positions have not been performed yet. The implementation of chillers for combined cycles has been studied as well [15], [16]; but there is little information about the feasibility of using chillers in a high humidity scenario as in Dominican Republic. In addition, an important topic for decarbonization is blending natural gas with hydrogen. The impact of blending on performance and its drawbacks are being analyzed [17], but little to no information is available for the feasibility of blending in Dominican Republic considering its ambient conditions.

To investigate combined cycle improvements, three strategies will be examined in this project:

- Open Rack Vaporizers (ORVs) placement.
- Chiller usage and sizing.
- Hydrogen Blending usage.

2.1.1.- ORVs.

Open Rack Vaporizers (ORVs) are heat exchangers which employ sea water to heat Liquified Natural Gas (LNG) from -163C up to 15C, to be later burned at the gas turbine. The heat exchanger consists of a series of aluminum tubes in contact that allows heat transfer between these two fluids. [18]. ORVs need an inlet of hot water and an outlet of cooler water, and their respective pumps. They do not require any additional source of heat or power. As sea water is required, the first step is deciding what are the possible sources of hot water, which can be found in the cooler circuit of the condenser, depicted in Figure 2.3.

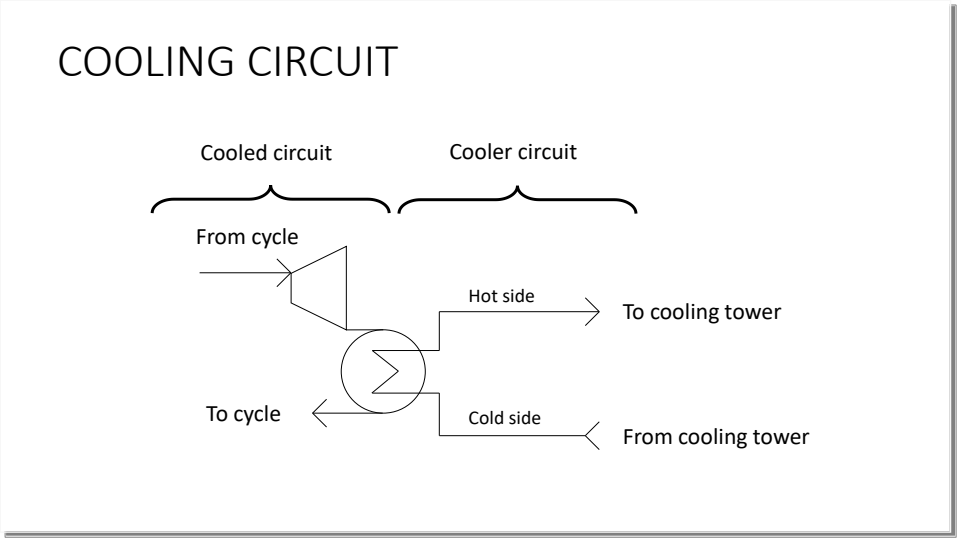

Figure 2.3 Cooling circuit of the steam turbine.

2.1.2.- Chillers.

In combined cycles, reducing inlet air temperature can increase combined cycle power output in a cost-effective manner. As the air cools down, its density increases, allowing a higher mass flow rate and increasing output power [19]. Air-cooled electric chillers and water-cooled absorption chillers can be used to obtain this effect, as shown in Figure 2.4 and Figure 2.5.

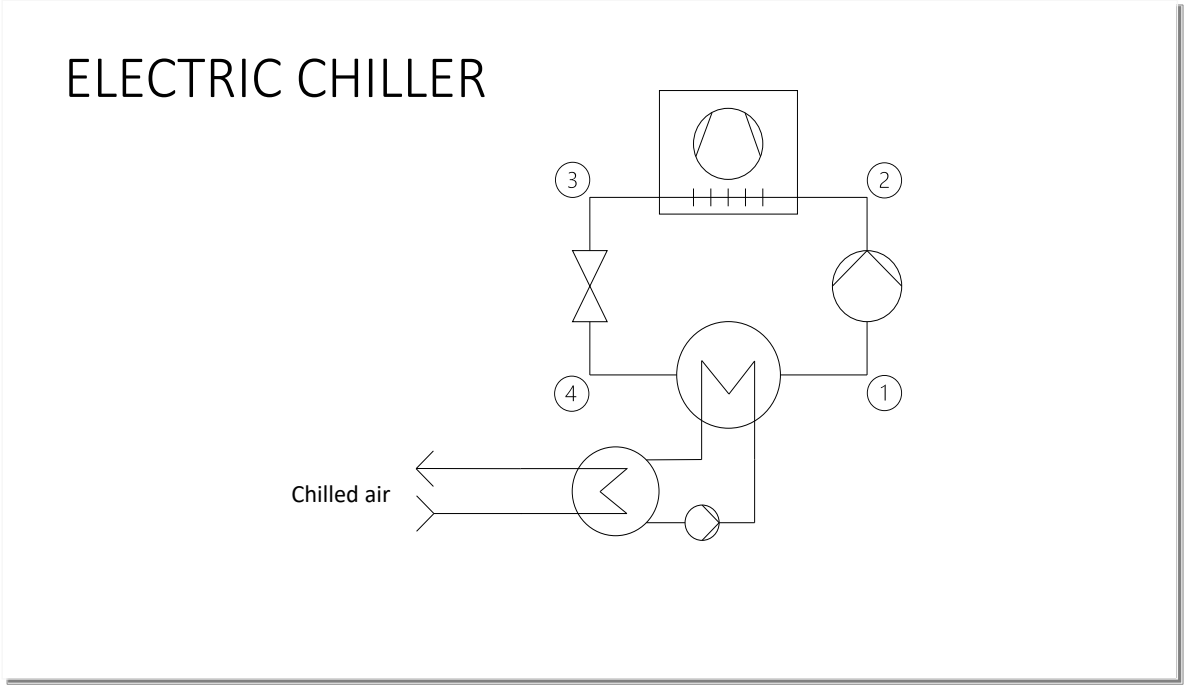

Figure 2.4 Electric chiller components.

Electric chillers work by circulating a refrigerant in a closed cycle, as seen in Figure 2.4. First, the liquid refrigerant is pumped and its pressure and temperature increase (steps 1 and 2). Then, it is cooled down with ambient air (step 3). Finally, the pressure drops in an isenthalpic valve which cools down the refrigerant used to take heat from the compressor inlet air (step 4). [20]

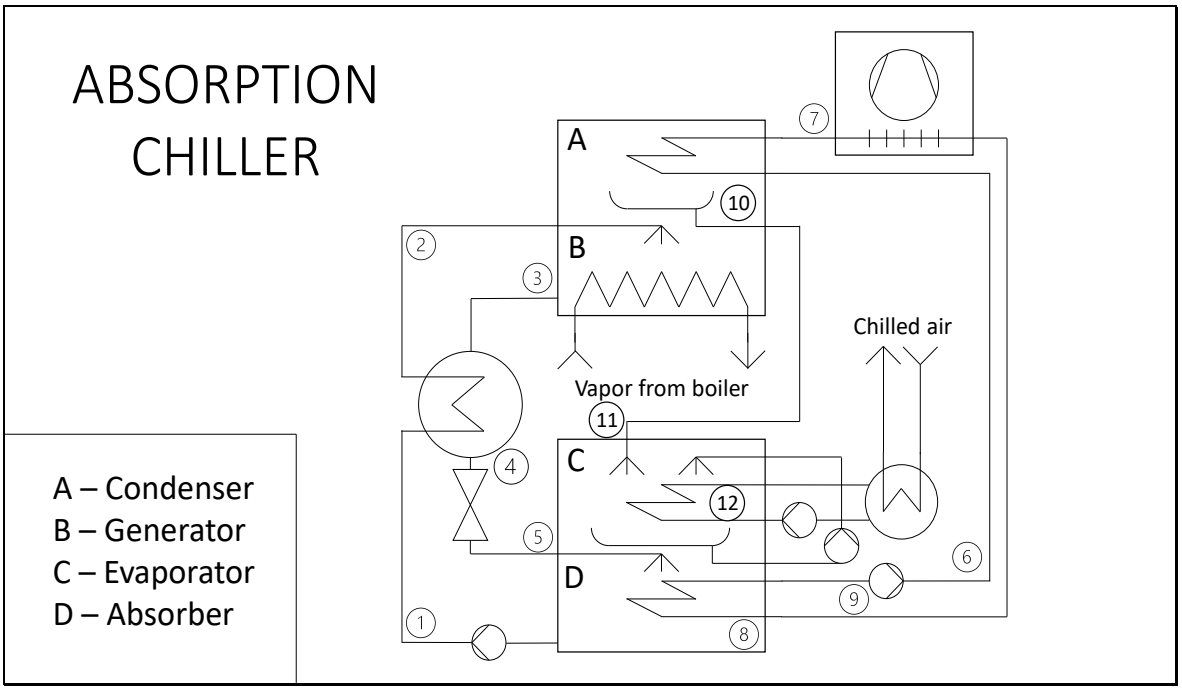

Figure 2.5 Absorption chiller components.

The absorption chiller has a similar working principle, but the refrigerant used is usually a mixture of water and lithium bromide, which has a high affinity for water. First, the lithium bromide solution is pumped into a generator (steps 1 and 2), where vapor from the boiler heats up the solution. As it is heated, lithium bromide loses affinity for water, and it evaporates into a condenser. The concentrated lithium bromide solution goes back to an absorber after being cooled down in a regenerator (steps 3 and 4). This concentrated solution is sprayed in the absorber, attracting water vapor from the evaporator (step 5), and completing the cycle. The evaporator has a low pressure, lowering the boiling point of water to around 4ºC.

The cycle that absorbs heat from the system to be cooled starts in the absorber, cooling down water vapor to enable a faster water absorption by the lithium bromide (steps 8 and 9). It also cools down the water vapor in the condenser (steps 6 and 7) and heat is later rejected with a fin-fan cooler.

On the other hand, the cooling circuit starts in the condenser, where evaporated water turns into liquid (step 10), which is sprayed in the evaporator (step 11) over the cooling water tubes (step 12) where it evaporates. Finally, cooling water enters a heat exchanger which cools down the air for the gas compressor inlet [21].

2.1.3.- Blending.

Another option to optimize combined cycles involves introducing hydrogen into the natural gas fuel mixture, a process known as hydrogen blending. This technique aims to decrease carbon dioxide emissions from gas turbines, thereby enabling more adaptable and versatile fuel usage. In Table 2.1 the differences between methane and hydrogen properties are compared.

Table 2.1 Hydrogen and methane properties. [22]

CHARACTERISTIC	UNITS	METHANE	HYDROGEN
Formula		CH_4	H_2
Molecular weight	kg/kmol	16	2
Molecular size	pm (10^{-12} m)	380	289
Lower/Upper flammability limits	-	4.4/17	4/75
Flame speed	cm/s	~30-40	~200-300
Adiabatic flame temperature	ºC	~1963	~2204
Lower Heating value	MJ/Nm^3	35.8	10.8
Lower Heating value	MJ/kg	50	120
Density (STP*)	kg/m^3	0.657	0.0899

*STP=Standard temperature and pressure

As shown in Annex C, some modifications in the equipment must be conducted prior to blending operation, but once installed, the operation is similar to operation with only natural gas.

2.2.-Objectives.

The main objective of this final degree project is to generate knowledge about possible strategies to improve the efficiency, reduce the carbon footprint and increase the power output of combined cycles. This main objective can be divided into the following specific ones:

- Perform a bibliographic review of the strategies for improving the efficiency of combined cycles, reduce their environmental impact and increase their power output.
- Study the effects of the placement of Open Rack Vaporizers in a combined cycle.
- Study the effects of implementing different chillers in a combined cycle.
- Study the effects of hydrogen blending in a combined cycle.

3. Methodology.

The methodology used in this work comprises the thermodynamic analysis of the three alternatives presented before. In the first strategy, the Open Rack Vaporizers are designed to work with sea water, and all the possible configurations will be compared with the aim of finding the most suitable location, given a turbine and its operating conditions. The other two strategies, the use of a chiller and blending, will be compared against the same cycle with no modifications, as a way of analyzing the viability and the expected return of a more complex cycle.

3.1.-Thermodynamic analysis.

For the Thermodynamic analysis, mass and energy balances have been performed for the relevant cycle equipment. The general mass balance is written as follows:

$$\sum \dot{m}_{in} = \sum \dot{m}_{out} \tag{3.1}$$

Where $\dot{m}_{in}$ and $\dot{m}_{out}$ are the mass flowrates in kg/s of incoming and outgoing streams. The general energy balance for open systems in steady regime, following the 1st Law of Thermodynamics, is

$$\dot{Q} - \dot{W} = \sum \dot{m}_{out} \cdot h_{out} - \sum \dot{m}_{in} \cdot h_{in} \tag{3.2}$$

Where $\dot{Q}$ is the thermal power in kW, $\dot{W}$ represents power in kW, and h_{in} and h_{out} are the specific enthalpy values of the incoming and outgoing streams in kJ/kg. Note that changes in kinetic and potential energy have been neglected in this analysis.

Equations 3.1 and 3.2 have been particularized for every cycle component. In the case of the cycle heat exchangers, the general formula 3.3 for heat transfer using the Logarithmic Mean Temperature Difference will be used to estimate the heat rate, and

for the analysis of heat exchanger, the second part of the equation 3.3 has been used to calculate the heat rate.

$$\dot{Q} = U \cdot A \cdot LMTD = \dot{m} \cdot C_P \cdot \Delta T \quad (3.3)$$

Where:

- $\dot{Q}$ is the heat transferred [kW]
- U is the overall heat transfer coefficient [kW/(m^2·ºC)]
- A is the area of the heat exchanger [m^2]
- $LMTD$ is the Logarithmic Mean Temperature Difference [ºC]

Heat transfer calculations depend on lots of different parameters, and even with the same heat exchanger shape, the fluid velocity, temperature, viscosity, density etc. can drastically change the heat transfer rate of a given surface. [23]

When comparing different operating conditions, a reasonable first approach is that the heat transfer rate is directly proportional to the temperature difference across the surfaces. While it is a good first approach, it does not perform good enough for small temperature differences, and it does not distinguish between co-current and counter-current flow.[24]

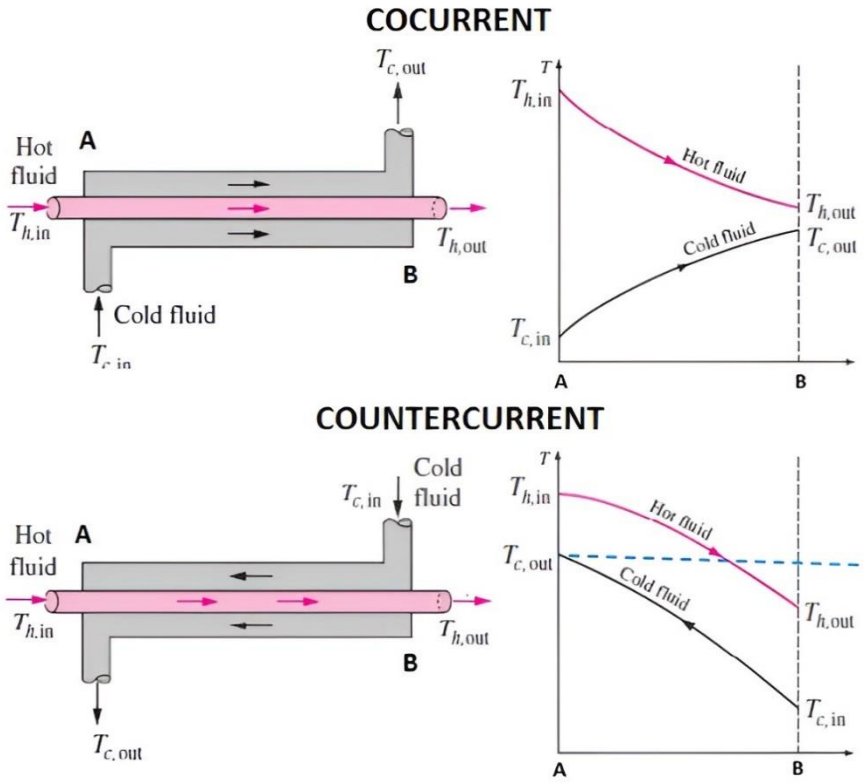

Figure 3.1 Comparison between co-current and counter-current flow [25]

As a way to solve these limitations, the LMTD is commonly used. In this method, the heat rate is proportional to the mean temperature difference between the two fluids across all the surface. For simplification, it is assumed that the temperature decreases linearly across the tubes. As shown in Figure 3.2, 'A' and 'B' represent the ends of the heat exchanger, and '1' and '2' represent the inlet and outlet of each flow.

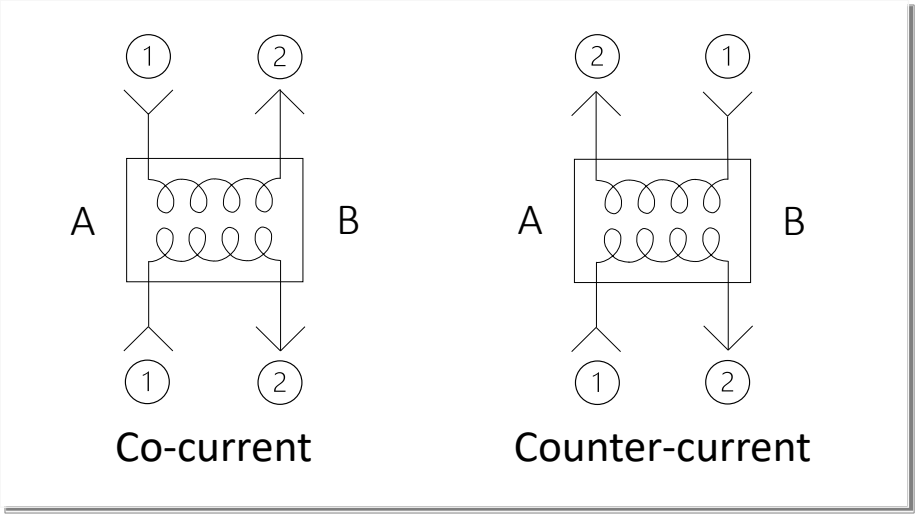

Figure 3.2 Co-current and counter-current configurations of a general heat exchanger.

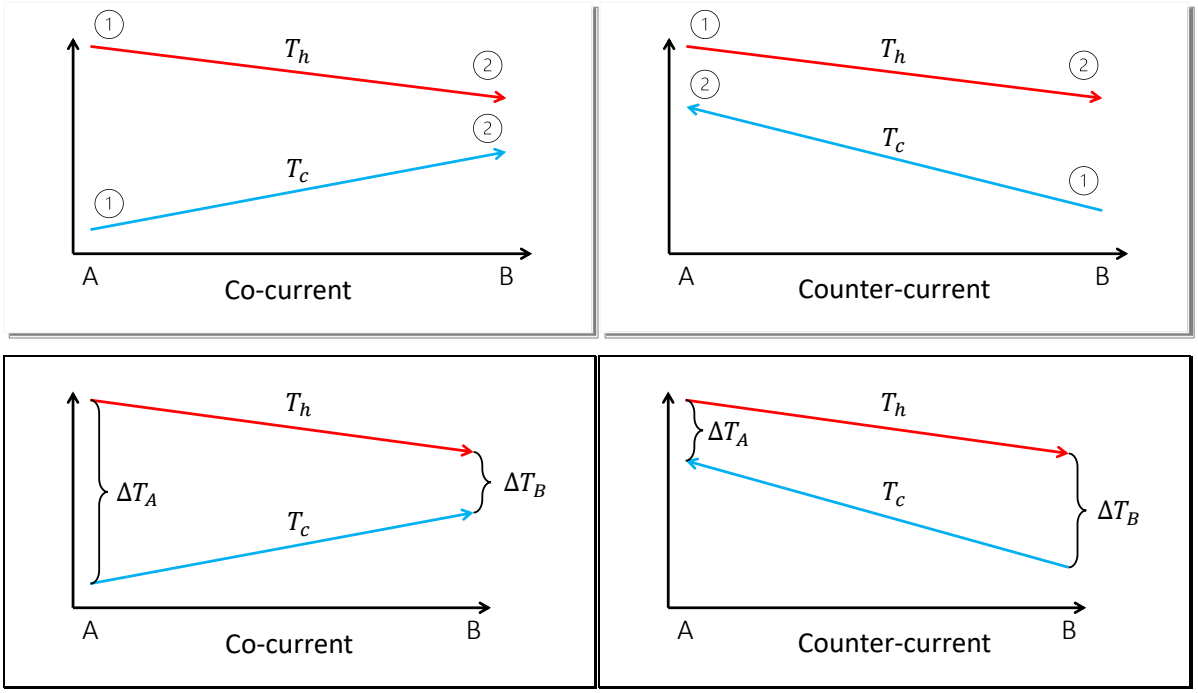

Figure 3.3 Temperature evolution in co-current and counter-current configurations.

The LMTD is calculated using the formula LMTD = $\frac{(\Delta T_A - \Delta T_B)}{\ln\left(\frac{\Delta T_A}{\Delta T_B}\right)}$. For a more detailed analysis on how to deduce it, see Annex A. LMTD formulation.

In order to achieve the proposed objectives, some calculation methods have been used to lower calculation time. If a complete analysis of a combined cycle had to be made by hand, using mass and energy balances, although possible, it would be very time-consuming for the simulation of different scenarios.

The main programs considered, their main strong points and limitations are collected in Table 3.1.

Table 3.1 Programs considered for the design of components and combined cycles.

Program name	Strong points	Limitations
Thermo-Calc	Detailed analysis of physical properties	Only one component at a time
ProSim (Matlab)	Thermophysical analysis of components	Simple analysis of components
EES	Accurate fluid properties	Code-intensive, difficult to add different components
Thermoflow	Complete cycle/components analysis	Iterative (requires computation time)

In this project, Thermoflow was selected as the software to be used, as it allows to perform a complete analysis of the cycle and its components. EES and an Excel Macro have been also used to obtain some fluid properties. The use of the Macro is described in Annex D. Microsoft Excel Macros.

The three components used from Thermoflow are described below.

3.1.1.- GTPro.

It is a software specially built for designing all types of gas turbine cycles, simple and combined, with different configurations. It takes input working conditions, such as the turbine model, ambient temperature, pressure and relative humidity, design boiler pressure… and simulates the cycle with different conditions until finding the ones that optimize its efficiency.

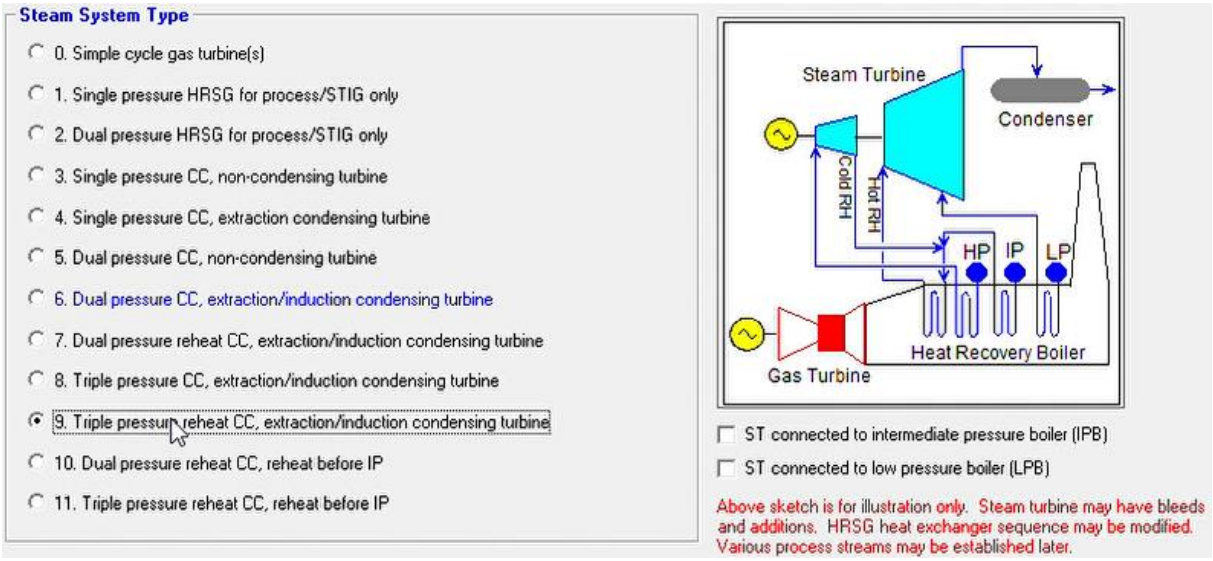

Figure 3.4 Screen capture of GTPro, showing different configurations for the type of cycle.

Once all the input parameters are set, GTPro gives a text and graphic output with the flow conditions in each point.

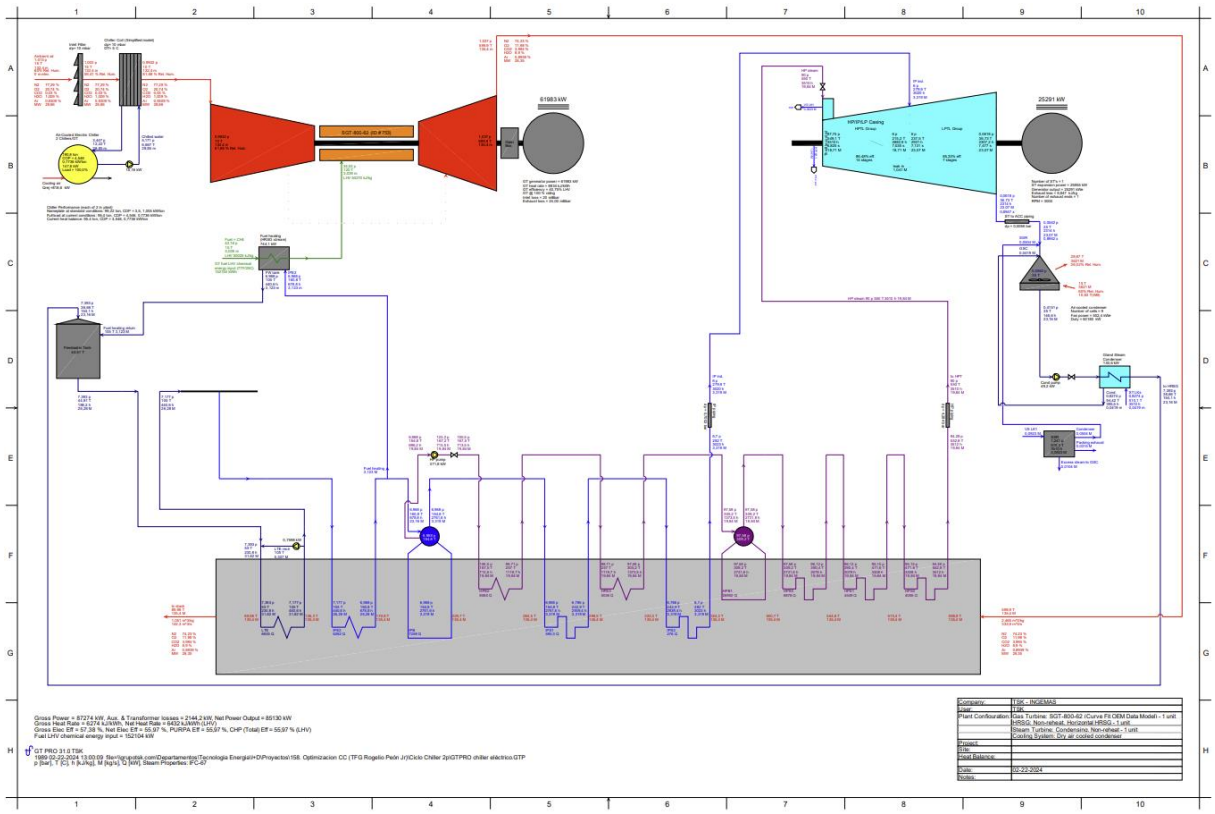

Figure 3.5 Screen capture of the general graphic output of GTPro -2LP cycle-.

This was the software used to design the combined cycle and the chillers. One of its features is being able to export the cycle, once simulated, to Thermoflex, the main component of Thermoflow.

3.1.2.- Thermoflex.

It is the most complete component of Thermoflow for performing thermodynamic analyses. The navigator used to select different working modes is depicted in Figure 3.6. The first step is the design of the cycle components from an extensive library, using the “Edit Drawing” option. Then, components are connected through pipes and initial cycle conditions are set.

Figure 3.6 Thermoflex navigator used to select different modes.

When the first “Play” button is pressed, the “Edit Inputs” button is activated. Clicking it opens a menu for the input of ambient conditions and the general site configuration. Then, the operating conditions of all components are set.

Thermoflex has three simulation procedures that must be run in order, using the second “Play” button:

1) Thermodynamic Design (TD): It uses the previously design conditions to simulate the behavior of its components, performing heat and mass balances.
2) Engineering Design (ED): It considers, as well as thermodynamic conditions, the actual size of components, choosing the next larger one for a required operation from the available libraries.
3) Off Design (OD): It fixes the components previously simulated, and it allows the user to change operation conditions without modifying the size of the equipment.

Thermoflex allows the user to change the design modes all at once or one by one, for fine-tuning design. In addition, in the business version of Thermoflex, the PEACE add-on is available, which gives a cost and size estimation of the equipment and resources used in the cycle, as shown in Figure 3.7.

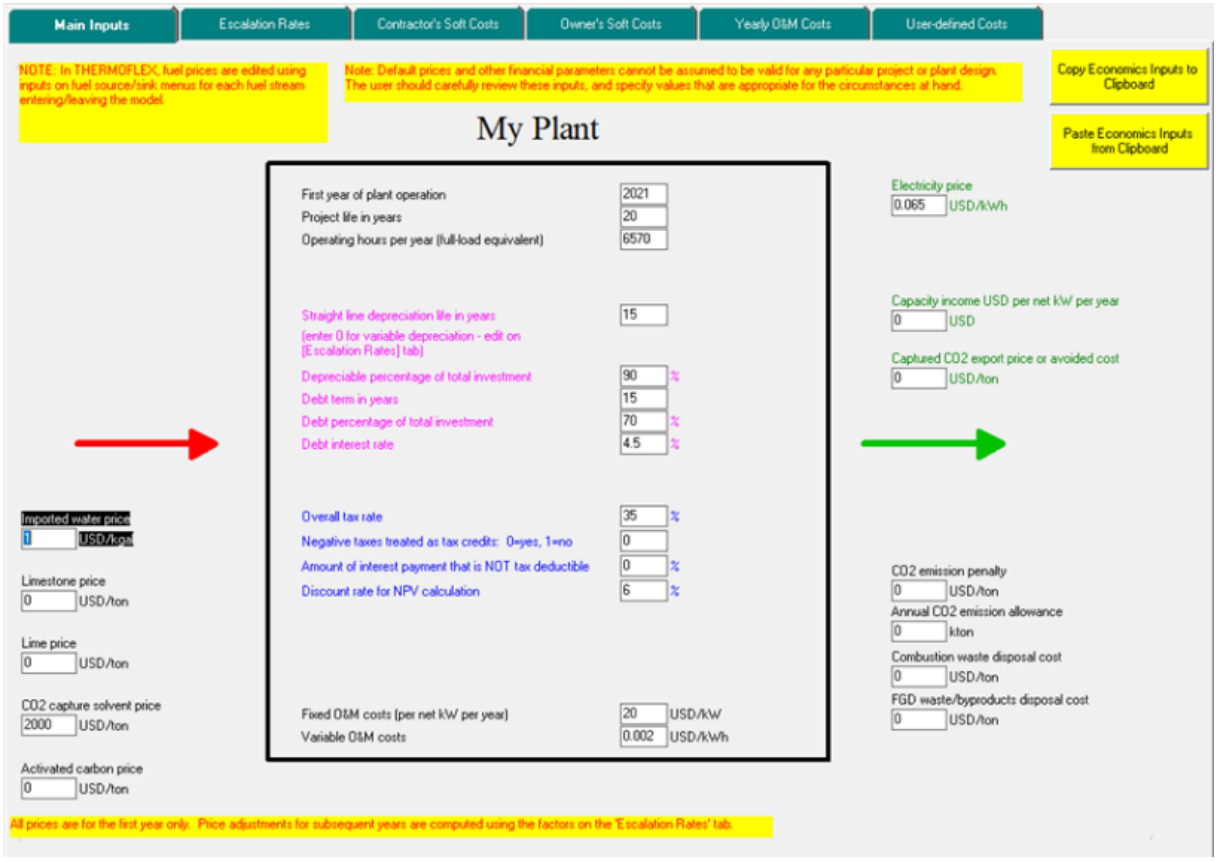

Figure 3.7 Screen capture of main PEACE configuration.

Once all the different steps of the simulation have been run, Thermoflex gives both text and graphic outputs of all the calculated parameters. Figure 3.8 shows the outline of the general graphic output of Thermoflex for a combined cycle with 3 pressure levels.

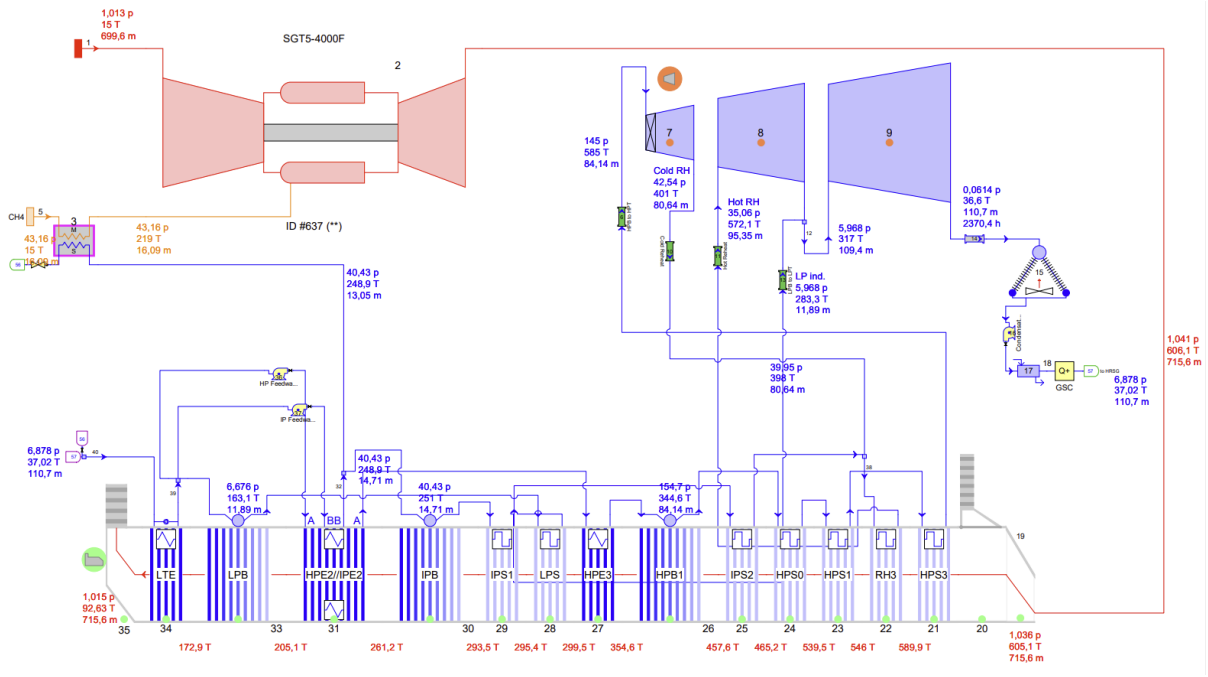

Figure 3.8 Screen capture of the general graphic output of Thermoflex -3LP cycle-.

3.1.3.- ELINK.

ELINK is a useful tool that allows the user to simulate GTPro and Thermoflex designs in Microsoft Excel, being able to simulate multiple operating conditions. Even though simulations in ELINK take longer and Thermoflex can also simulate multiple operating conditions, the tool allows to analyze the results in a more orderly way. Figure 3.9 shows the interface used to run and modify simulations.

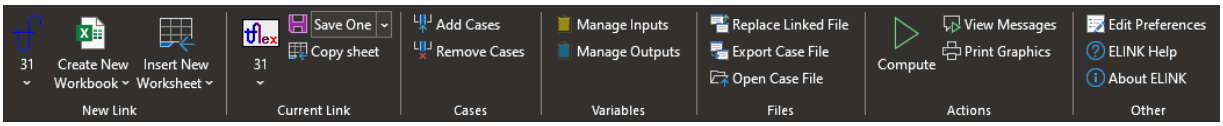

Figure 3.9 Screen capture of ELINK options.

3.2.-Strategies for improving combined cycles.

After describing the software used for the thermodynamic analysis, the strategies studied for improving combined cycles will be introduced.

For the second and third strategies, Dominican Republic conditions have been studied as the country relies heavily on fossil fuels for electricity generation, and a fast adoption of green sources of energy is not achievable.

Firstly, only the heat rejection related components of the cycle were studied, allowing to evaluate the optimal placement position of ORVs. Afterwards, the whole cycle was considered for studying the introduction of chillers and fuel blending.

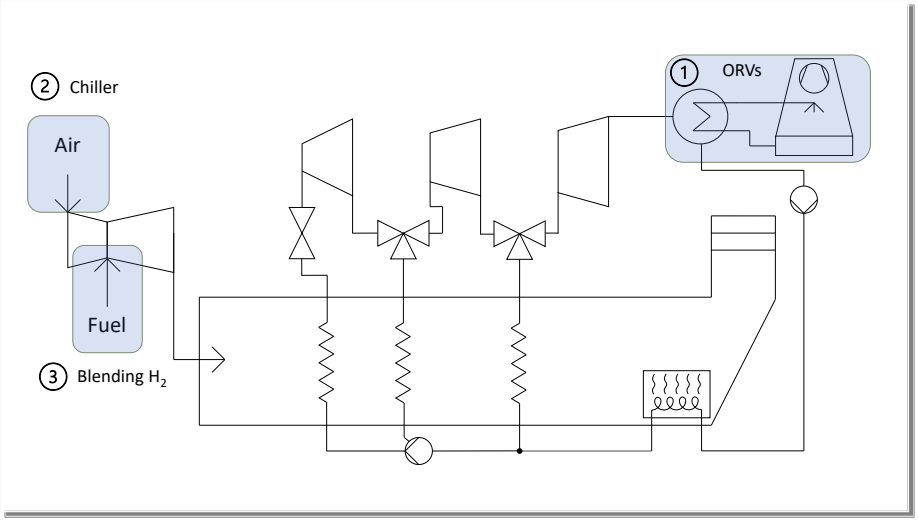

Figure 3.10 Combined cycle with the three areas to be analyzed.

3.2.1.- Placement of Open Rack Vaporizers.

Before studying the position of ORVs, the conditions of the cooling system of the turbine needed to be fixed. As previously commented, for this first study it is enough to focus on the heat rejection circuit of the cycle.

The steam turbine works with a design exhaust pressure between 0.085 bar and 0.075 bar. The same condenser was considered for both levels of pressure; therefore, it was designed for the most demanding case, 0.075 bar. The main input and output properties are indicated in Table 3.2 and Table 3.3 for both pressure levels.

Table 3.2 Turbine and condenser fluid properties in the main cycle.

First Pressure Level – 0.085 bar					
	Pressure [bar]	Temperature [ºC]	Mass flow [t/h]	Enthalpy [kJ/kg]	State [-]
ST Input	165	565	489.6	3437	Superheated Vapor
ST Output	0.085	42.69	489.6	2,231.2	Liquid-Vapor mixture
Condenser Output	0.444	42.69	489.6	178.7	Subcooled liquid
Second Pressure Level – 0.075 bar					
	Pressure [bar]	Temperature [ºC]	Mass flow [t/h]	Enthalpy [kJ/kg]	State [-]
ST Input	165	565	489.6	3473	Superheated Vapor
ST Output Condenser	0.075	40.33	489.6	2,219.6	Liquid-Vapor mixture
Condenser Output	0.434	40.32	489.6	117.7	Subcooled liquid

Table 3.3 Condenser fluid properties in the cooling cycle.

First Pressure Level – 0.085 bar					
	Pressure [bar]	Temperature [ºC]	Mass flow [t/h]	Enthalpy [kJ/kg]	State [-]
Condenser Input	3	30.43	26,035	127.8	Subcooled liquid
Condenser Output	2	39.69	26,035	166.5	Subcooled liquid
Second Pressure Level – 0.075 bar					
Condenser Input	Pressure [bar]	Temperature [ºC]	Mass flow [t/h]	Enthalpy [kJ/kg]	State [-]
ST Input	2	28.00	25,903	117.7	Subcooled liquid
Condenser Output	3	37.30	25,903	156.4	Subcooled liquid

The design of the condenser was made on Thermoflex, according to input and output temperatures. In an effort to use the same condenser area for both pressure levels, the Logarithmic Mean Temperature Difference (LMTD) has been used to design its cold-side input temperature for the high-pressure scenario. To make calculations simpler, it was assumed that for both levels of pressure, the heat exchanged in the condenser was the same. As U and $\dot{Q}$ are considered constant, to keep the same heat exchanger area -or size-, the LMTD must be constant.

For both pressure levels, the outlet temperature of the cooling cycle after the condenser was set to three degrees lower than condensing temperature of the main cycle. For the first pressure level, the cooling cycle condenser inlet temperature was obtained from the simulation. With this result, the LMTD was calculated, so that the cooling cycle condenser inlet temperature for the second pressure level can be calculated from the

definition of the LMTD (see Annex A). As the main cycle condenser inlet and outlet temperatures are the same (condensing process) for each pressure level, co-current and counter-current configurations give the same result. The calculated operating temperatures were fixed for all the examined cases:

$$\Delta T_A = T_{main,cond} - T_{cooling,in} \quad (3.4)$$

$$\Delta T_B = T_{main,cond} - T_{cooling,put} \quad (3.5)$$

After fixing these operating temperatures, the study of ORV placement position can proceed. The limitations for the design are:

- The ORVs must discharge to the sea.
- The sea temperature is 25ºC and the maximum discharge temperature allowed by the company is 31.5ºC.
- The air wet bulb approach to incoming warm water of the cooling tower is 4ºC.
- The heat rate required for the ORVs is set by the cases which have them installed in the outlet of the cold side of the cooling circuit.
- The evaporative cooling tower blowdown is taken from the cooling tower and pumped out by the circulating pump, being discharged directly to the sea and bypassing ORVs.

There are two possible locations for the flow inlet and outlet: before the cooling tower (CT) - the hot side - or before the condenser - the cold side -. There are also two possible placements for the ORVs, in the inlet pipeline or the outlet pipeline. These four possibilities are depicted in Figure 3.11.

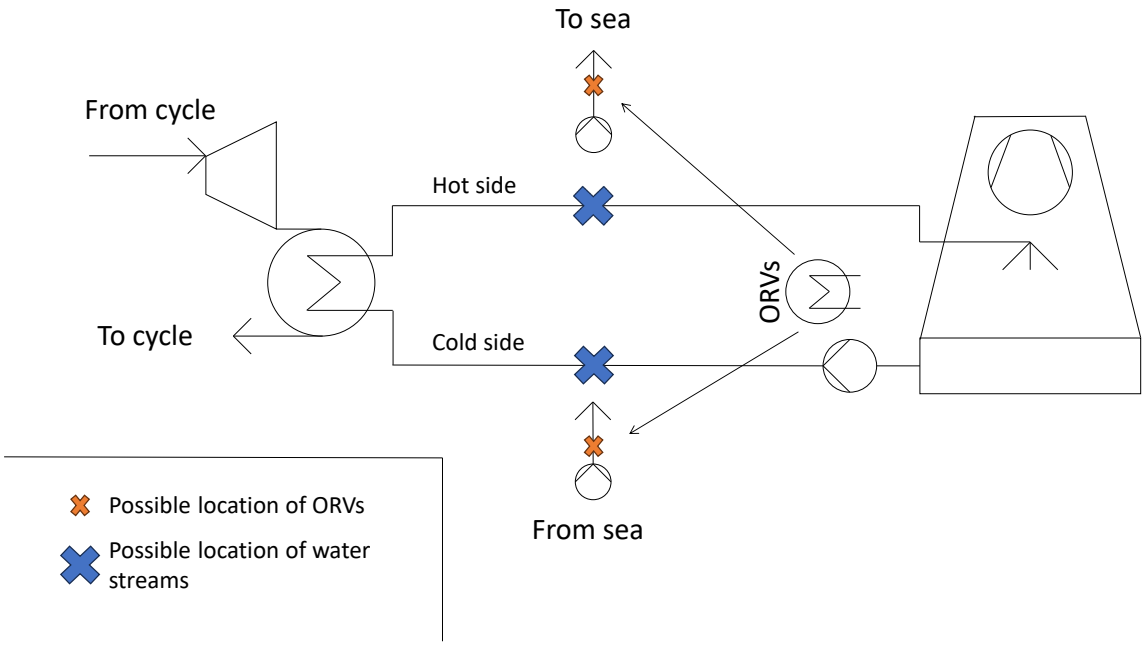

Figure 3.11 Possible locations for inlet or outlet pipes and ORVs.

Out of all twelve possible setup combinations for each pressure, six have been calculated for the first pressure level and five for the second pressure level. The reasons for discarding a setup were:

- Discharge to sea from the hot side without ORVs, due to the high temperature discharge limitations.
- The situations where the order of discharge from the same side was worse (the inlet pipe located prior to the outlet pipe) if the other order was available.
- The situations where the inlet pipe connects to the hot side and the outlet pipe connects to the cold side, as very similar possibilities are better due to the lower water flow through the condenser.

The remaining configurations were considered, and named according to these conditions:

- The four main configurations were named with letters from A to D.

- Cases with a ‘1’ in the name correspond to low-pressure scenarios. Cases for high-pressure scenarios do not have the additional number.
- Case CI was added in parallel to the C high-pressure scenario due to temperature limitations.
- Cases BI and BI1 were named in parallel to B and B1 due to their similarity but correspond to separate cases.

The configuration of all cases may be compared in Figure 3.12 and Table 3.4.

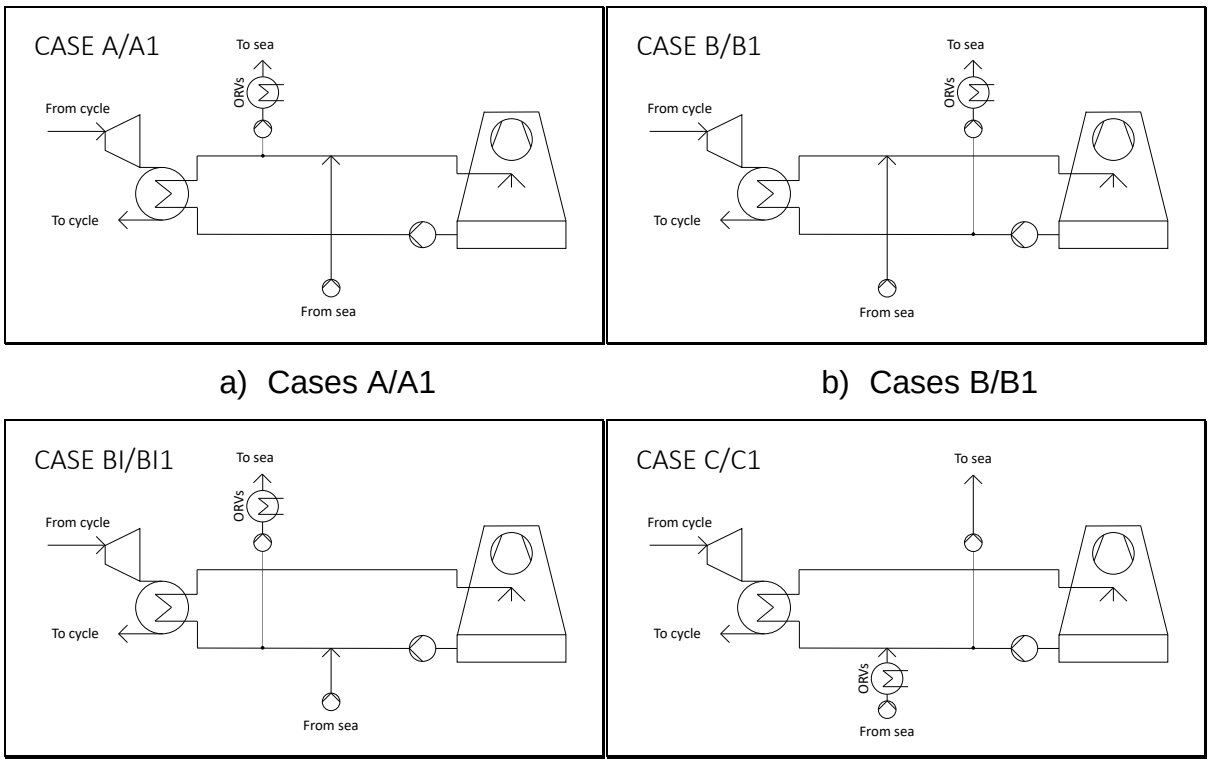

a) Cases A/A1

b) Cases B/B1

c) Cases BI/BI1

d) Cases C/C1

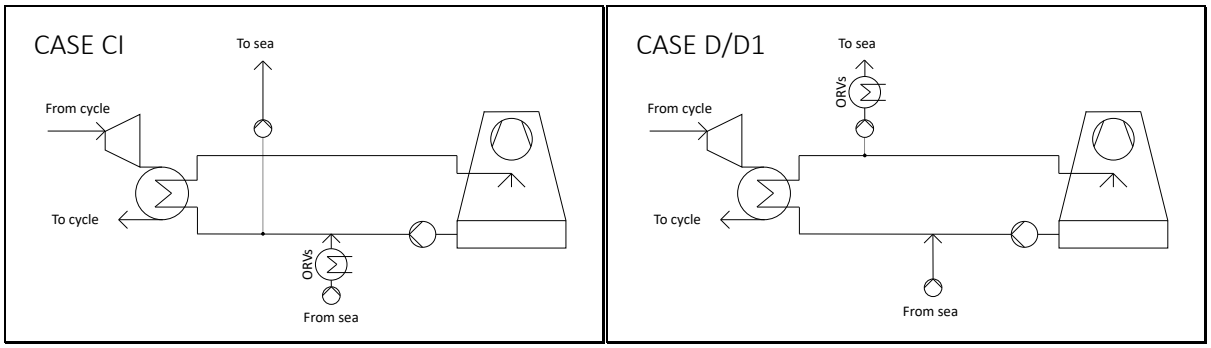

e) Case CI f) Case D/D1

Figure 3.12 Different locations for inlet and outlet streams and the ORV placement.

Table 3.4 Inlet and outlet pipes and ORV placement.

Case	Seawater intake	Seawater release	ORV location
A	Before CT	After condenser	Release
B	After condenser	After CT	Release
BI	After CT	Before Condenser	Release
C	Before Condenser	After CT	Intake
CI	After CT	Before Condenser	Intake
D	After CT	After Condenser	Release

For calculating the power output, only the steam turbine and the cooling circuit will be considered, to simplify calculations. Although this prevents obtaining the total power output and economic benefit due to the disregard of the rest of cycle equipment, the differential power output and cost can be easily calculated and compared, allowing to select the best configuration for ORVs.

3.2.2.- Introduction of air chillers.

To evaluate the feasibility of introducing a chiller in the cycle, two different combined cycles with two (2LP) and three (3LP) pressure levels were considered. The three-pressure cycle, depicted in Figure 3.13, consists of a 329 MW gas turbine, the SGT5-4000F, and a general 3-stage vapor turbine provided by the software. The two-pressure

cycle, shown in Figure 3.14, consists of a 62.5 MW gas turbine, the SGT-800-62, and a general 2-stage vapor turbine.

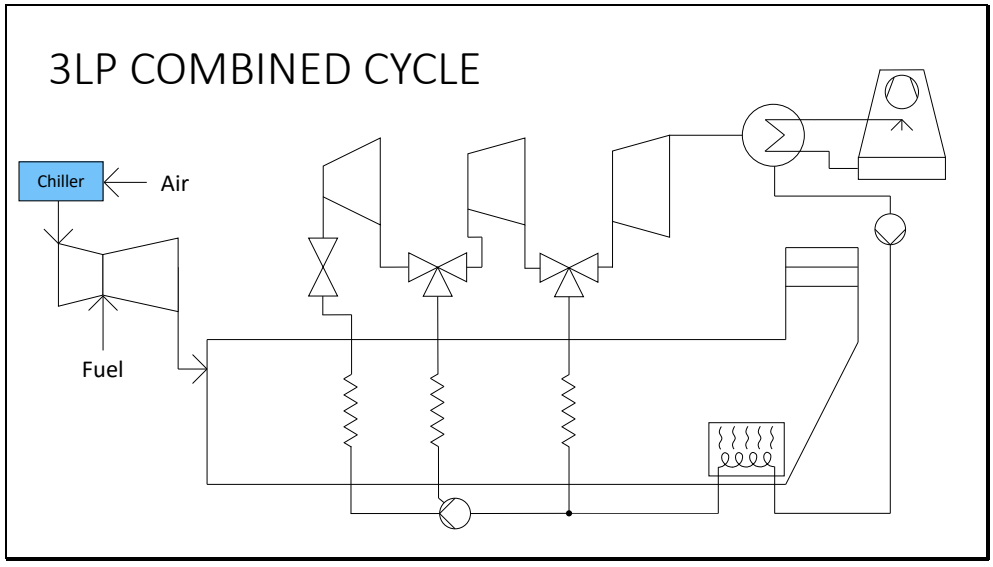

Figure 3.13 3LP combined cycle with the location of a possible chiller.

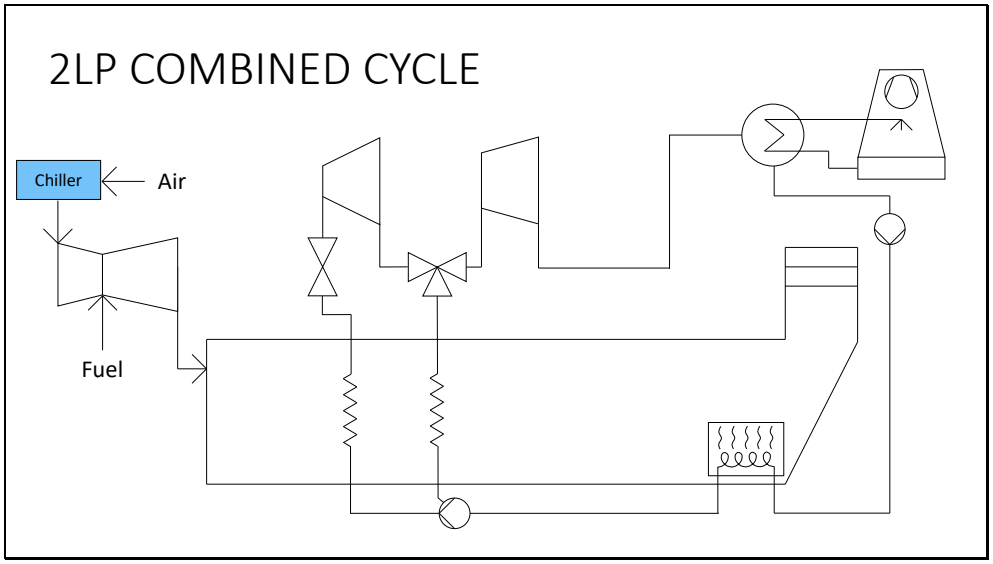

Figure 3.14 2LP combined cycle with the location of a possible chiller.

As usual operation of the plant is in the combined cycle configuration, the simple cycle configuration will use the same chiller equipment designed for the combined cycle. The

chillers are designed to decrease compressor air inlet temperature down to 10ºC. A lower value may cause ice generation at the first compressor stages, and, as pressure increases, it can cause permanent damage.

For both cycles, two distinctive operation modes (simple, with only the gas turbine; and combined, with both turbines) and design ambient conditions were studied:

- Scenario 1: Combined cycle at 15ºC ambient temperature and 100% relative humidity (RH)
- Scenario 2: Combined cycle at 30ºC and 60% RH
- Scenario 3: Simple cycle at 15ºC and 100% RH
- Scenario 4: Simple cycle at 30ºC and 60% RH

With the purpose of allowing the comparison between scenarios, both cycles have been calculated for ISO ambient relative humidity, 60% [26]. Therefore, scenarios 1 and 3 at 60% relative humidity and 20ºC ambient temperature are considered equivalent to the design conditions, as the same cooling power is required. Results for the design conditions of the first scenario are available in Annex B. Hence, scenarios 1 and 3 consider a smaller chiller able to decrease ambient temperature from 20ºC to 10ºC at 60% RH. On the other hand, the second and fourth scenarios consider a larger chiller able to decrease ambient temperature from 30ºC to 10ºC. As a result, it is possible to detect if there is an increased benefit of increasing the chiller size, due to economies of scale and the additional cooling for warmer conditions. Table 3.5 collects the chiller design conditions.

Table 3.5 Chiller design conditions.

Size	Cycle	Scenarios	Design Temperature	Design RH	Chiller type
Small	2LP	1, 3	15ºC	100%*	Electric, absorption and none.
	3LP				
Large	2LP	2, 4	30ºC	60%	
	3LP				

* Simulations were performed at 60%, following ISO standard, to allow the comparison between the chiller sizes.

As the influence of the chiller affects the whole combined cycle, the entire cycle was simulated to evaluate all variations. Three chiller types were considered for each cycle and scenario:

- Electric chiller
- Absorption chiller
- No chiller

Off-design simulations were performed for several ambient conditions, with the purpose of collecting data about the performance for a wide range of real operating conditions. For the sake of avoiding an excessive number of graphs while showing the most amount of valuable, some values were normalized. The raw values obtained are available in Annex B.

As the third and fourth scenarios correspond to the simple cycle simulations - using only the gas turbine -, they may not be a primary consideration for the design of the equipment. For the sake of brevity, these scenarios have also been included in Annex B.

3.2.3.- Hydrogen Blending.

To evaluate the effects of hydrogen blending, both combined cycles used for the previous analyses -2LP and 3LP- were simulated with blending. Differences in hydrogen and methane (representing natural gas) properties could complicate the design of the combined cycle components depending on the amount of hydrogen in the mix. These differences are explained in Annex C. A significant difference is the use of a Selective Catalytic Reductor which lowers the nitrous oxide emissions (NO_x), at the cost of the price for the equipment and a pressure drop.

As the goal set by Siemens - the turbine manufacturer - is to develop gas turbines until they can handle up to 100% hydrogen, in the Thermoflex simulations, the percentage in volume of hydrogen has been simulated from 0% (no blending at all) up to 100% (only hydrogen as fuel).

3.3.-Economics & Environmental analysis.

To study the profitability of a project, the Net Present Value (NPV) was used considering a 20-year timeframe. As operating expenses are considered in Thermoflex with the 'PEACE' addon, it is straight-forward to calculate the NPV with the cost of fuel and electricity.

The formula for the NPV for a constant annual benefit is: [27]

$$NPV = B \cdot \frac{1-(1+r)^{-n}}{r} - I \tag{3.6}$$

Where:

- B is the annual benefit or loss.
- r is the annual interest rate, approximately 3%.

- n is the number of years of operation.
- I is the initial investment that must be made to build the plant.

In the first strategy studied, the ORVs, only the steam turbine and the cooling cycle were considered for calculating power generation, and only the cooling circuit cost was considered. This means that the calculated profits cannot be considered as absolute, but will only serve as a basis to calculate differential prices between alternatives and select the most profitable one. The add-on 'PEACE' from Thermoflex provides all equipment costs except for the ORVs. Therefore, ORV cost was calculated from the value of 5.5 MUSD, information provided by the manufacturer for the studied case CI. To make an estimation for different ORV sizes, it was assumed that the cost was proportional to the required contact surface, with the surface being proportional to the LMTD, as the geometrical shape is similar, and the heat rate is the same for all different cases.

For the second and third strategies, the introduction of a chiller and blending, the cost and earnings of the whole cycle were analyzed.

For Dominican Republic, the price of acquisition of electricity for producing facilities is 108 USD/MWh [28]. The price of the natural gas used in the power plant is 4USD/GJ. For the estimation of hydrogen prices, there is a high uncertainty, as no local production is available. An Italian company, EN.IT, is planning to build a 350 MW green hydrogen plant that could reach a Levelized Cost of Hydrogen (LCOH) between 12 and 4.35 USD/kg [29]. The Hydrogen Insights Report estimated a green hydrogen production cost of 2.3 USD/kg for 2030 and lower than 2 USD/kg for 2050, perhaps too optimistic expectations[29], [30].The actual price of hydrogen depends on its electricity source, as acquiring energy for the grid is neither competitive nor sustainable. Currently, the best alternative is using energy from wind farms, which give a LCOH of around 6 USD/kg[31]. This was the value selected to check profitability. With that price and

considering gas properties, the price per heating value of the fuel was obtained as a function of the amount of hydrogen in the blend, as shown in Figure 3.15.

A cost estimation analysis was performed using the simulation results to assess the feasibility of blending. The determination of this estimate proved to be challenging as even a slight variation in the price of hydrogen, natural gas, or electricity had the potential to yield substantial effects on the net present value (NPV) of the plant. The result is subject to price fluctuations, but the general trend is clearly visible in Figure 3.15: at current prices, hydrogen has a price per unit power higher than methane - around 15 times higher for the estimated prices -.

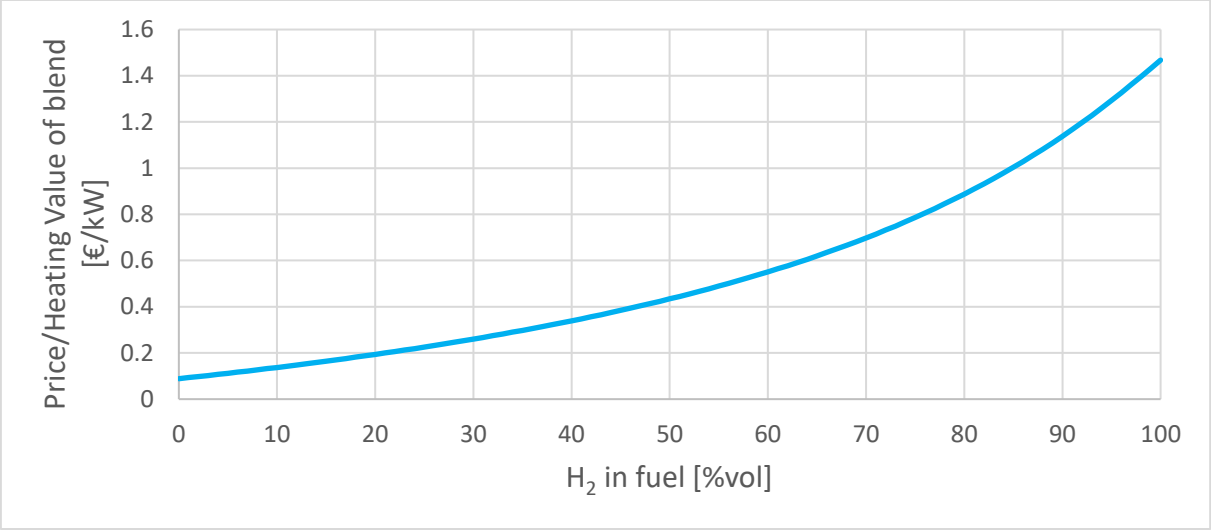

Figure 3.15 Price of fuel blend for the same heating value.

In order to obtain the yearly operation conditions of the cycle and calculate the NPV, the average hourly temperature data for each month has been obtained from Weather Spark for the Dominican Republic [32]. The relative frequency of each temperature was calculated dividing the absolute frequency by the total amount of values taken, 288 (24 hours times 12 months). The results of relative frequencies of temperatures are depicted in Figure 3.16.

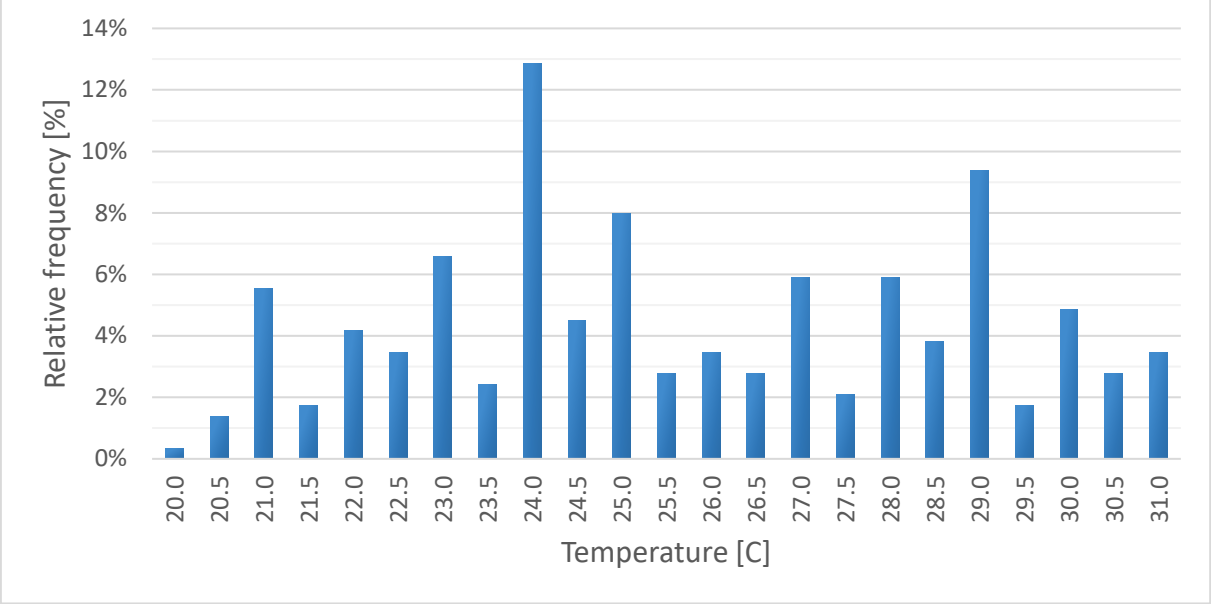

Figure 3.16 Relative frequency of average hourly temperature in Dominican Republic.

For humidity conditions, an average of 90% has been estimated, with the performance values interpolated between the 60% and 100% scenarios.

Finally, the NPV of each alternative was calculated by multiplying values by their relative frequency and adding them up or subtracting them from the total earnings depending on their sign.

In blending operation, using hydrogen has two additional benefits: it reduces carbon emissions, lowering the environmental impact of the power plant and resulting in less carbon emission taxes. To estimate the extent of these positive impacts, the Hydrogen Decarbonization Calculator from Siemens Energy has been used [33]. Dominican Republic currently has no tax for carbon emissions, but as the communities become more aware of climate problems, a carbon tax could be implemented in the near future [34].

4. Results.

4.1.-ORVs.

With the known low-pressure scenario temperatures, an LMTD value of 6.579 was obtained at the cycle condenser, resulting in an inlet temperature of the cooling circuit side of 30.43ºC. If the change in the heat rate was considered (278,913 kW to 279,133 kW from the low-pressure to the high-pressure case), the LMTD obtained for the high-pressure would be 6.584ºC and the inlet temperature of the cooling circuit side would be 30.41ºC, a negligible difference with the previous value.

After performing Thermoflex simulations, cases A, C and D resulted in an output temperature higher than the maximum allowable one, 31.5ºC. Even though their results are displayed, they cannot be implemented due to regulations and environmental concerns.

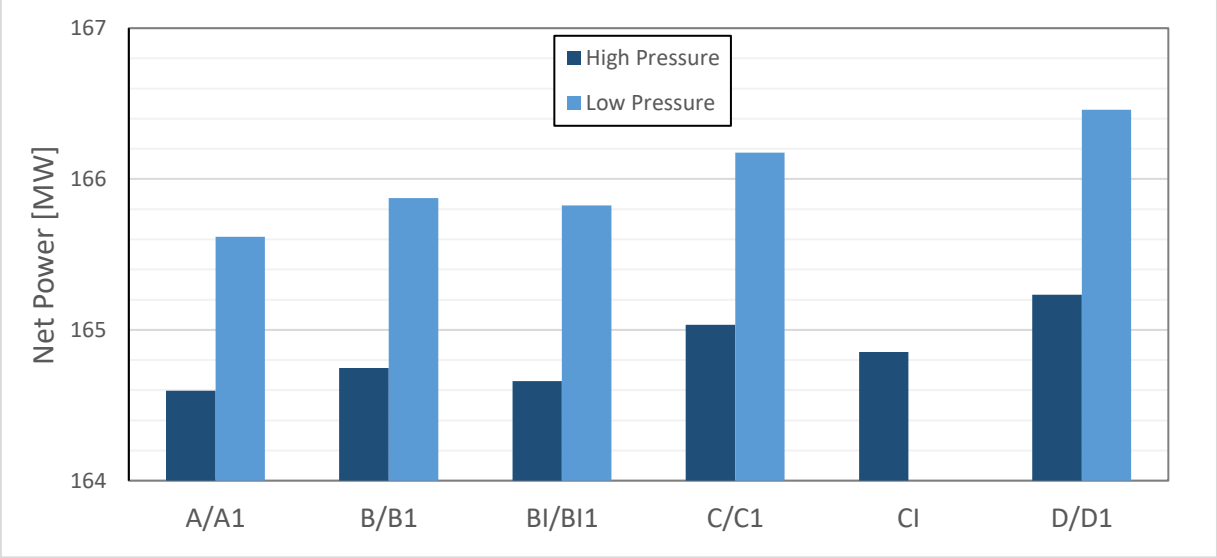

Figure 4.1 Net power generated for all cases.

Figure 4.1 shows the net power generated for all studied cases. All low-pressure cases are able to give more power than high-pressure cases. The highest output power for high-pressure and low-pressure cases are D and D1, respectively.

ORV price is inversely proportional to the LMTD, as previously defined. Using inlet and outlet gas and water temperatures, the values for the LMTD shown in Figure 4.2 are obtained.

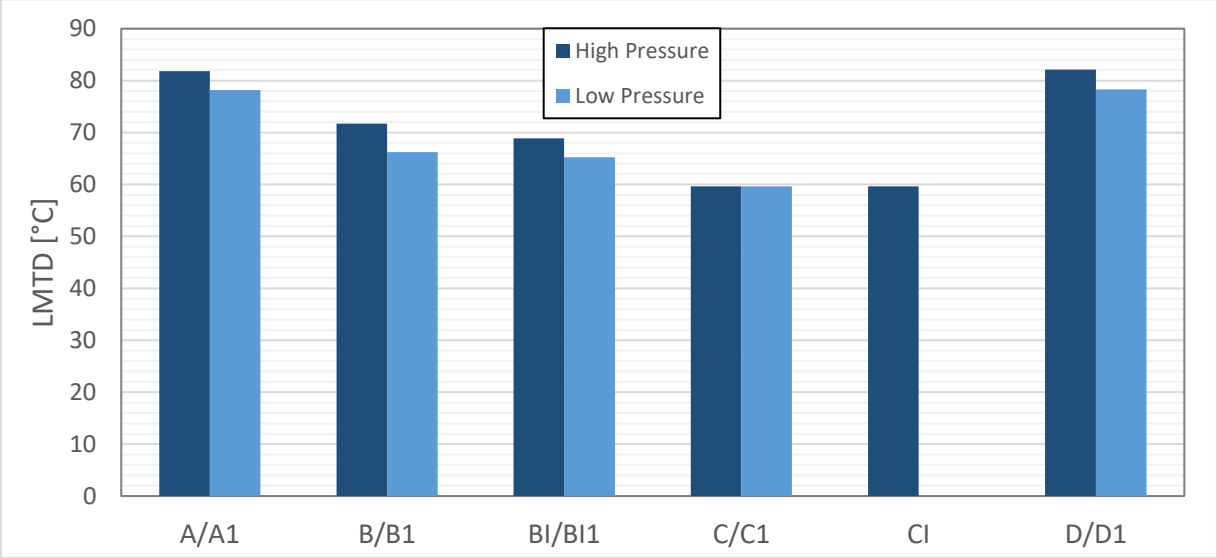

Figure 4.2 LMTD of ORVs for all cases - The higher the better.

The LMTD is higher in the scenarios where the ORVs are placed in the outlet of the high-temperature side (cases A/A1 and D/D1) as higher sea water temperature improves the heat rate to the cold LNG.

If the equipment cost given by Thermoflex and the calculated cost of ORVs is added, the overall installation cost is obtained, as shown in Figure 4.3.

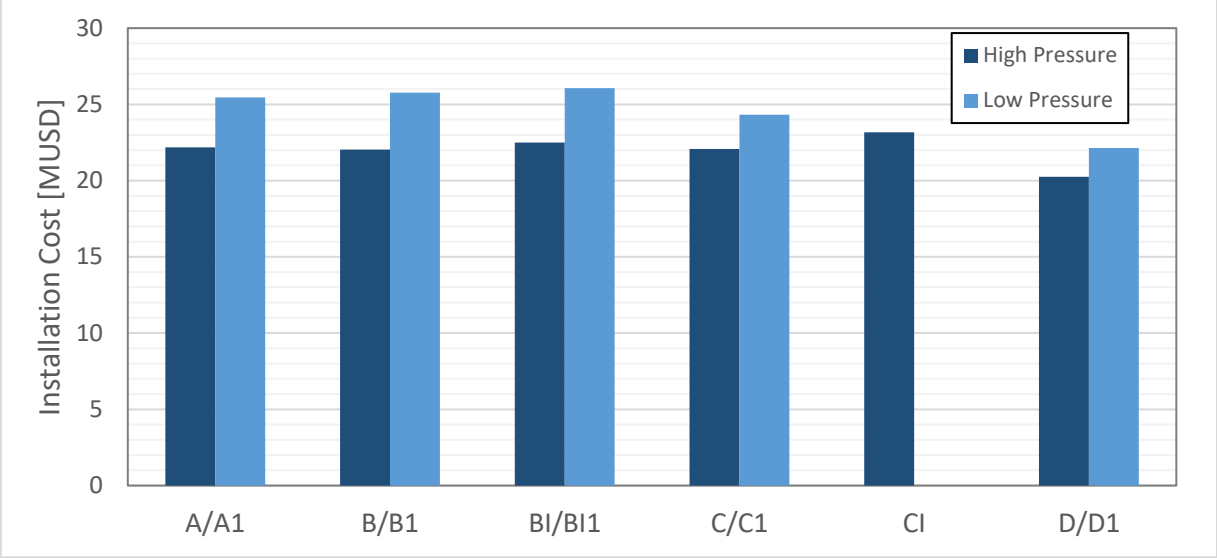

Figure 4.3 Total installation cost for each case, in MUSD.

With the installation cost and the cost of electricity in Dominican Republic, 108 USD/MWh, it was possible to compare all alternatives using the NPV within a timeframe of 20 years.

Table 4.1 Net profit for the different alternatives, considering an amortization time of 20 years.

High Pressure	Case A	Case B	Case BI	Case C	Case CI	Case D
Net Profit [MUSD]	2,074.3	2,075.3	2,078.6	2,084.1	2,086.2	2,091.8
Low Pressure Cases	A1	B1	BI1	C1	CI1	D1
Net Profit [MUSD]	2,077.1	2,079.6	2,084.1	2,086.4	-	2,098.0

Figure 4.4. shows the net differential profit of all alternatives with respect to the worst-case scenario, case A. The benefit of the other alternatives is clearly patent, as more power is produced and the net profit is higher.

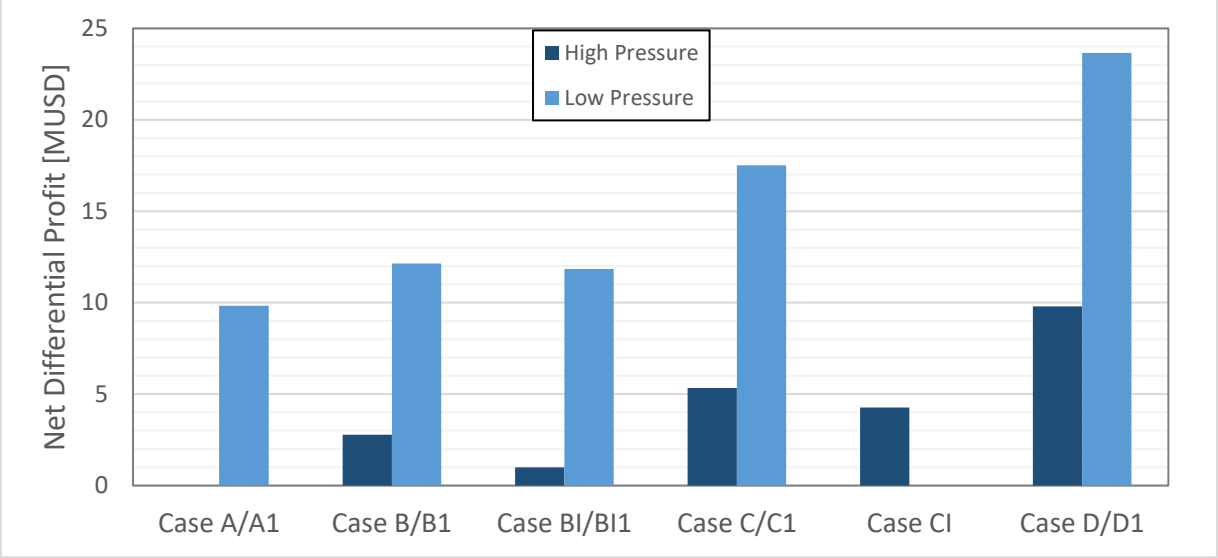

Figure 4.4 Net differential profit, taking case A as reference.

4.2.-Chillers.

Firstly, the results from the analysis of the cycles without a chiller are presented enable the examination of the system efficiency and energy consumption with and without the chiller and provide valuable insights for further optimization. The power and efficiency obtained without chillers are summarized in Table 4.2 for the corresponding levels of pressure (LP).

Table 4.2 Net power and efficiency for both cycles without chillers at ISO conditions.

Cycle simulated	Net Power Output	Net Electric Efficiency (LHV)
2LP, no chiller	84.5MW	55.87%
3LP, no chiller	464.5MW	57.87%

Please note that, for the sake of brevity, additional information for the studied scenarios is available in Annex B, to allow focusing in the most relevant results in the following subsections.

4.2.1.- First Scenario.

After running the simulations, values of the net power and compressor inlet temperature for the different chiller configurations, cycle pressure levels and ambient temperatures have been displayed in Figure 4.5 and Figure 4.6. Net power has been normalized with respect to the lowest value of the base cycle.

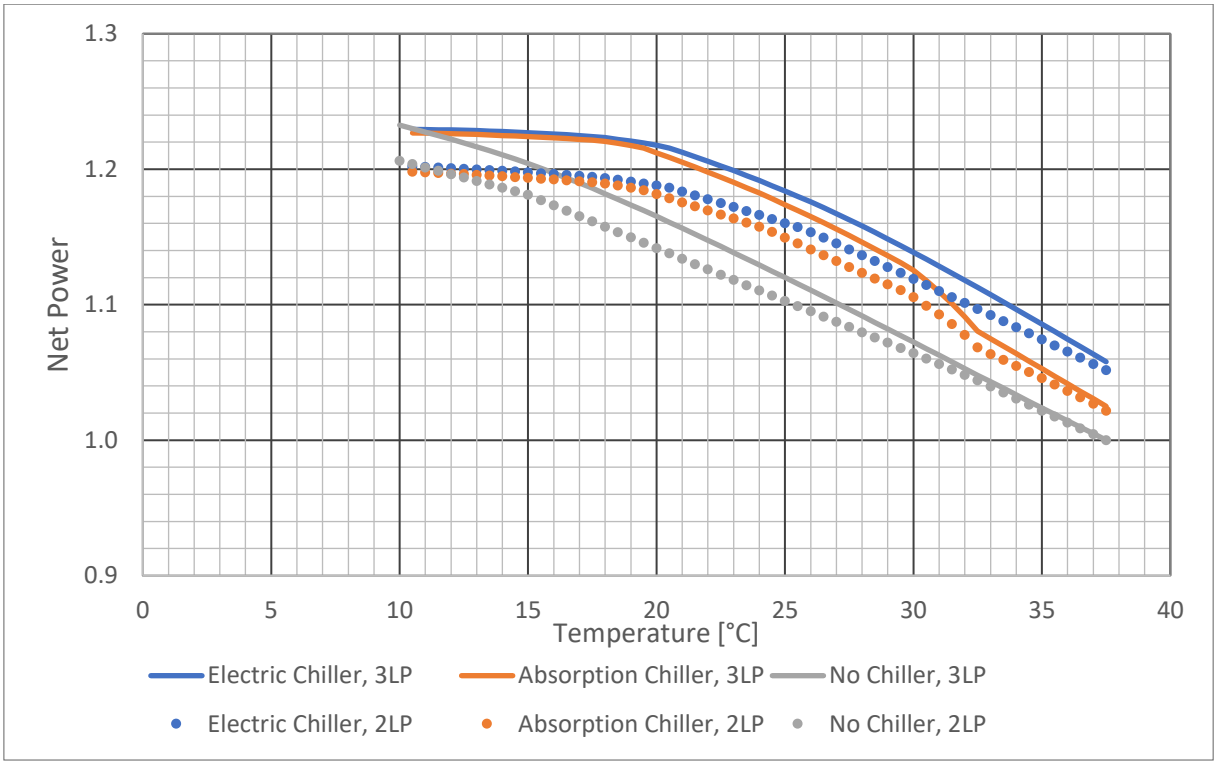

Figure 4.5 Normalized net power output for 60%RH.

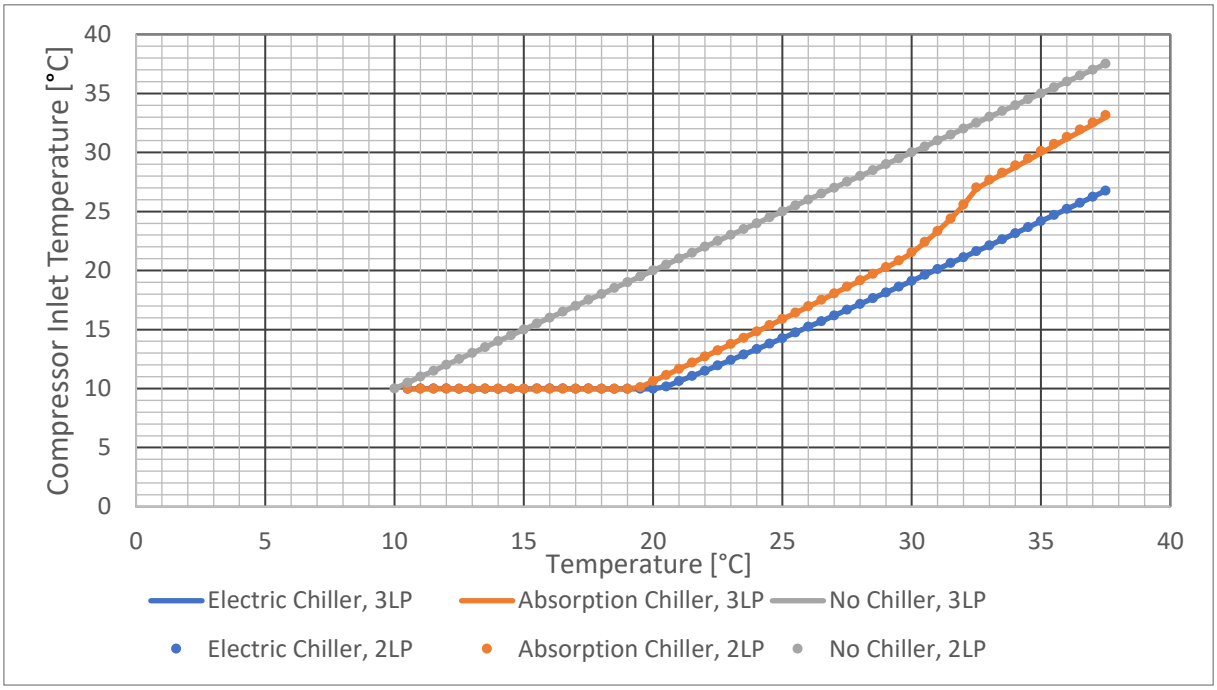

Figure 4.6 Compressor inlet temperature for 60%RH.

By looking at Figure 4.5 and Figure 4.6, it can be deduced that the decrease in power output of the cycles after 20 ºC is a consequence of the chiller reaching its maximum cooling capacity.

It can also be observed that, from 30ºC to 32.5ºC, there is a sudden drop in power output in the absorption chiller compared to the electric chiller. If the 2LP absorption chiller is analyzed, its performance is mostly stable, as shown in the following Energy Efficiency Ratio (EER) graph:

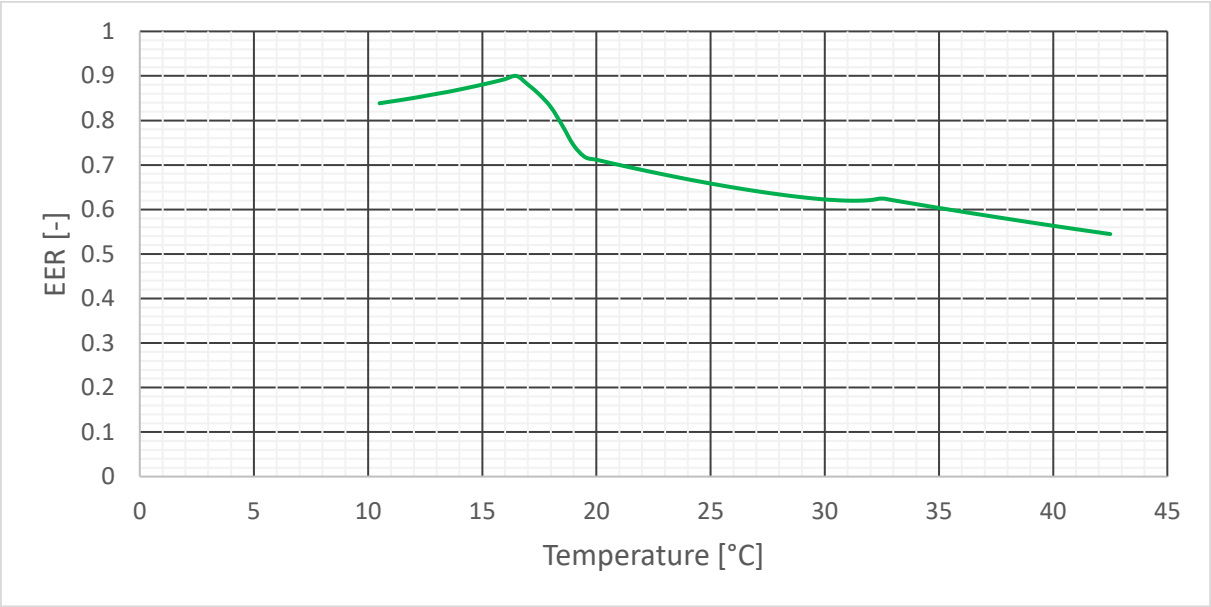

Figure 4.7 Energy Efficiency Ratio of the absorption chiller in the 2LP cycle.

Therefore, the effect of the change in ambient temperature at this temperature range cannot be the cause of the decrease in performance. However, a decrease in the steam input flow in that range of temperatures was found, indicating that the chiller is demanding less steam. Therefore, the chiller cooling circuit, in particular, the fin-fan cooler, was analyzed, being the LMTD the most relevant parameter, as there is no phase change of the fluids and conditions are not extreme, it should be a great indicator of heat transfer.

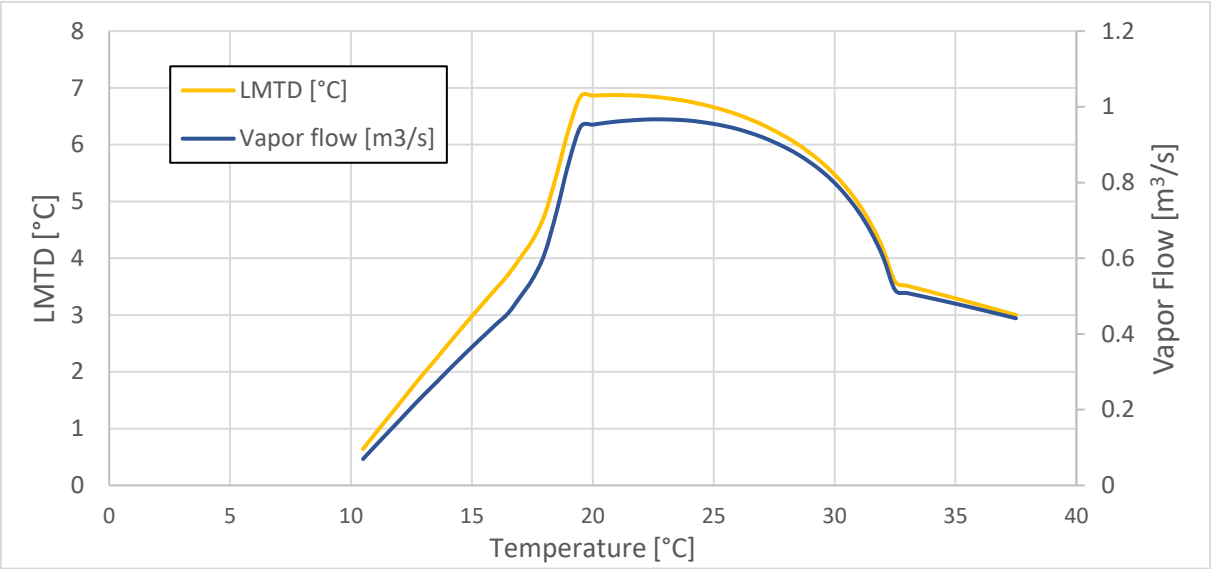

Figure 4.8 LMTD and vapor flow of the fin-fan cooler of the absorption cooler from 2LP cycle.

As seen in Figure 4.8, the LMTD has almost the same shape as the vapor flow, so it may be concluded that the fin-fan cooler is the chiller bottleneck, limiting its cooling capacity.

In Figure 4.9 the efficiency for the different types of chiller has been computed. It can be seen that the cycle efficiency with a chiller is lower, but its power output is larger.

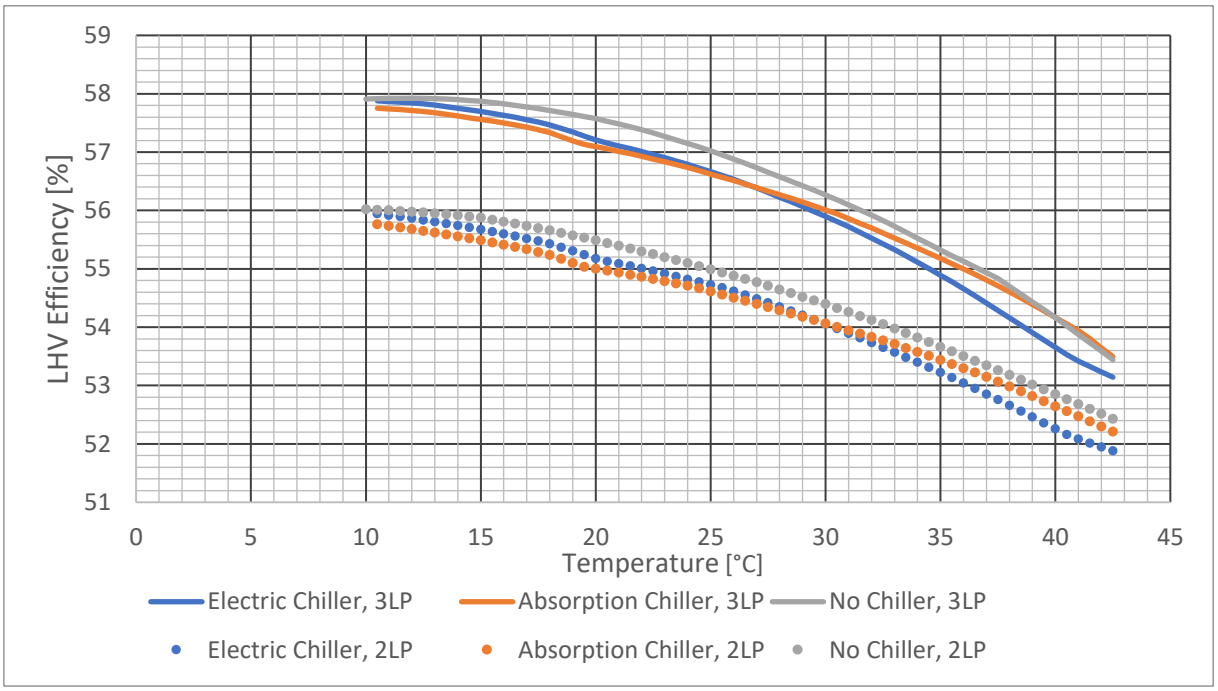

Figure 4.9 LHV efficiency for 60%RH.

Figure 4.10, Figure 4.11, Figure 4.12 and Figure 4.13 collect the results from the price estimates, including labor costs.

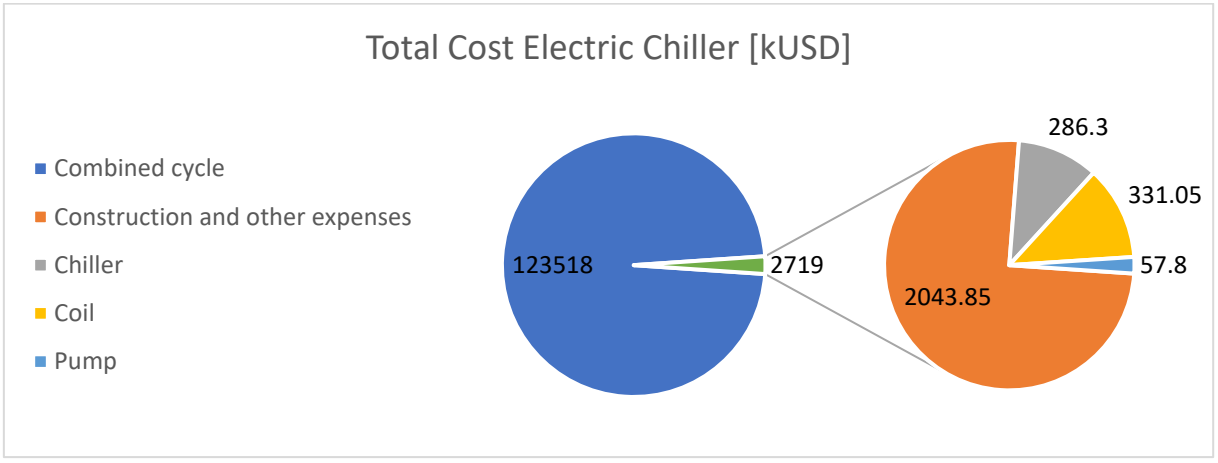

Figure 4.10 Total cost of 2LP combined cycle and electric chiller.

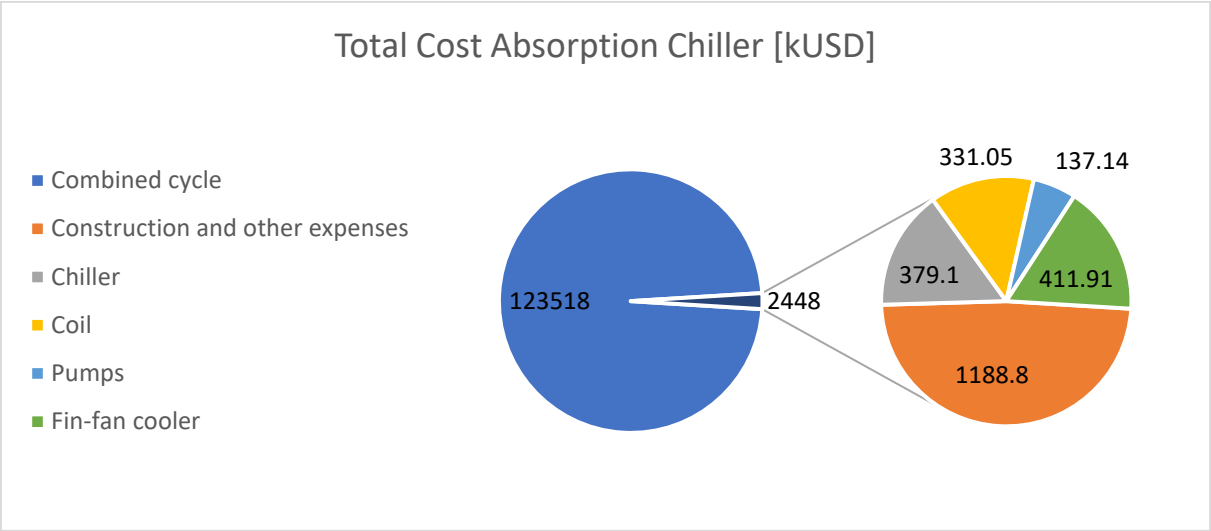

Figure 4.11 Total cost of 2LP combined cycle and absorption chiller.

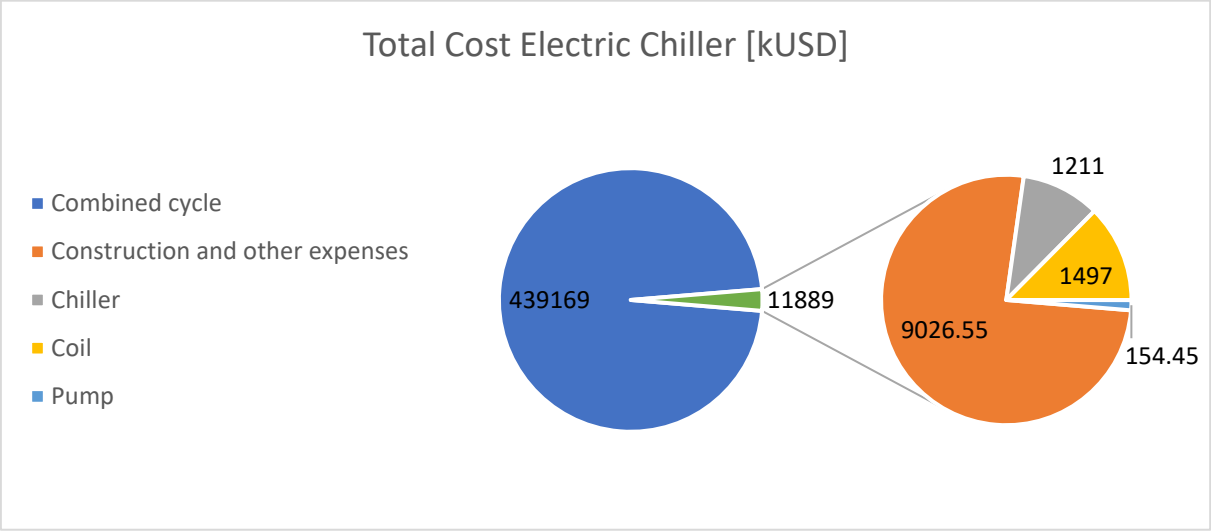

Figure 4.12 Total cost of 3LP combined cycle and electric chiller.

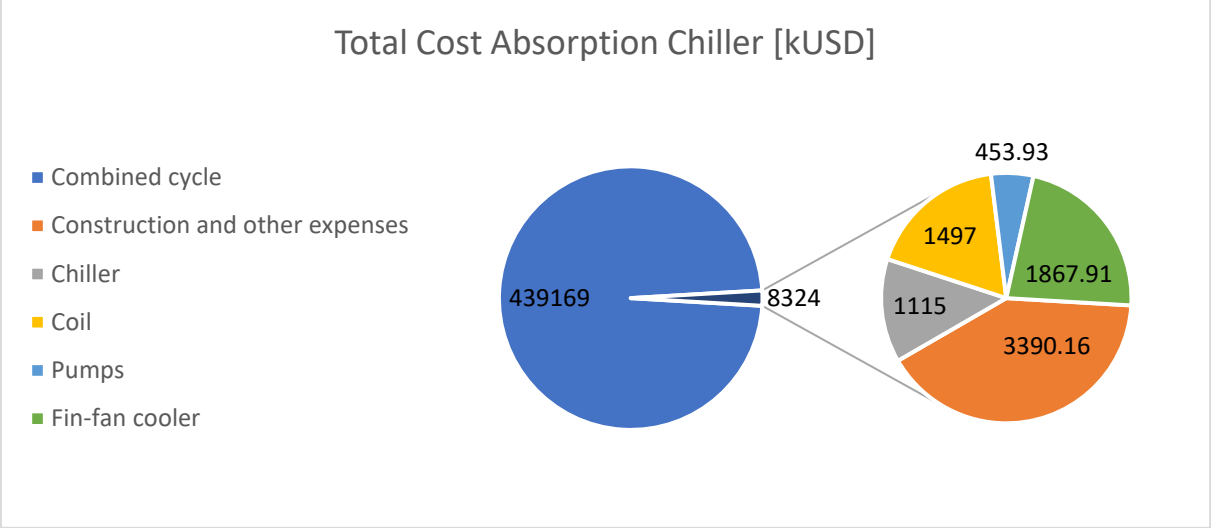

Figure 4.13 Total cost of 3LP combined cycle and absorption chiller.

This allowed to obtain an estimation of the cost per unit power for each alternative with respect to ambient temperature, depicted in Figure 4.14.

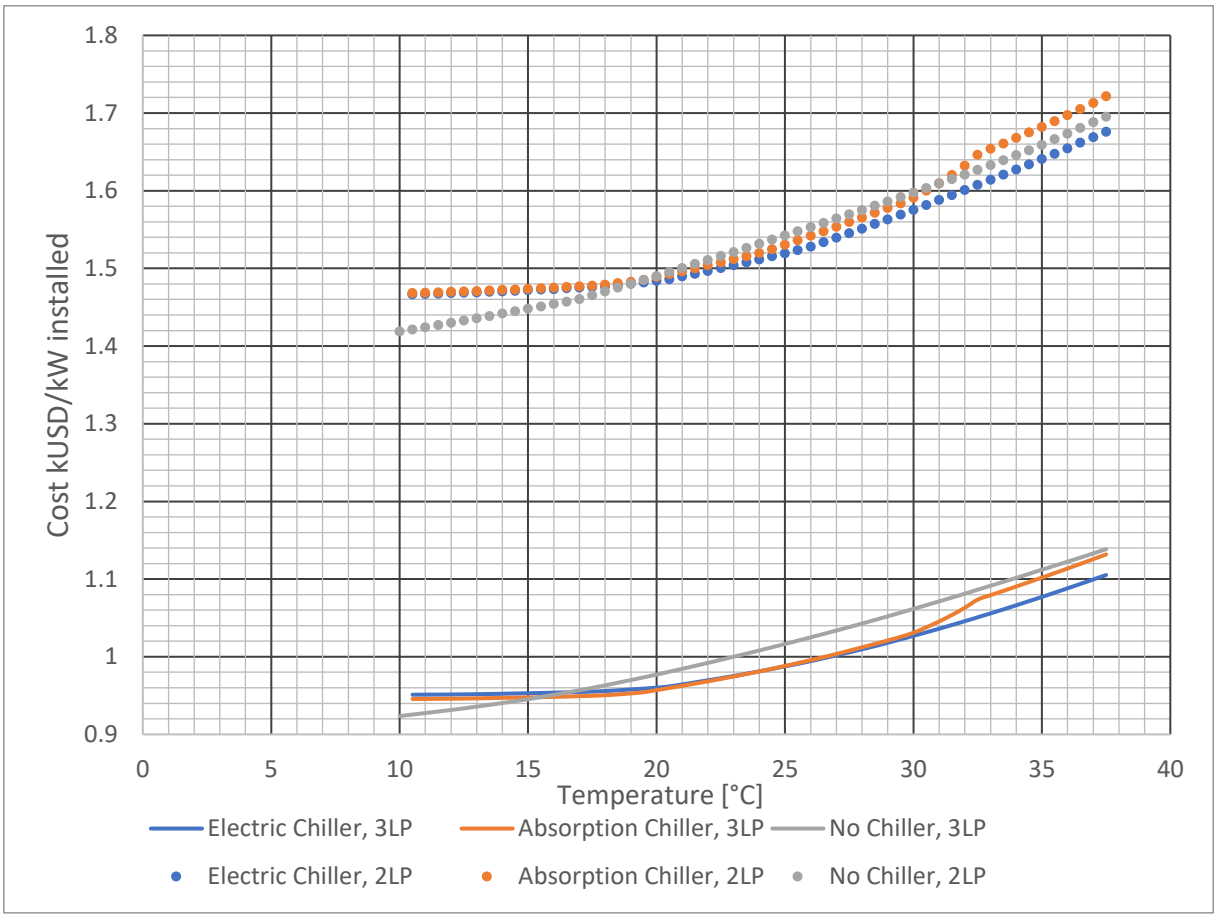

Figure 4.14 Cost of the installed power in the plant for 60%RH -the lower the better-.

As the 3LP cycle has a higher efficiency and associated cost decrease relative to the power generated, the cost per installed kW is also lower. At ambient temperatures higher than 16ºC and 18ºC, for the 3LP and 2LP cycles, the chillers can manage to reduce the cost per kW of the plant relative to the cycle with no chiller. Even though the cost per kW installed is lower, the decrease in generation efficiency could lower overall plant returns. For that reason, the NPV was calculated for 20 years of operation and is shown in the next scenario to be compared with its chiller.

4.2.2.- Second Scenario.

All the following graphs have been calculated for the relative humidity designed, 60%, and designed for an ambient temperature of 30ºC.

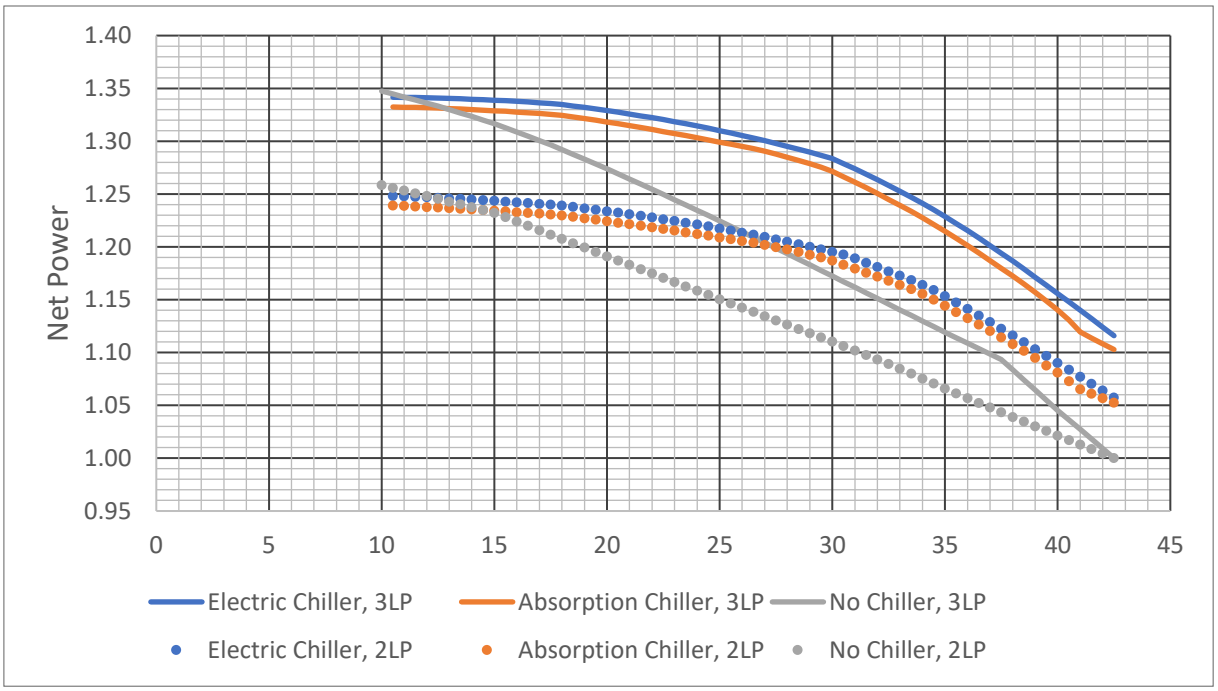

Figure 4.15 Normalized net power output for 60%RH.

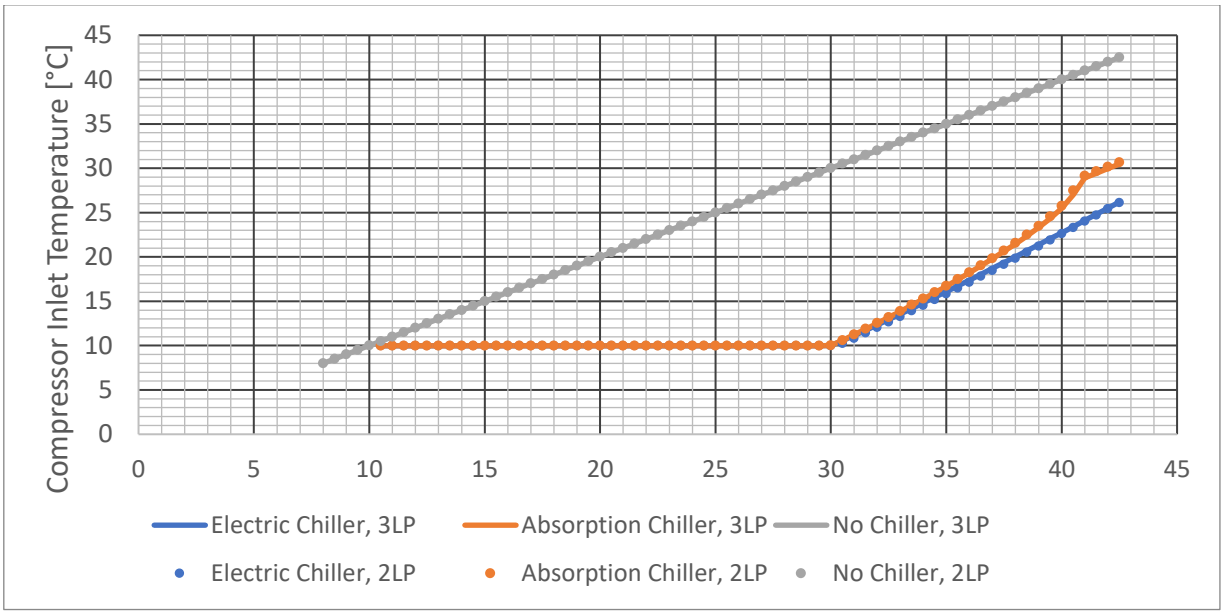

Figure 4.16 Compressor inlet temperature for 60%RH.

In Figure 4.16, looking at the electric chiller and no chiller slopes, it can be observed that the temperature drop the chiller generates is lower for higher values of ambient

temperature. This is mostly due to the decrease in the EER of the electric chiller - see Figure 4.17 - and partly due to the air specific heat (C_P), which increases with temperature as seen in the Figure 4.18 obtained from [35]. Therefore, with a constant heat transfer rate, a lower temperature drop is achieved for higher temperatures.

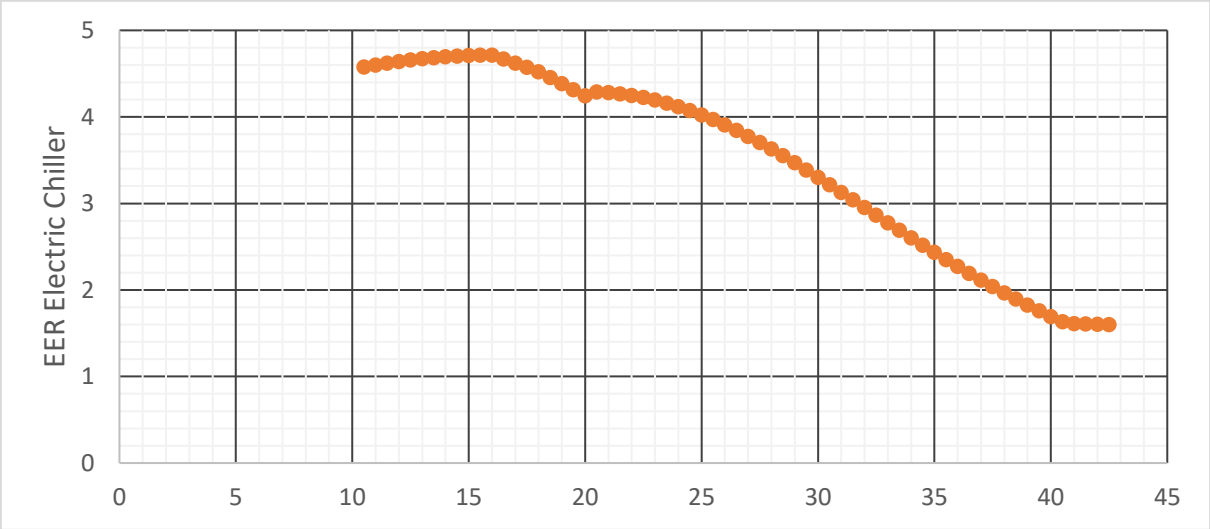

Figure 4.17 EER of the electric chiller for the 2LP cycle.

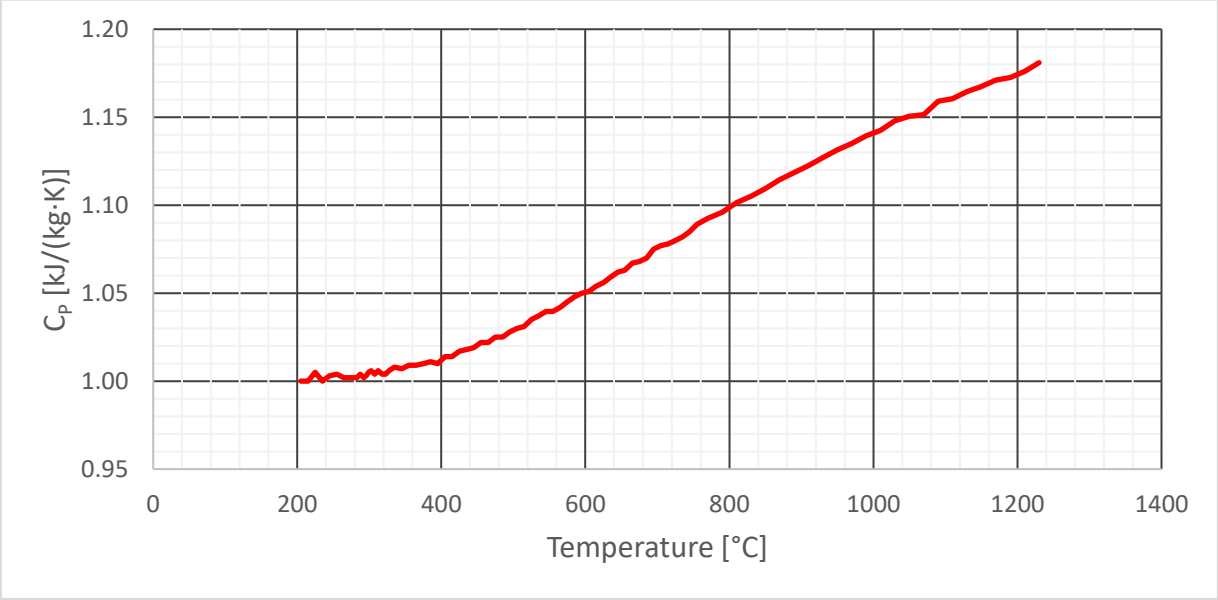

Figure 4.18 Increase in the calorific power of the air as a function of temperature [35].

Figure 4.19, Figure 4.20, Figure 4.21 and Figure 4.22 show the cost of the alternatives with an electric chiller.

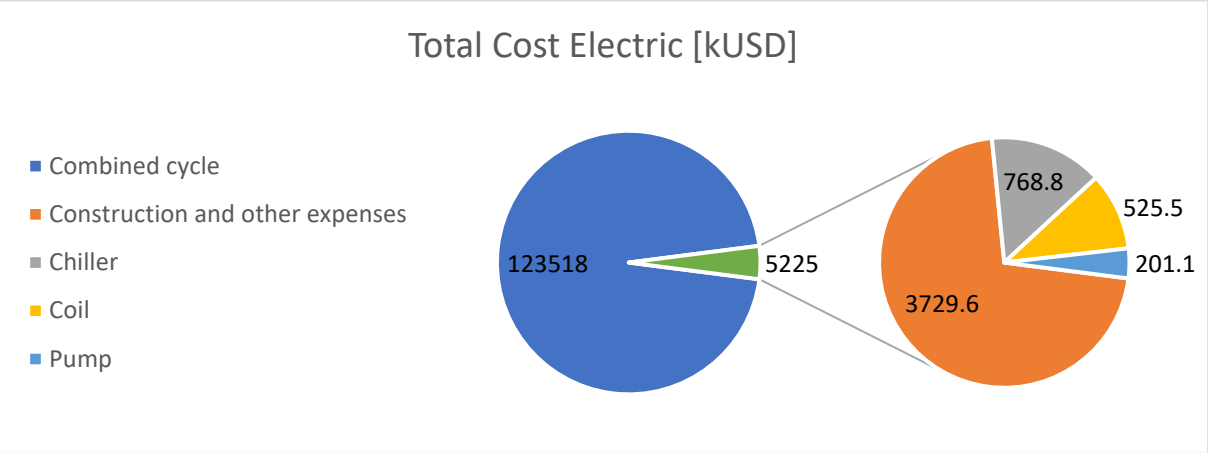

Figure 4.19 Total cost of 2LP combined cycle and electric chiller.

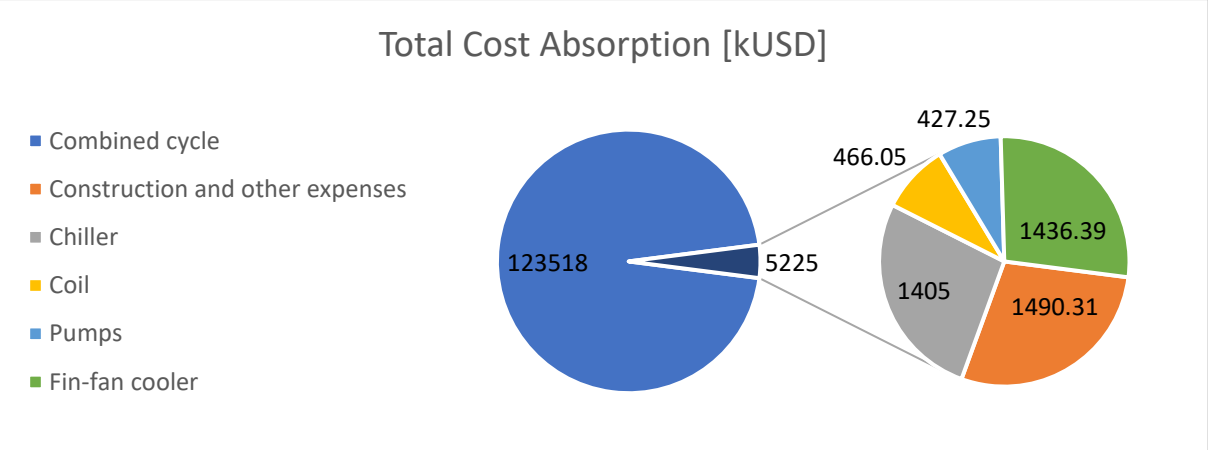

Figure 4.20 Total cost of 2LP combined cycle and absorption chiller.

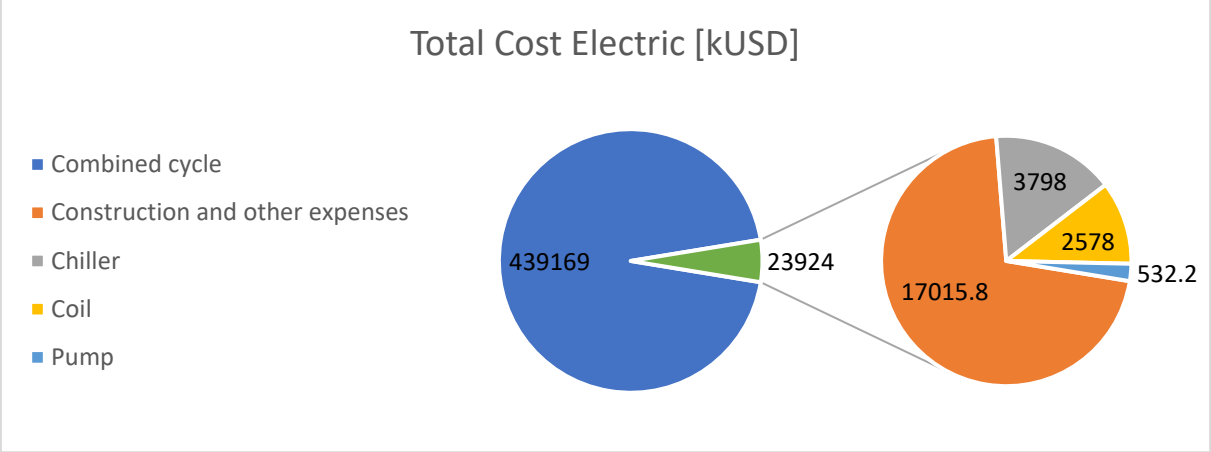

Figure 4.21 Total cost of 3LP combined cycle and electric chiller.

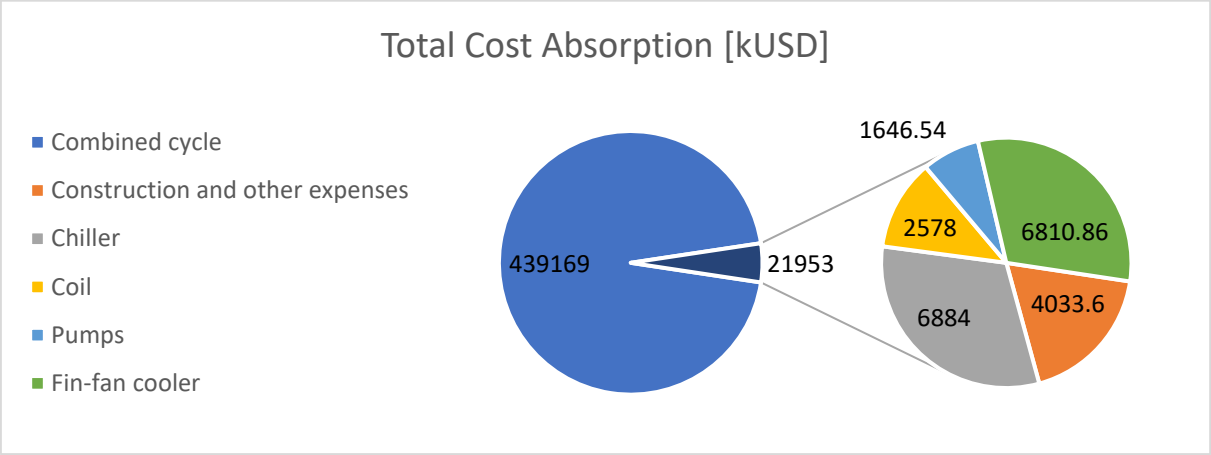

Figure 4.22 Total cost of 3LP combined cycle and absorption chiller.

The installation cost is higher than the previous chillers but the cost per net kW can be lower as their cooling capacity is higher.

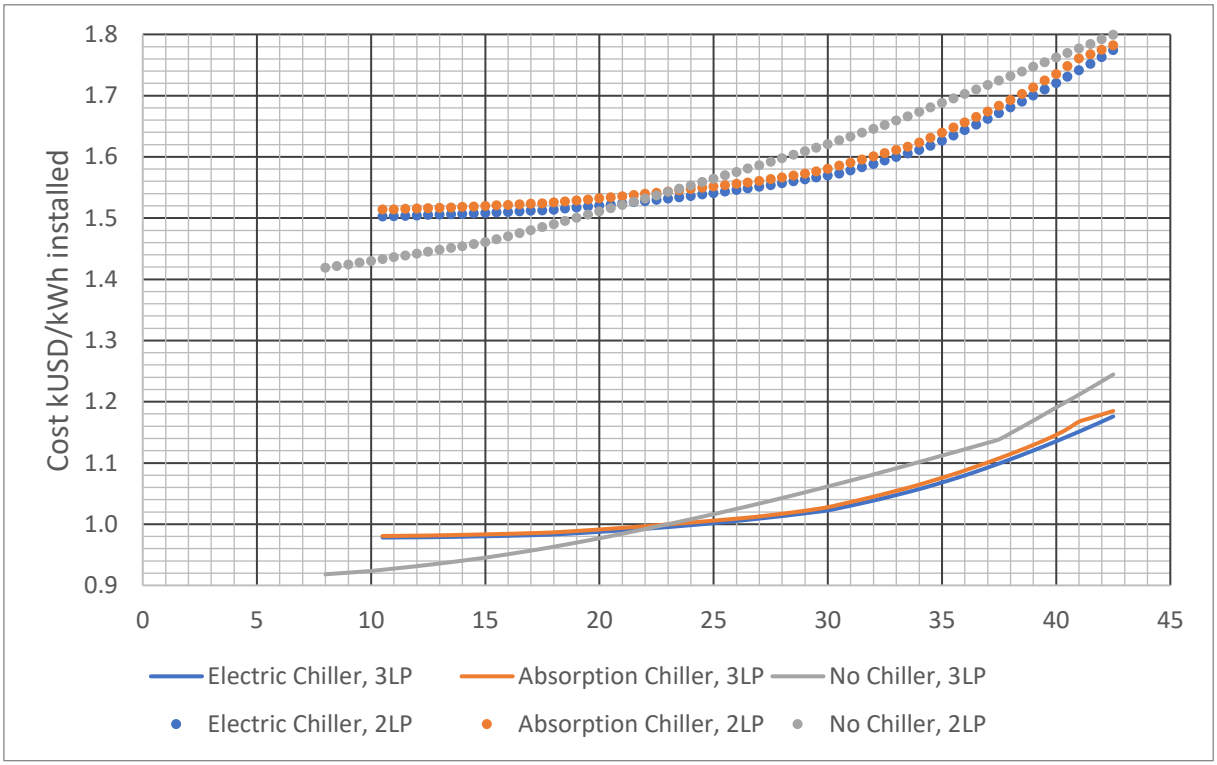

Figure 4.23 Cost of power generation capacity installed for the 3LP plant -The lower the better-.

Finally, the NPV of chiller implementation was obtained and compared with the values for the first scenario. From Figure 4.24 it can be deduced that chillers have a higher return when the temperature drop is higher, and a bigger design – the second scenario- performs better at higher temperatures while a smaller design is more suitable for temperatures up to 25ºC.

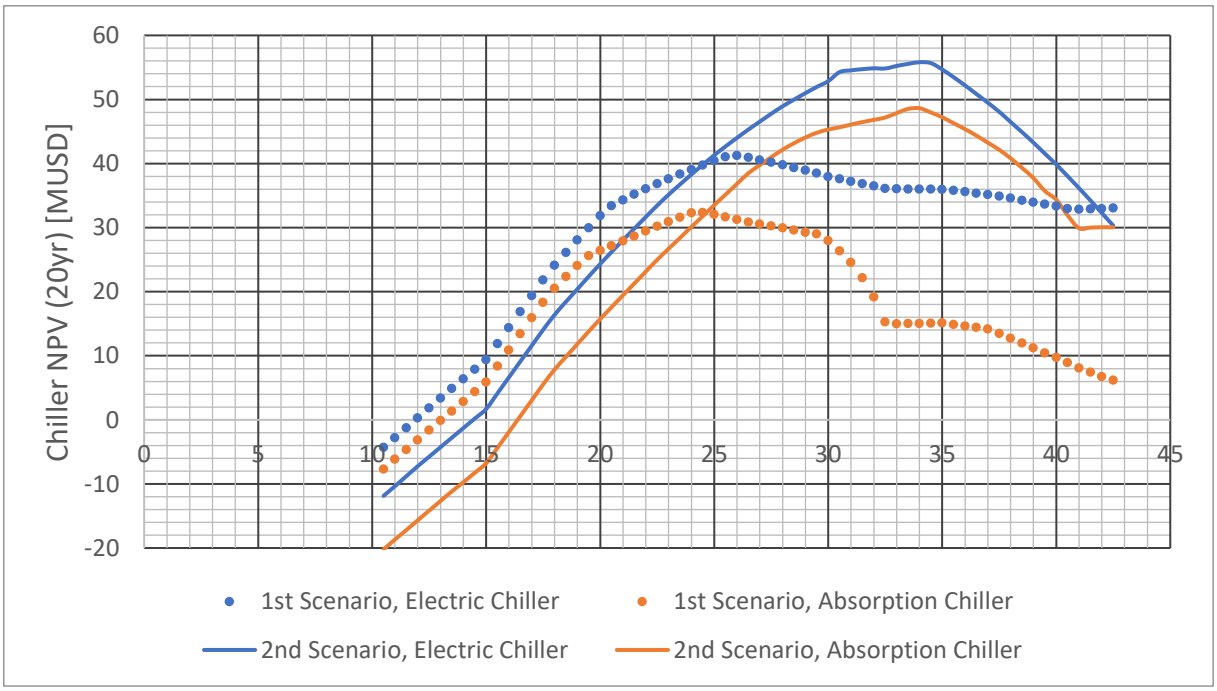

Figure 4.24 NPV of using electric and absorption chillers of two different sizes, with respect to the 2LP combined cycle operation with no chiller.

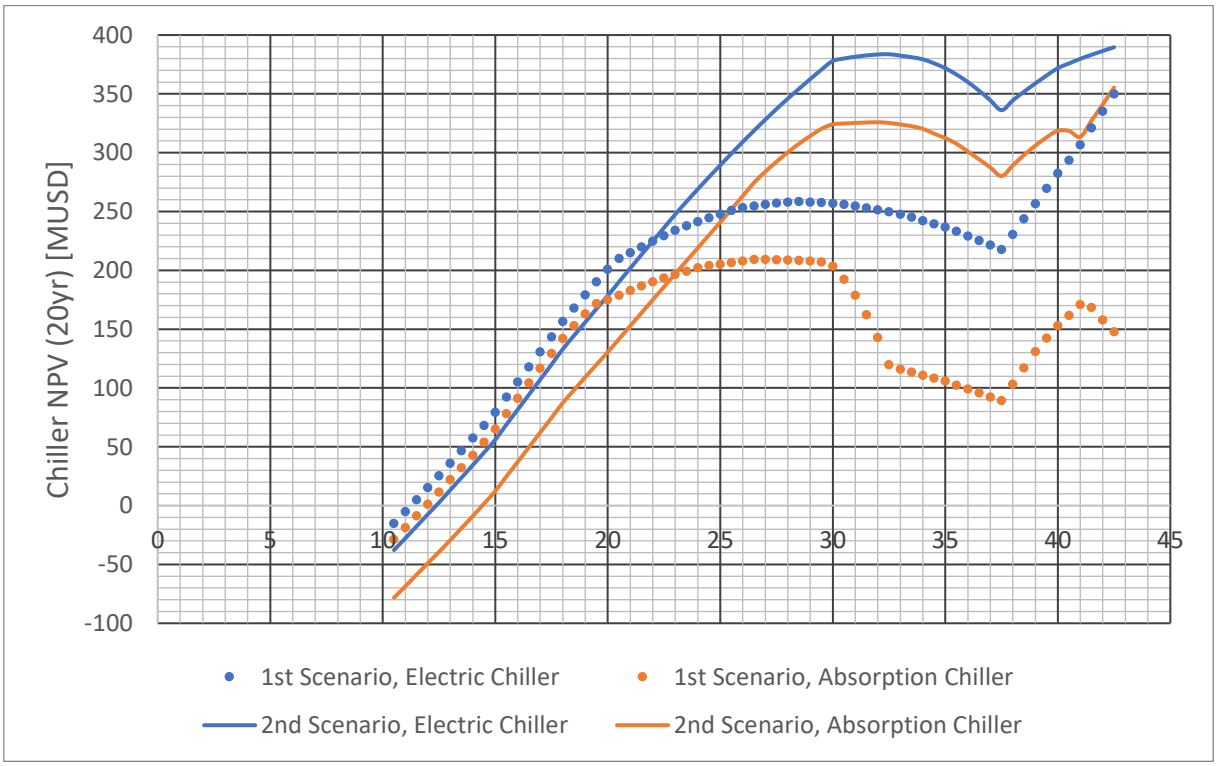

Figure 4.25 NPV of using electric and absorption chillers of two different sizes, with respect to the 3LP combined cycle operation with no chiller.

In the specific environment of Dominican Republic, if its ambient conditions across the Typical Meteorological Year (TMY) are used to calculate its production, Table 4.3 is obtained with the expected returns of each alternative considered.

Table 4.3 Shows for each type of chiller the NPV (20yr) [MUSD] compared to the operation with no chiller.

Chiller used		**2LP**		**3LP**	
		Combined cycle	**Simple Cycle**	**Combined cycle**	**Simple Cycle**
Electric	**Small**	13.97	12.00	105.95	50.26
	Large	28.11	22.64	160.79	92.19
Absorption	**Small**	6.75	7.64	63.11	28.08
	Large	21.10	22.71	115.99	74.76

4.3.-Blending.

Results considering blending of natural gas and hydrogen are presented in this section. For blending operation, the ambient temperature and relative humidity simulated were 25ºC and 90%, close to the ambient conditions of Dominican Republic.

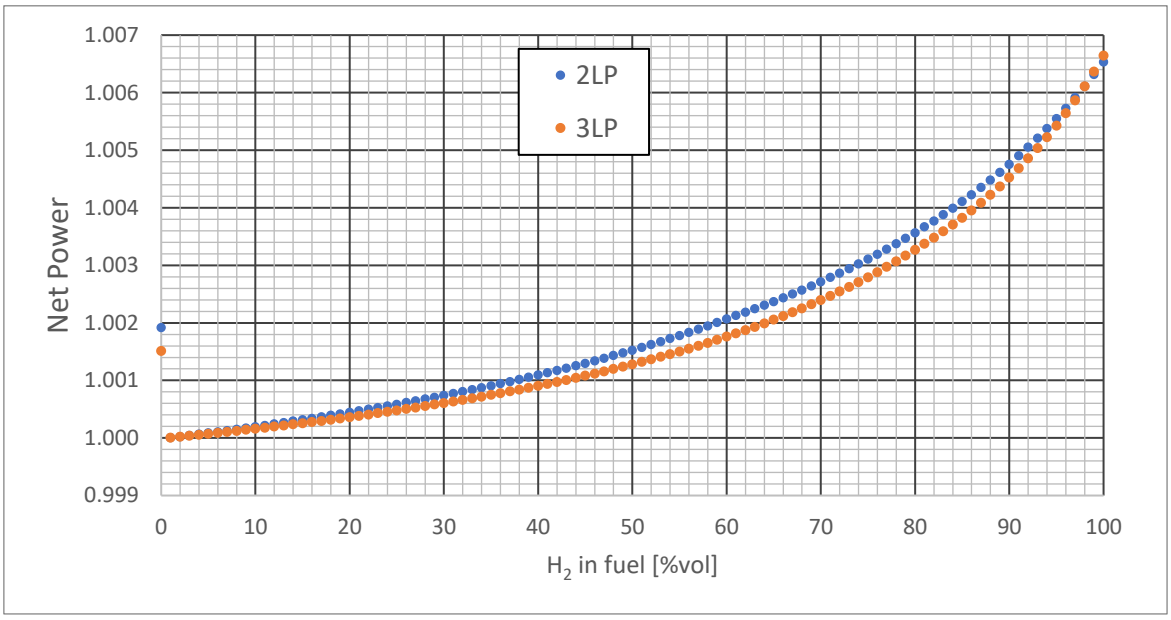

Figure 4.26 Normalized net power as a function of the hydrogen volume percent for both plants.

The power output difference for zero percent volume is due to the absence of a selective catalytic reductor (SCR), and is only considered if the plant was not designed for hydrogen, as it does not account for the pressure drop caused by the SCR. This indicates that around 55-60% of hydrogen is needed to justify the use of an SCR from the technical point of view.

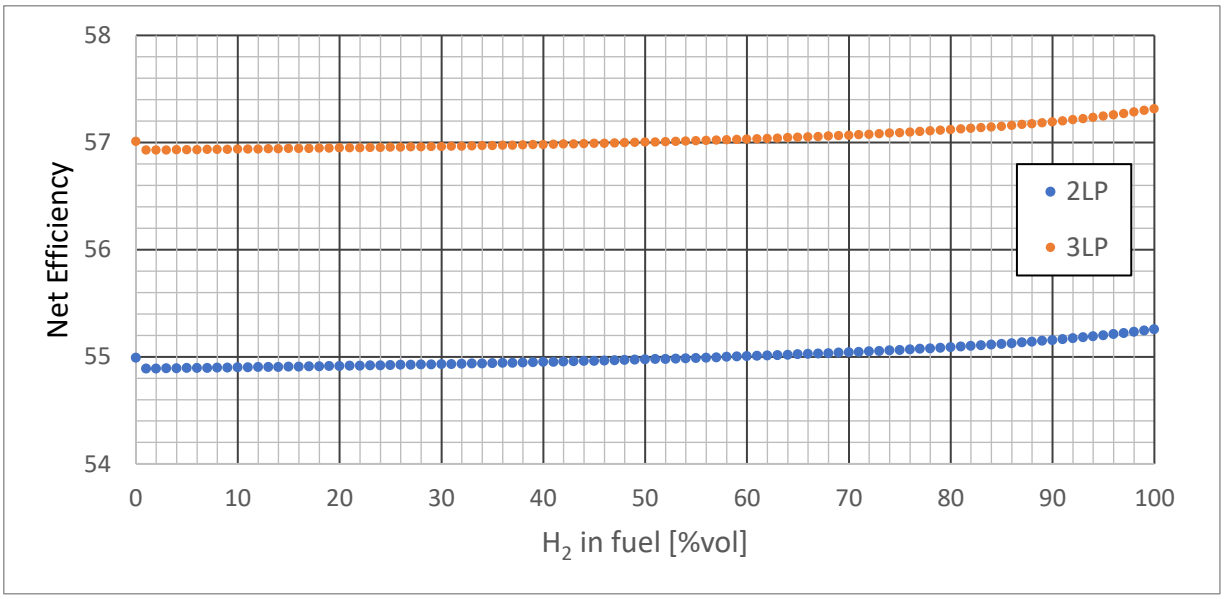

Figure 4.27 Net efficiency depending on the hydrogen volume percent for both plants.

The net power and efficiency increase as more hydrogen is included in the blend, due to the higher output temperatures achieved in the gas turbine. More information about this temperature rise is available in Annex B. Detailed results.

Nevertheless, when comparing the NPV of the different alternatives, blending does not seem so profitable, as shown in Figure 4.28 and Figure 4.29. For the current price of 6 USD/kg of hydrogen, blending is not very profitable for high percentage blends. However, a small percentage is feasible. In addition, that would not change drastically the cycle configuration as operation with low hydrogen percentage can be carried out with less modifications.

If we consider that hydrogen price will drop to 2USD/kg, the breakeven point is for 92% and 97% for 2LP and 3LP, respectively.

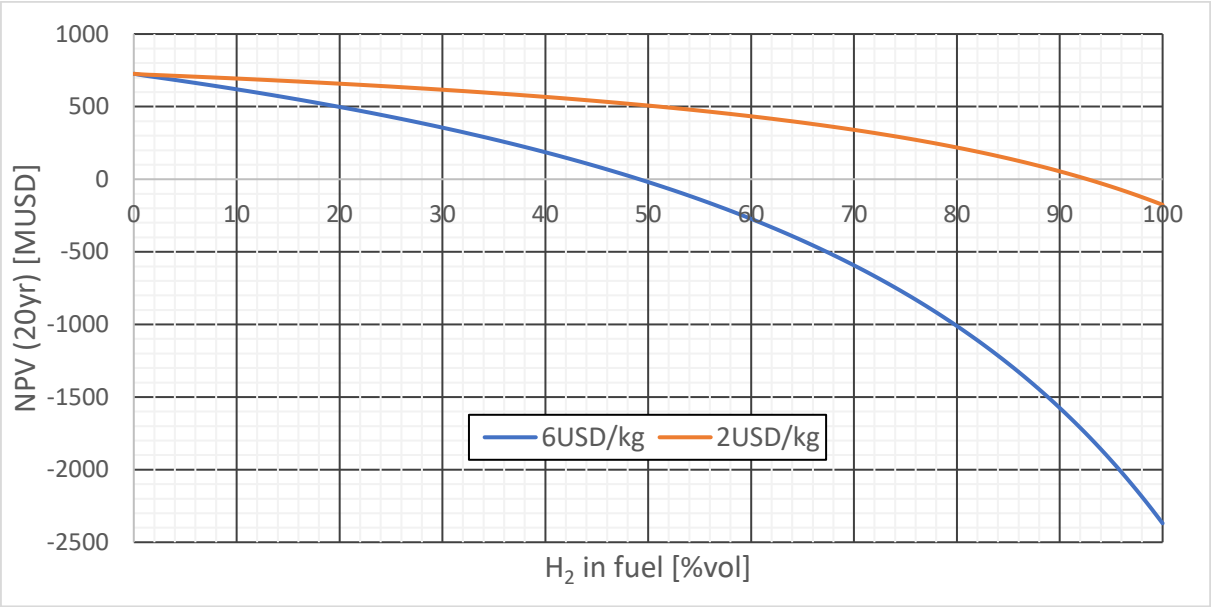

Figure 4.28 Profit expected when using hydrogen blending for the 2LP cycle.

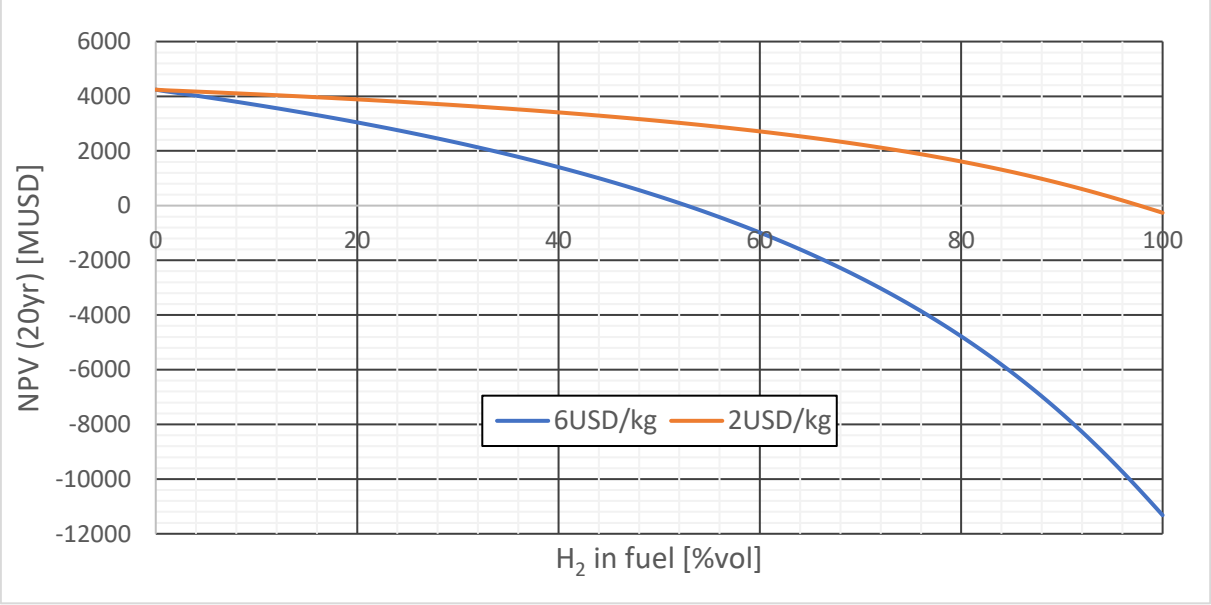

Figure 4.29 Profit expected when using hydrogen blending for the 3LP cycle.

If we plot the electricity price needed for breakeven as a function of hydrogen price, as in Figure 4.29, it may be observed that for delivering energy with the electricity price considered, 108 USD/MWh, hydrogen price would have to be 2 USD/kg or lower to break even.

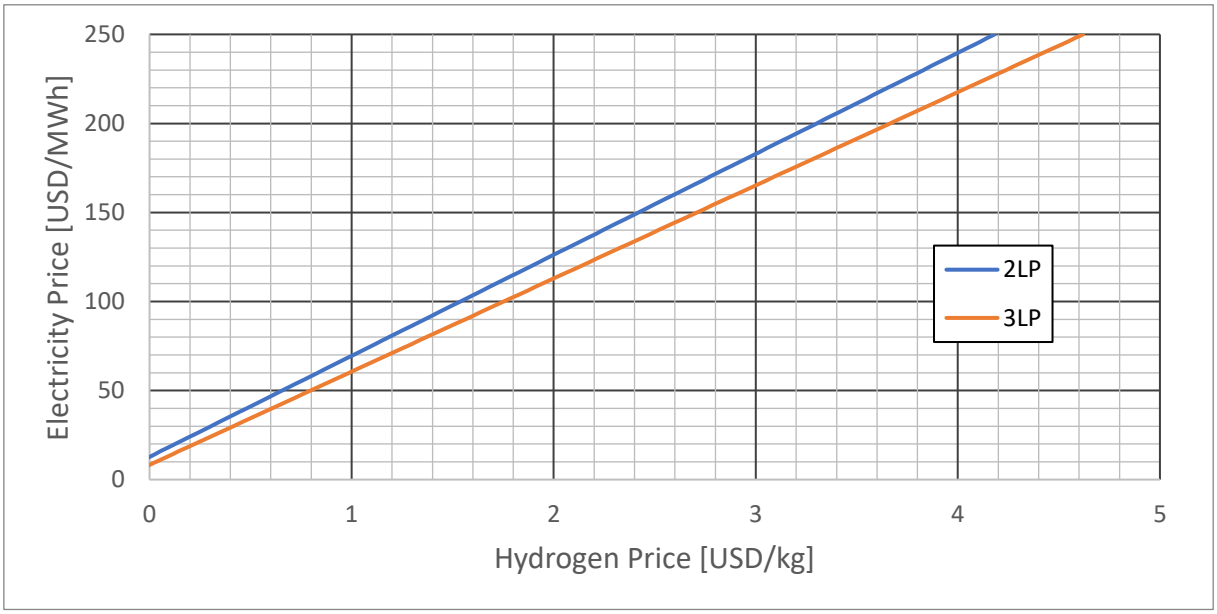

Figure 4.30 Price of the electricity needed to get a NPV of zero.

5. Conclusions.

The objectives set in this work have been fulfilled, ORVs, chillers and blending analysis have been performed and their impact on the cycle has been quantified.

All three alternatives for improving combined cycles have been analyzed and simulated. The main results obtained from this work are summarized in the following paragraphs.

For the environmental conditions considered for natural gas preheating, Case D1 (with the sea water intake in the cold side and the outlet in the hot side with the preheaters) outperformed all the other possible configurations for any pressure level in the turbine. Case CI (preheaters in the water intake, placed in the cold side and outlet in the cold side) performed the best only considering high-pressure scenarios.

Considering the introduction of chillers, the electric chiller was in most cases the best alternative, and makes combined cycles more competitive, allowing for higher power operation.

Regarding blending with hydrogen, the expected return is lower than with natural gas. However, future environmental regulations may limit carbon emissions associated to power generation, forcing operation with hydrogen. In this context blending is profitable up to 49% hydrogen in case of a two-levelled pressure cycle and 52% in case of a 3LP cycle, for the actual price of 6USD/kg.

Future research lines could analyze different chiller types, other methods for obtaining cheaper hydrogen for combined cycles. On the other hand, the use of chillers and more efficient cycles can improve the feasibility of blending. The integration of these three combined cycle improvements could be synergetic and require further investigation.

6. Schedule and budget.

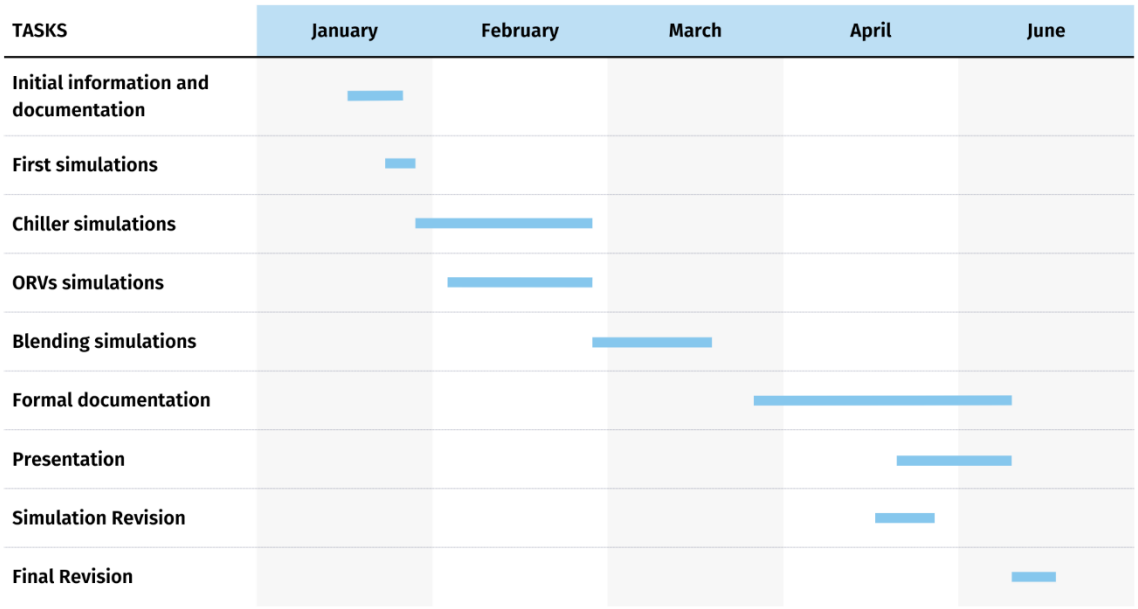

Figure 6.1 Schedule for the project development.

Table 6.1 Cost of the investigation.

Description	Quantity	Unit Price	Total Price
Business Laptop	1	100€/yr	100€
Thermoflex License	1	12,000€/yr	3,000€
GTPro License	1	6,000€/yr	1,500€
Investigation hours	400	40€/h	16,000€
Professor hours	40	50€/h	2,000€
Office Equipment	1	200€/yr	50€
Indirect Costs	3%		679.50€
Total Cost			23,329.50€

References.

[1] U.S. Department of Commerce, “Global Monitoring Laboratory - Carbon Cycle Greenhouse Gases.” Accessed: Feb. 27, 2024. [Online]. Available: https://gml.noaa.gov/ccgg/trends/

[2] V. Masson-Delmotte *et al.*, “Working Group I Contribution to the Sixth Assessment Report of the Intergovernmental Panel on Climate Change Edited by,” 2021, Accessed: Feb. 27, 2024. [Online]. Available: www.ipcc.ch

[3] L. Byers, J. Friedrich, R. Hennig, A. Kressig, C. Mccormick, and L. Malaguzzi Valeri, “A GLOBAL DATABASE OF POWER PLANTS,” Mar. 2021, Accessed: Apr. 01, 2024. [Online]. Available: http://globalenergyobservatory.org

[4] H. Ritchie, P. Rosado, and M. Roser, “Electricity Mix,” *Our World in Data*, Jan. 2024, Accessed: Feb. 28, 2024. [Online]. Available: https://ourworldindata.org/electricity-mix

[5] MET Group Countries, “Natural gas vs Coal – environmental impacts,” NATURAL GAS VS COAL – ENVIRONMENTAL IMPACTS. Accessed: Mar. 09, 2024. [Online]. Available: https://group.met.com/en/mind-the-fyouture/mindthefyouture/natural-gas-vs-coal

[6] I. - International Energy Agency, “Electricity Market Report 2023”, Accessed: Mar. 09, 2024. [Online]. Available: www.iea.org

[7] F. Aquino *et al.*, “ELABORADO POR REVISADO POR APROBADO POR FECHA DE SALIDA ORGANISMO COORDINADOR DEL SISTEMA ELÉCTRICO NACIONAL INTERCONECTADO DE LA REPÚBLICA DOMINICANA, INC. INFORME ANUAL DE OPERACIONES Y TRANSACCIONES ECONÓMICAS DEL AÑO 2023,” Feb. 2024, Accessed: Apr. 26, 2024. [Online]. Available: https://www.oc.org.do/Informes/Administrativos/Informe-Anual/EntryId/193520

[8] Process Control Team, “Details Home.” Accessed: Apr. 01, 2024. [Online]. Available: https://blog.parker.com/site/usa/details-home-page/natural-gas-combined-cycle-power-plants-history-trends-and-outlook-us

[9] L. Aramayo and M. Morey, “New natural gas-fired capacity additions expected to total 8.6 gigawatts in 2023 - U.S. Energy Information Administration (EIA).” Accessed: Apr. 01, 2024. [Online]. Available: https://www.eia.gov/todayinenergy/detail.php?id=60663

[10] K. Mathews, “Power Plant Technology Combined Cycle and Renewable Energy Power Systems (Lecture 1) by Mohamad Firdaus Basrawi, Dr. (Eng) Mechanical Engineering Faculty. - ppt download.” Accessed: May 09, 2024. [Online]. Available: https://slideplayer.com/slide/13700024/

[11] Ø. Flatebø and L. O. Nord, “Off-design Simulations of Offshore Combined Cycles,” Jul. 2012.

[12] A. Baudoux, F. Demeyer, and W. De Paepe, “Advanced configurations of amine based post-combustion carbon capture process applied to combined cycle gas turbine,” *Energy Conversion and Management: X*, vol. 22, p. 100537, Apr. 2024, doi: 10.1016/J.ECMX.2024.100537.

[13] Y. Khan, R. S. Mishra, and A. P. Singh, “Performance comparison of organic Rankine cycles integrated with solar based combined cycle: A thermodynamic and exergoenvironmental analysis,” *https://doi.org/10.1177/09544062231167069*, vol. 238, no. 1, pp. 233–248, Apr. 2023, doi: 10.1177/09544062231167069.

[14] X. Shi, B. Agnew, D. Che, and J. Gao, “Performance enhancement of conventional combined cycle power plant by inlet air cooling, inter-cooling and LNG cold energy utilization,” *Appl Therm Eng*, vol. 30, no. 14–15, pp. 2003–2010, Oct. 2010, doi: 10.1016/J.APPLTHERMALENG.2010.05.005.

[15] S. F. Afzali and V. Mahalec, “Optimal design, operation and analytical criteria for determining optimal operating modes of a CCHP with fired HRSG, boiler, electric chiller and absorption chiller,” *Energy*, vol. 139, pp. 1052–1065, Nov. 2017, doi: 10.1016/J.ENERGY.2017.08.029.

[16] K. Agnieszka and W. Szaflik, “Absorption and adsorption chillers applied to air conditioning systems,” *Archives of Thermodynamics*, vol. 31, no. 2, pp. 77–94, 2010, doi: 10.2478/v10173-010-0010-0.

[17] J. Y. Ryu, S. Park, C. Lee, S. Hwang, and J. Lim, “Techno-Economic Analysis of Hydrogen–Natural Gas Blended Fuels for 400 MW Combined Cycle Power Plants (CCPPs),” *Energies 2023, Vol. 16, Page 6822*, vol. 16, no. 19, p. 6822, Sep. 2023, doi: 10.3390/EN16196822.

[18] Cryonorm, “LNG Open Rack Vaporizer - Cryonorm.” Accessed: Apr. 19, 2024. [Online]. Available: https://cryonorm.com/liquefied-natural-gas/vaporizers/open-rack-vaporizer/

[19] A. P. Santos and C. R. Andrade, “Analysis of Gas Turbine Performance with Inlet Air Cooling Techniques Applied to Brazilian Sites,” *Journal of Aerospace Technology and Management*, vol. 4, no. 3, pp. 341–353, 2012, doi: 10.5028/JATM.2012.04032012.

[20] Inst Tools, “Difference between HVAC Absorption Chillers and Electric Chillers.” Accessed: Apr. 19, 2024. [Online]. Available: https://instrumentationtools.com/difference-between-hvac-absorption-chillers-and-electric-chillers/

[21] P. Evans, “Absorption Chiller, How it works - The Engineering Mindset.” Accessed: Apr. 19, 2024. [Online]. Available: https://theengineeringmindset.com/absorption-chiller-works/

[22] Dr. J. Goldmeer and J. Catillaz, “Hydrogen for power generation Experience, requirements, and implications for use in gas turbines www.ge.com/gas-power/future-of-energy,” Mar. 2022, Accessed: Apr. 09, 2024. [Online]. Available: www.ge.com/gas-power/future-of-energy

[23] Shri. K. A. Gavhane, “Heat Transfer - V. P. Isachenko, V. A. Osipova, Aleksandr Semenovič Sukomel - Google Libros.” Accessed: Apr. 01, 2024. [Online]. Available: https://books.google.es/books?hl=es&lr=&id=3Om2k2Amo9wC&oi=fnd&pg=PA22&dq=heat+transfer&ots=skmKU2ON6h&sig=QJ74eaPbrZMSp0L7WScxTGKdi6s#v=onepage&q=heat%20transfer&f=false

[24] C. J. Renedo, “Ingeniería Térmica y de Fluidos (II) Ingeniería Eléctrica y Energética Máquinas y Motores Térmicos,” Feb. 2009, Accessed: Apr. 03, 2024. [Online]. Available: http://personales.unican.es/renedoc/index.htm

[25] S. Nath, “Why is a counter flow heat exchanger better than a parallel flow heat exchanger? - Quora.” Accessed: Apr. 01, 2024. [Online]. Available: https://www.quora.com/Why-is-a-counter-flow-heat-exchanger-better-than-a-parallel-flow-heat-exchanger

[26] ISO, “ISO 3977-2:2023 - Gas turbines — Procurement — Part 2: Standard reference conditions and ratings.” Accessed: Apr. 22, 2024. [Online]. Available: https://standards.iteh.ai/catalog/standards/iso/0bf7c7bf-0eef-4e83-82b9-ab1d2abc2935/iso-3977-2-2023

[27] “How to calculate NPV — AccountingTools.” Accessed: Apr. 04, 2024. [Online]. Available: https://www.accountingtools.com/articles/how-to-calculate-npv.html

[28] J. Luis Moreno San Juan, “LA TARIFA ELÉCTRICA EN REPÚBLICA DOMINICANA,” Aug. 2022.

[29] A. Vilela, “Planean un centro de producción de hidrógeno verde de 350 MW en República Dominicana - H2 Business News.” Accessed: Apr. 11, 2024. [Online]. Available: https://h2businessnews.com/planean-un-centro-de-produccion-de-hidrogeno-verde-de-350-mw-en-republica-dominicana/

[30] McKinsey & Company, “Hydrogen Insights A perspective on hydrogen investment, market development and cost competitiveness,” Feb. 2021, Accessed: Apr. 11, 2024. [Online]. Available: www.hydrogencouncil.com.

[31] I. De la Cruz, “¿Es viable producir hidrógeno verde en República Dominicana? - Diario Libre.” Accessed: Apr. 11, 2024. [Online]. Available: https://www.diariolibre.com/economia/energia/2023/10/22/es-viable-producir-hidrogeno-verde-en-republica-dominicana/2497841

[32] Weather Spark, “Dominican Republic December Weather, Average Temperature (Dominican Republic) - Weather Spark.” Accessed: Apr. 18, 2024. [Online]. Available: https://weatherspark.com/m/150222/12/Average-Weather-in-December-in-Dominican-Republic#Figures-Temperature

[33] Siemens Energy, “Hydrogen Decarbonization Calculator.” Accessed: Apr. 18, 2024. [Online]. Available: https://www.siemens-energy.com/global/en/home/products-services/solutions-usecase/hydrogen/hydrogen-decarb-calculator.html

[34] United Nations Climate Change, “Defining the Carbon Pricing Instrument Road Map in the Dominican Republic | UNFCCC.” Accessed: Apr. 26, 2024. [Online]. Available: https://unfccc.int/about-us/regional-collaboration-centres/rcc-st-george/about-the-rcc-st-george-s/defining-the-carbon-pricing-instrument-road-map-in-the-dominican-republic

[35] Y. A. Çengel and M. A. Boles, “Termodinámica – Çengel, Boles – 7ma Edición,” 2012.

[36] SidewinderX, “File:Combustor diagram componentsPNG.png - Wikimedia Commons.” Accessed: Apr. 15, 2024. [Online]. Available: https://commons.wikimedia.org/wiki/File:Combustor_diagram_componentsPNG.png

[37] M. Utschick and T. Sattelmayer, “Flame Holding in the Premixing Zone of a Gas Turbine Model Combustor After Forced Ignition of H2–Natural Gas–Air Mixtures,” *J Eng Gas Turbine Power*, vol. 139, no. 4, Oct. 2016, doi: 10.1115/1.4034647.

[38] ILPI, “The MSDS HyperGlossary: Flammable Limits.” Accessed: Apr. 10, 2024. [Online]. Available: http://www.ilpi.com/msds/ref/flammablelimits.html

[39] “Gas turbines from 2 to 593 MW,” 2023.

[40] G. Dutt, “Methane Density,” MGM International. Accessed: Apr. 11, 2024. [Online]. Available: https://cdm.unfccc.int/methodologies/inputsconsmeth/MGM_methane.pdf

[41] “Hydrogen - Wikipedia.” Accessed: Apr. 11, 2024. [Online]. Available: https://en.wikipedia.org/wiki/Hydrogen

[42] “Diagrama psicrométrico online y cálculo de las propiedades del aire húmedo.” Accessed: Apr. 17, 2024. [Online]. Available: https://www.herramientasingenieria.com/onlinecalc/spa/psicrometricos/psicrometricos.html

[43] “Psychrometric Chart Use - Swineweb.com - Complete Swine News, Markets, Commentary, and Technical Info.” Accessed: Apr. 17, 2024. [Online]. Available: https://www.swineweb.com/facilities-equipment/psychrometric-chart-use/

[44] UCDavis, “Software Resource & Applications - Western Cooling Efficiency Center.” Accessed: Apr. 17, 2024. [Online]. Available: https://wcec.ucdavis.edu/resources/software-resource-applications/

[45] M. May, S.J., and A. Bart, “Finding Numerical Solutions with Goal Seek.” Accessed: Apr. 17, 2024. [Online]. Available: https://mathstat.slu.edu/~may/ExcelCalculus/sec-1-6-GoalSeek.html

Annexes.

Annex A. LMTD formulation.

In order to obtain the formula for the LMTD, the general equation of heat transfer is used:

$$\dot{dQ} = U \cdot dA \cdot \Delta T = U \cdot A \cdot LMTD \tag{A.1}$$

For this demonstration, all inlet flows are considered in point A excluding the cold flow in counter-current. The subscript 'h' corresponds to the hot fluid and the subscript 'c' corresponds to the cold fluid, as shown in the following image.

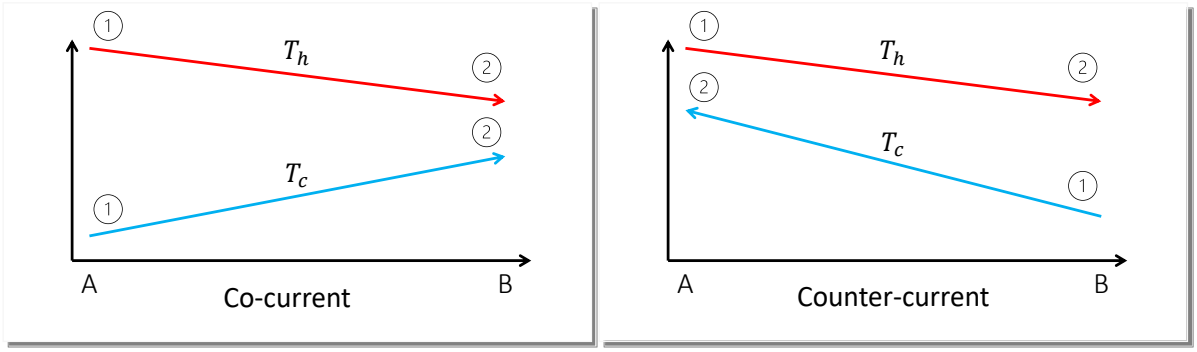

Figure A.1 Flow temperature for co-current and counter-current configurations.

The heat transferred from the hot side to the cold side is the same, and it is given by this equation:

$$\dot{dQ}_h = d\dot{Q}_c = \dot{m}_h \cdot C_{P,h} \cdot dT_h = \dot{m}_c \cdot C_{P,c} \cdot dT_c \tag{A.2}$$

To simplify the representation, phi is defined as $\Phi = \frac{dT_c}{dT_h} = \frac{\dot{m}_h \cdot C_{P,h}}{m_c \cdot C_{P,c}}$, $\Delta T = T_h - T_c$, and $d(\Delta T) = dT_h - dT_c = \Delta T_h - \Delta T_c$, where the differential and differences are measured from left to right -or from A to B-.

First, both heat transfer equations are made equal, for instance, from the hot side:

$$d\dot{Q}_h = U \cdot dA \cdot \Delta T = \dot{m}_h \cdot C_{P,h} \cdot dT_h \quad \text{(A.3)}$$

$\mathrm{dT_h}$ can be expressed in terms of ΔT and Φ using previous equations:

$$dT_h = d(\Delta T) + dT_c = d(\Delta T) + \Phi \cdot dT_h \quad \text{(A.4)}$$

$$dT_h = \frac{d(\Delta T)}{1 - \Phi} \quad \text{(A.5)}$$

And substituting it in the previous equation:

$$U \cdot dA \cdot \Delta T = \dot{m}_h \cdot C_{P,h} \cdot \frac{d(\Delta T)}{1 - \Phi} \quad \text{(A.6)}$$

In order to integrate, $1 - \Phi$ is converted back to temperatures using its definition:

$$1 - \Phi = 1 - \frac{\mathrm{dT}_c}{\mathrm{dT}_h} = \frac{\mathrm{dT}_h - \mathrm{dT}_c}{\mathrm{dT}_h} \quad \text{(A.7)}$$

As the rate of change of temperatures as a function of the position is constant, differentials can be substituted by differences:

$$1 - \Phi = \frac{\Delta \mathrm{T}_h - \Delta \mathrm{T}_c}{\Delta \mathrm{T}_h} \quad \text{(A.8)}$$

Then, the numerator is rewritten as a function of inlet and outlet temperatures:

$$1 - \Phi = \frac{\mathrm{T}_{h,B} - T_{h,A} - \left(\mathrm{T}_{c,B} - T_{c,A}\right)}{\Delta \mathrm{T}_h} = \frac{T_{h,A} - \mathrm{T}_{h,B} - T_{c,A} + \mathrm{T}_{c,B}}{-\Delta \mathrm{T}_h} \quad \text{(A.9)}$$

In this arrangement, ΔT_A and ΔT_B represent left-side and right-side temperature differences:

$$\Delta T_A = T_{h,A} - T_{c,A} \quad \text{(A.10)}$$

$$\Delta T_B = T_{h,B} - T_{c,B} \quad \text{(A.11)}$$

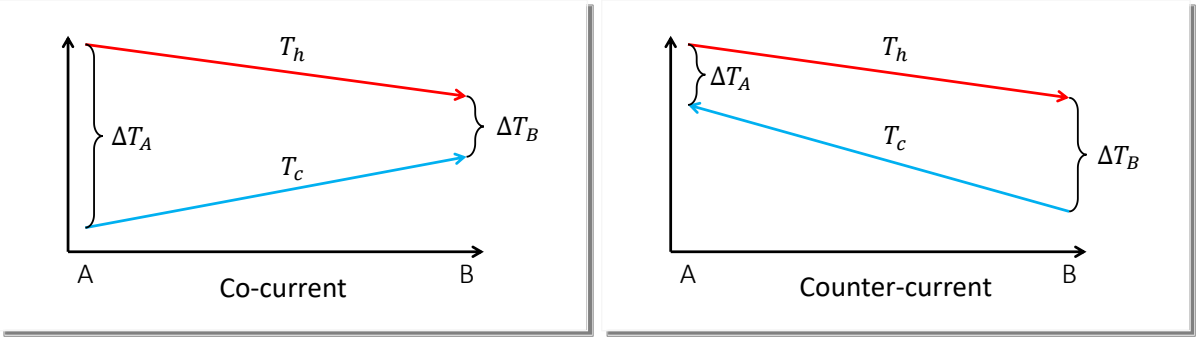

Figure A.2 ΔT_A and ΔT_B in co-current and counter-current configurations.

After substituting $T_{h,A} = T_{h,1}$ and $T_{h,B} = T_{h,2}$, the following expression is obtained:

$$1 - \Phi = \frac{\Delta T_A - \Delta T_B}{T_{h,1} - T_{h,2}} \quad \text{(A.12)}$$

Following with the previous equation, and substituting $1 - \Phi$:

$$U \cdot dA \cdot \Delta T = \dot{m}_h \cdot C_{P,h} \cdot \frac{-d(\Delta T) \cdot \Delta T_h}{\Delta T_A - \Delta T_B} \quad \text{(A.13)}$$

Simplifying and rearranging,

$$U \cdot dA \cdot \frac{(\Delta T_A - \Delta T_B)}{\Delta T_h} = \dot{m}_h \cdot C_{P,h} \cdot \frac{-d(\Delta T)}{\Delta T} \quad \text{(A.14)}$$

To eliminate differentials, the expression is integrated:

$$\int_A^B U \cdot dA \cdot \frac{(\Delta T_A - \Delta T_B)}{\Delta T_h} = \int_A^B \dot{m}_h \cdot C_{P,h} \cdot \frac{-d(\Delta T)}{\Delta T} \tag{A.15}$$

Next, the constants are moved out of the integral and the integration is performed:

$$U \cdot \frac{(\Delta T_A - \Delta T_B)}{\Delta T_h} \cdot \int_A^B dA = -\dot{m}_h \cdot C_{P,h} \cdot \int_A^B \frac{d(\Delta T)}{\Delta T} \tag{A.16}$$

$$U \cdot \frac{(\Delta T_A - \Delta T_B)}{\Delta T_h} \cdot A = -\dot{m}_h \cdot C_{P,h} \cdot [ln(\Delta T_B) - \ln(\Delta T_A)] \tag{A.17}$$

Rearranging to get to the heat flow,

$$U \cdot A \cdot \frac{(\Delta T_A - \Delta T_B)}{\ln\left(\frac{\Delta T_A}{\Delta T_B}\right)} = \dot{m}_h \cdot C_{P,h} \cdot \Delta T_h = \dot{Q}_h \tag{A.18}$$

Hence, it is shown that LMTD = $\frac{(\Delta T_A - \Delta T_B)}{\ln\left(\frac{\Delta T_A}{\Delta T_B}\right)}$.

Annex B. Detailed results.

The detailed values of combined cycle simulations can be revised in this annex.

B.1.- First Scenario.

If the first scenario at its design humidity conditions is simulated, the following power output is obtained:

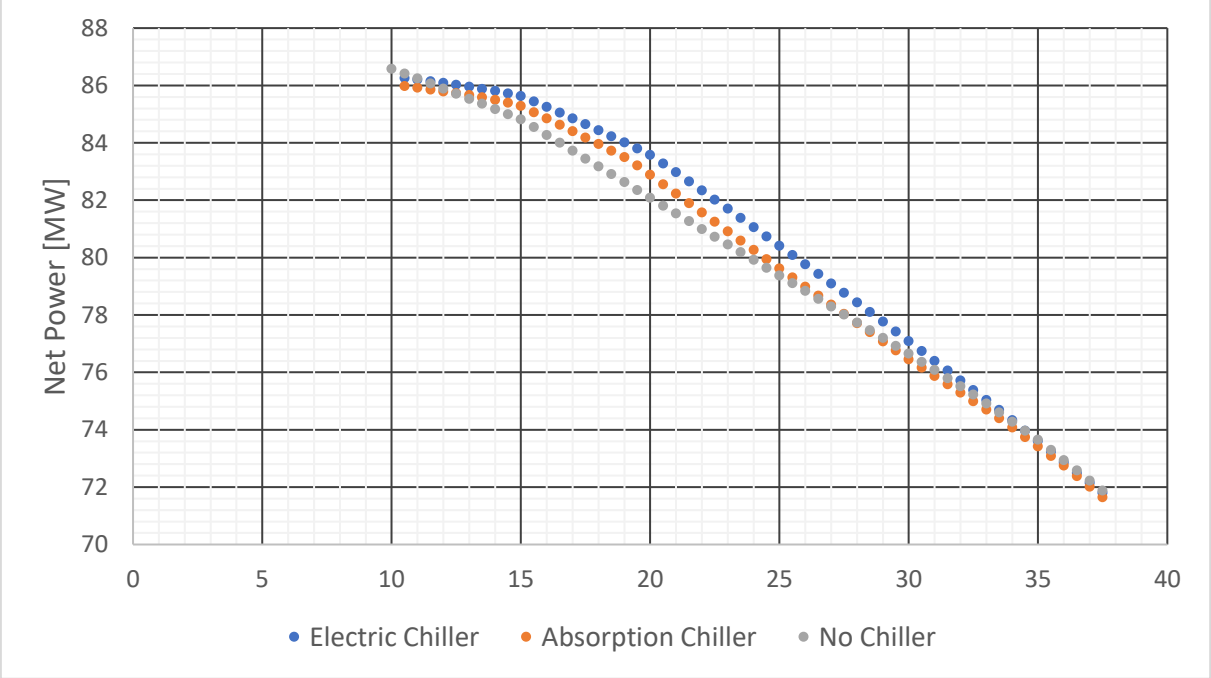

Figure B.1 Net power output of 2LP combined cycle operation at 100%RH.

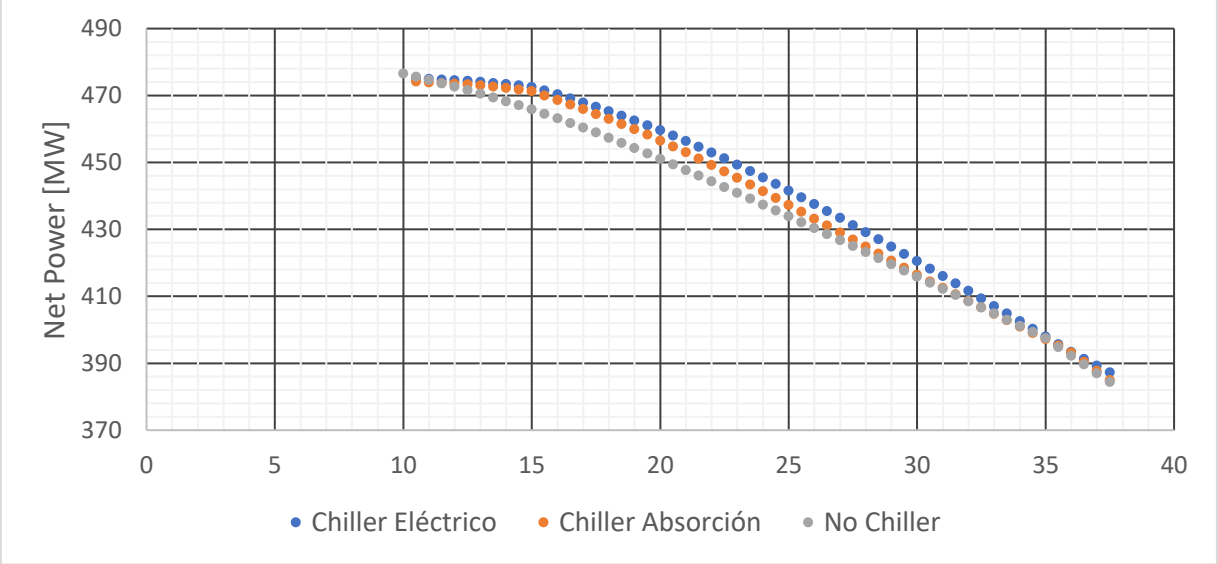

Figure B.2 Net power output of 3LP combined cycle operation at 100%RH.

The fuel and air flow show a similar shape:

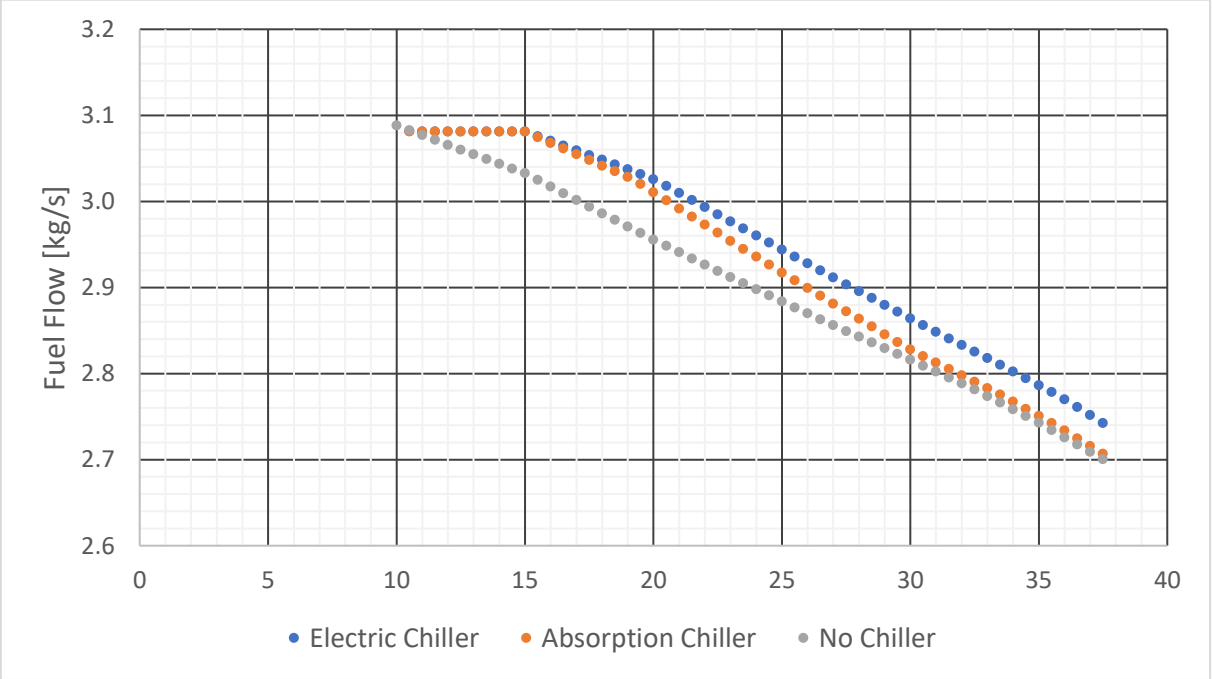

Figure B.3 Fuel flow into the gas turbine for the 2LP cycle, 100%RH.

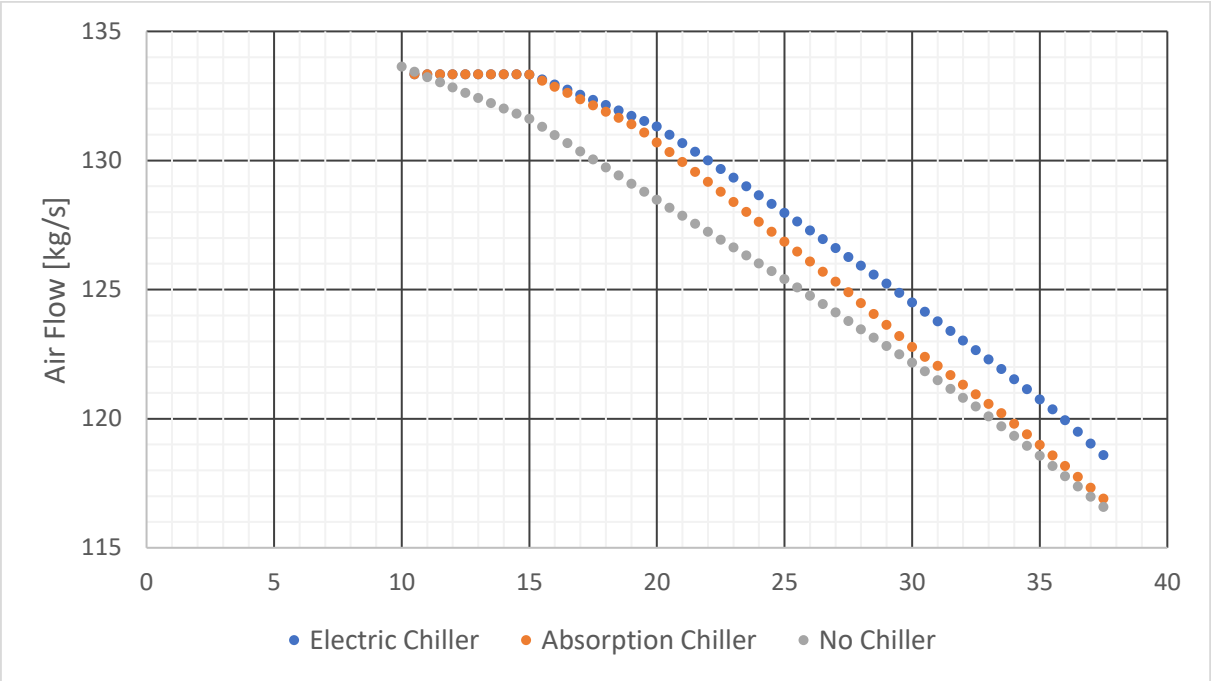

Figure B.4 Air flow into the gas turbine for the 2LP cycle, 100%RH.

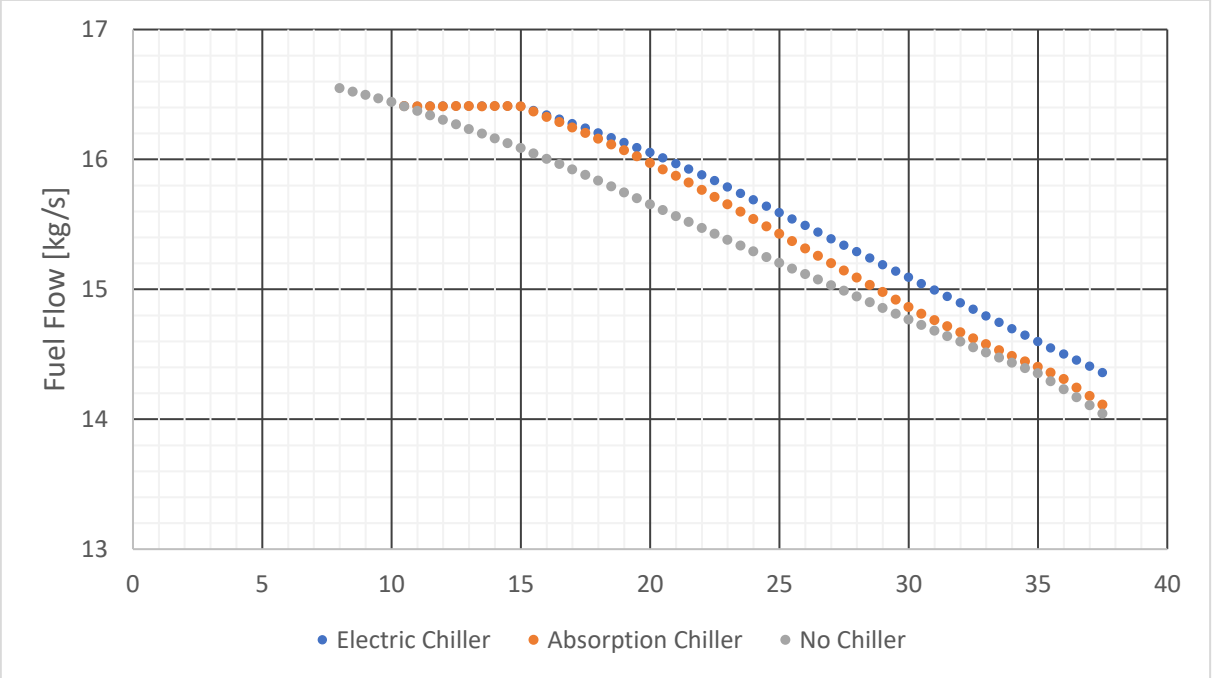

Figure B.5 Fuel flow into the gas turbine for the 3LP cycle, 100%RH.

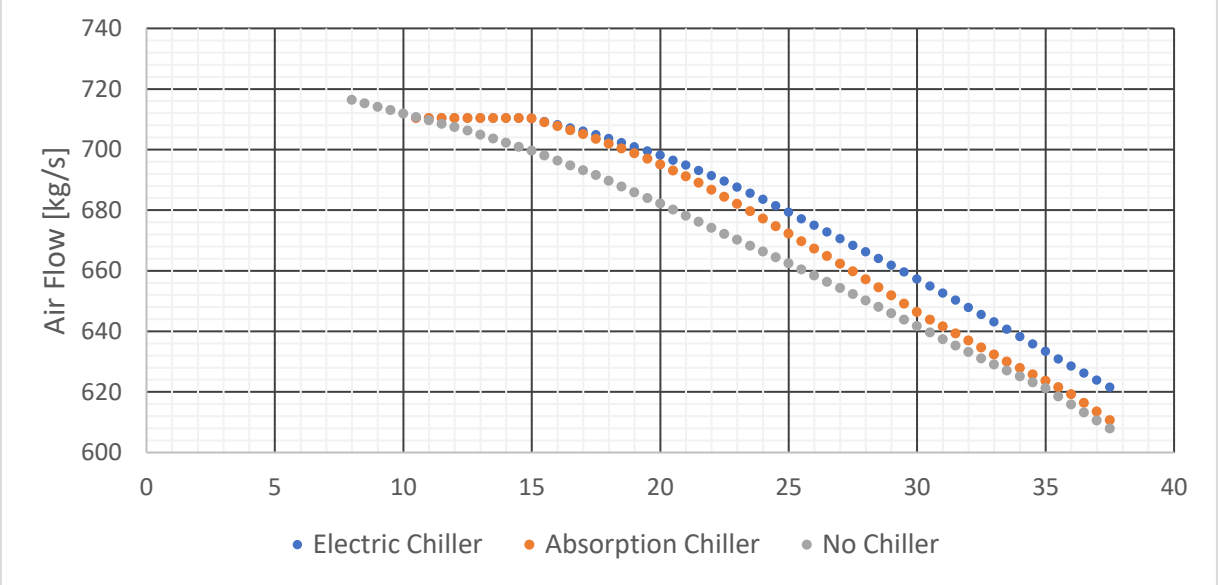

Figure B.6 Air flow into the gas turbine for the 3LP cycle, 100%RH.

The chiller´s performance can be measured as the air temperature difference between ambient and compressor inlet temperature.

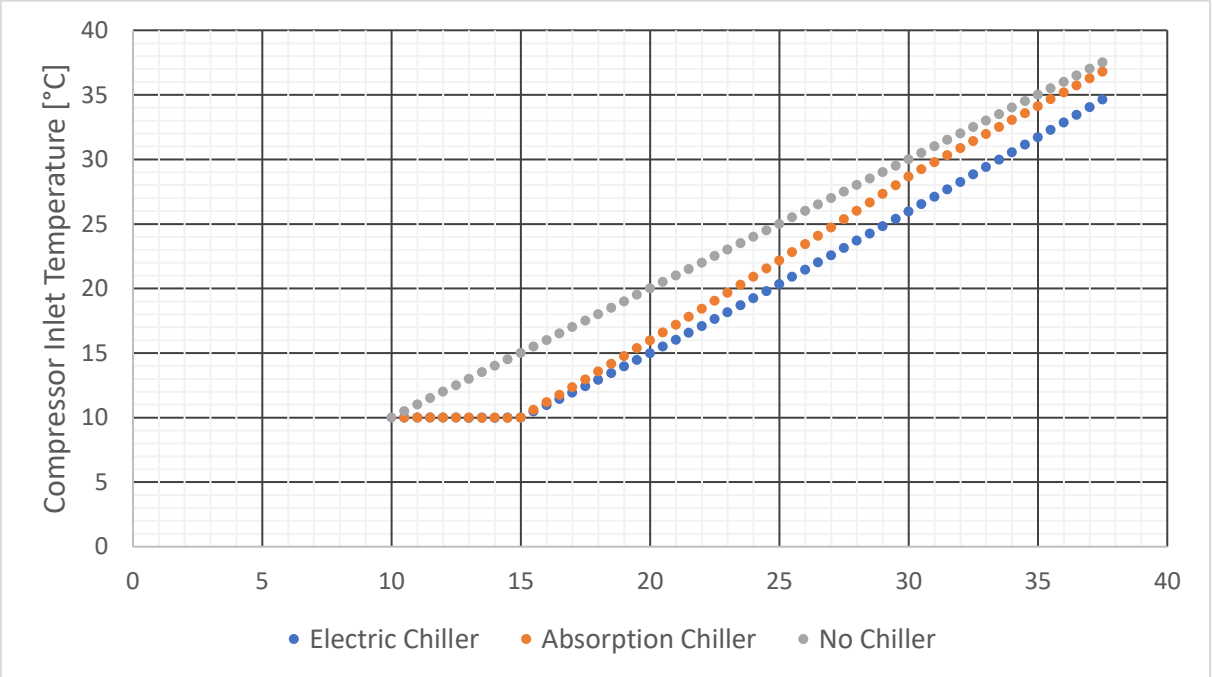

Figure B.7 Compressor inlet air temperature of 2LP cycle at 100%RH.

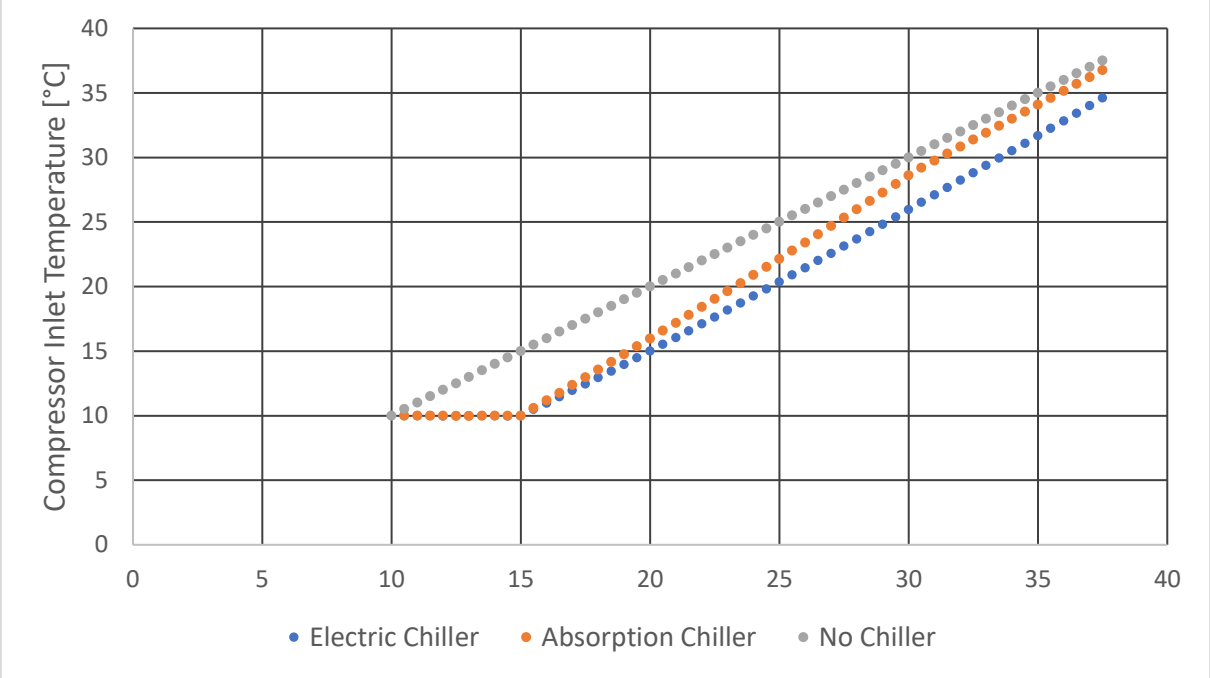

Figure B.8 Compressor inlet air temperature of 3LP cycle at 100%RH.

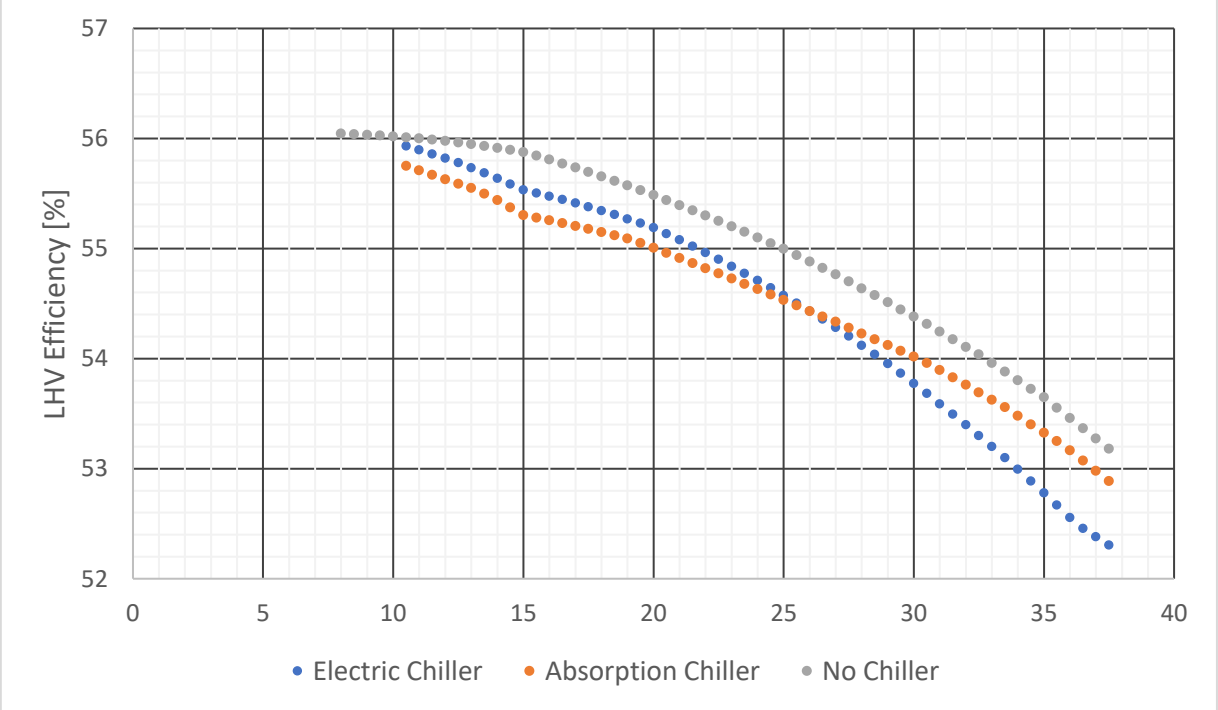

Figure B.9 LHV efficiency of the 2LP cycle at 100%RH.

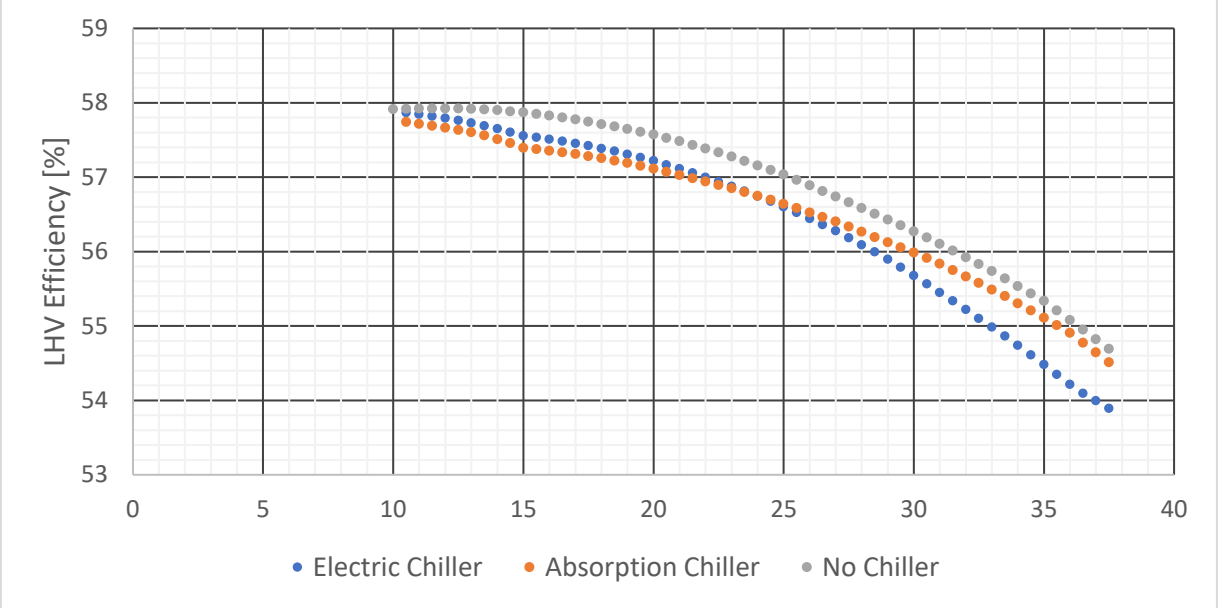

Figure B.10 LHV efficiency of the 3LP cycle at 100%RH.

The next graphs show the results for ISO humidity, 60%.

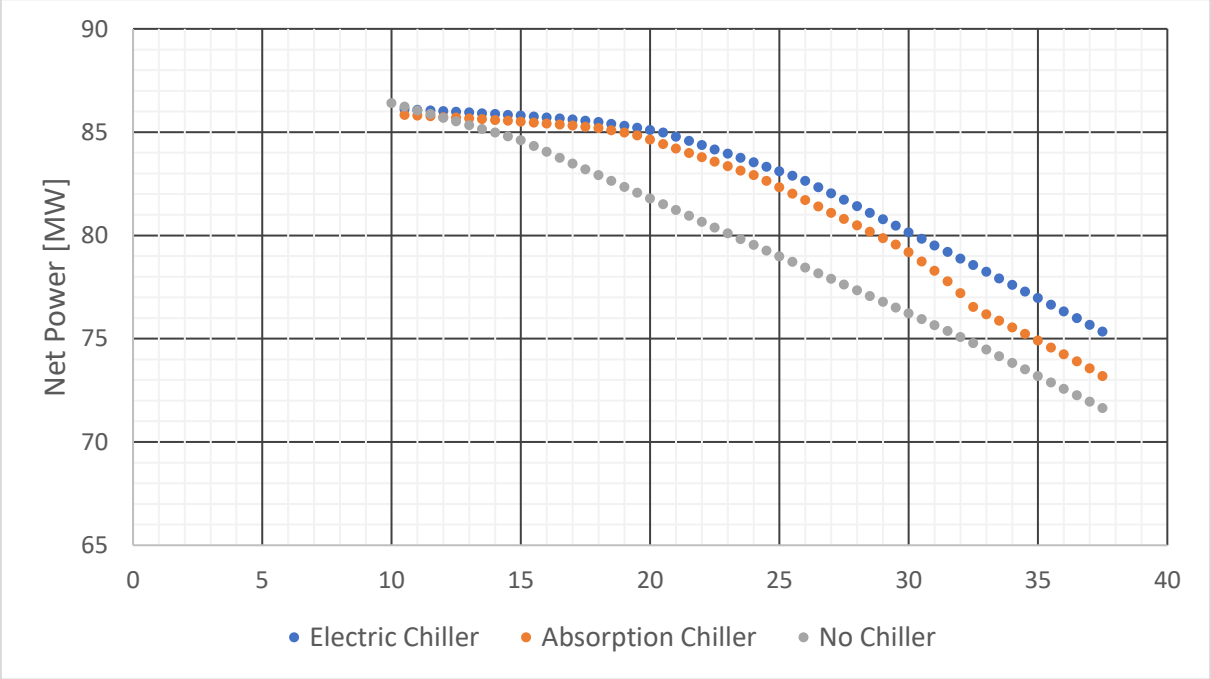

Figure B.11 Net power output of the 2LP combined cycle at 60%RH.

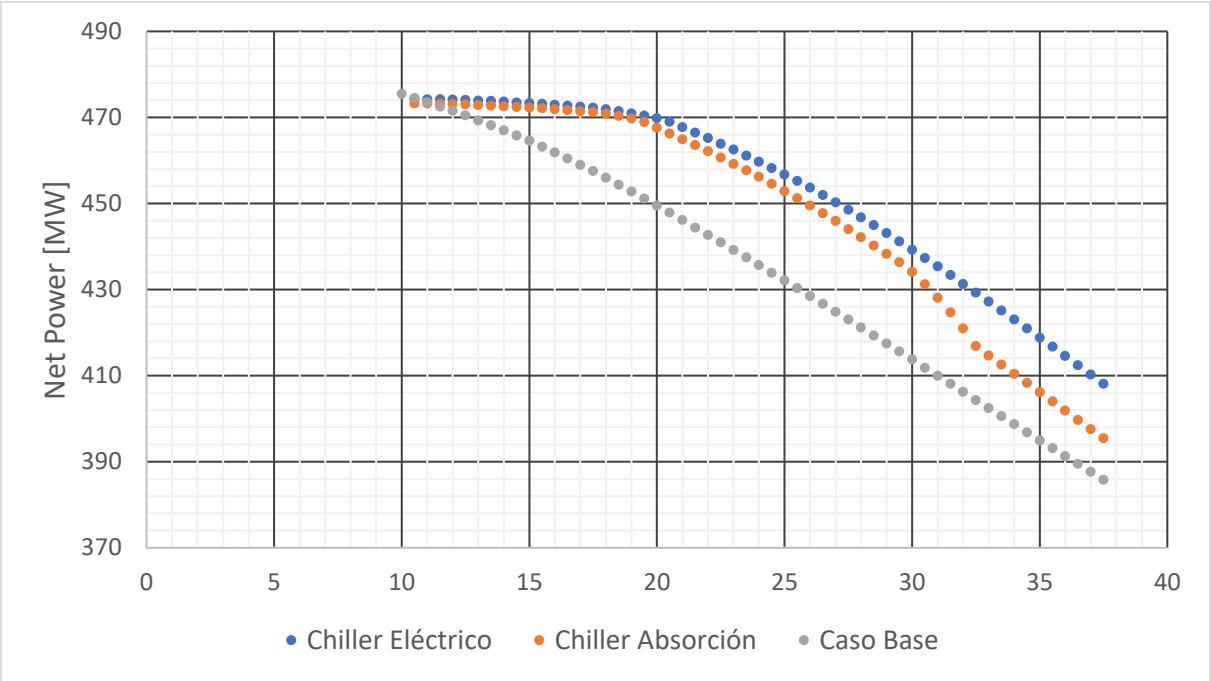

Figure B.12 Net power output of the 3LP combined cycle at 60%RH.

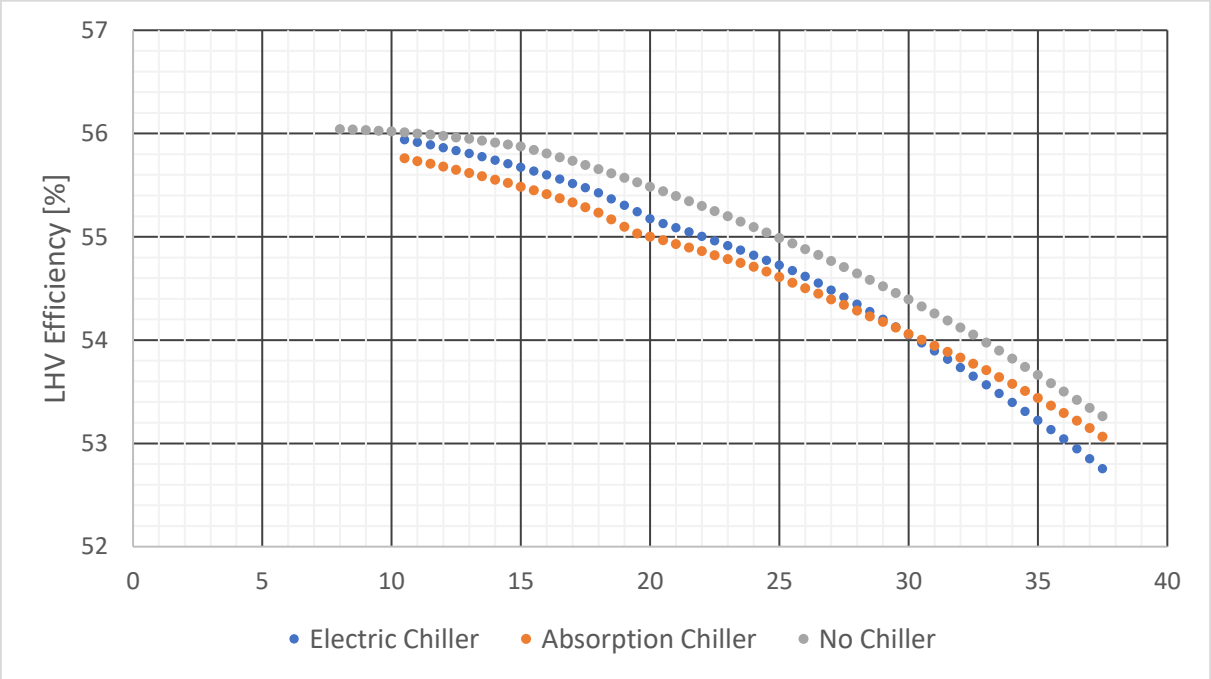

Figure B.13 LHV efficiency of the 2LP cycle at 60%RH.

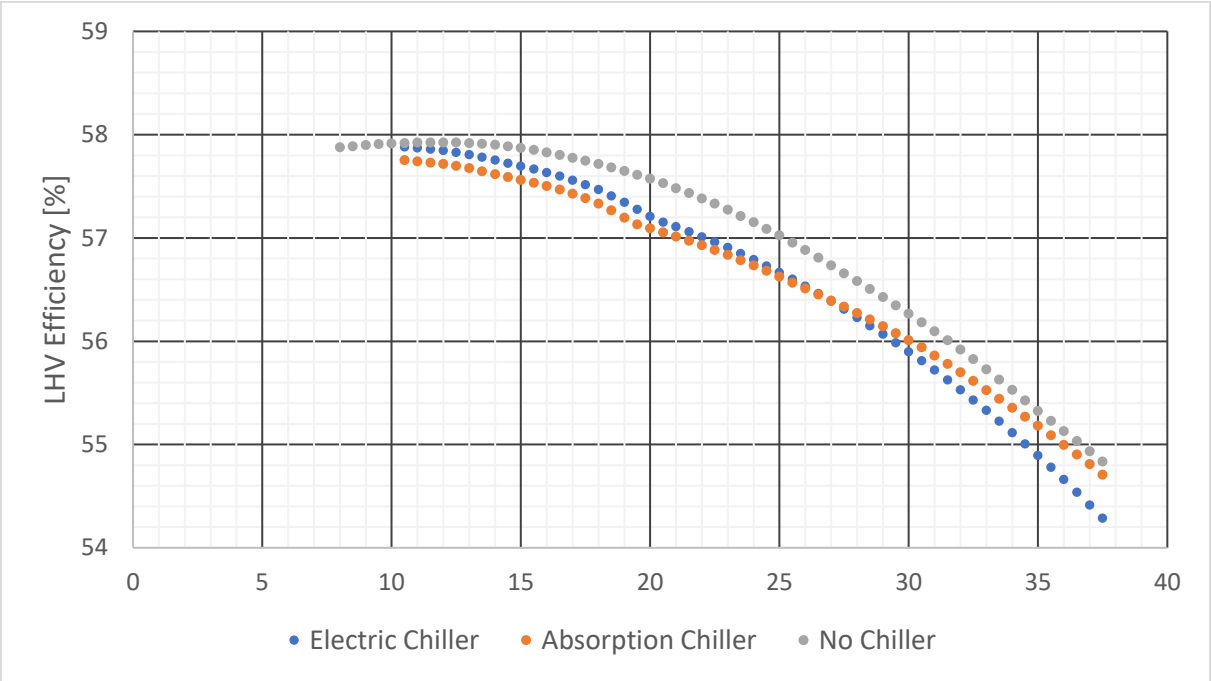

Figure B.14 LHV efficiency of the 3LP cycle at 60%RH.

B.2.- Second scenario.

The following information was obtained for 100%RH.

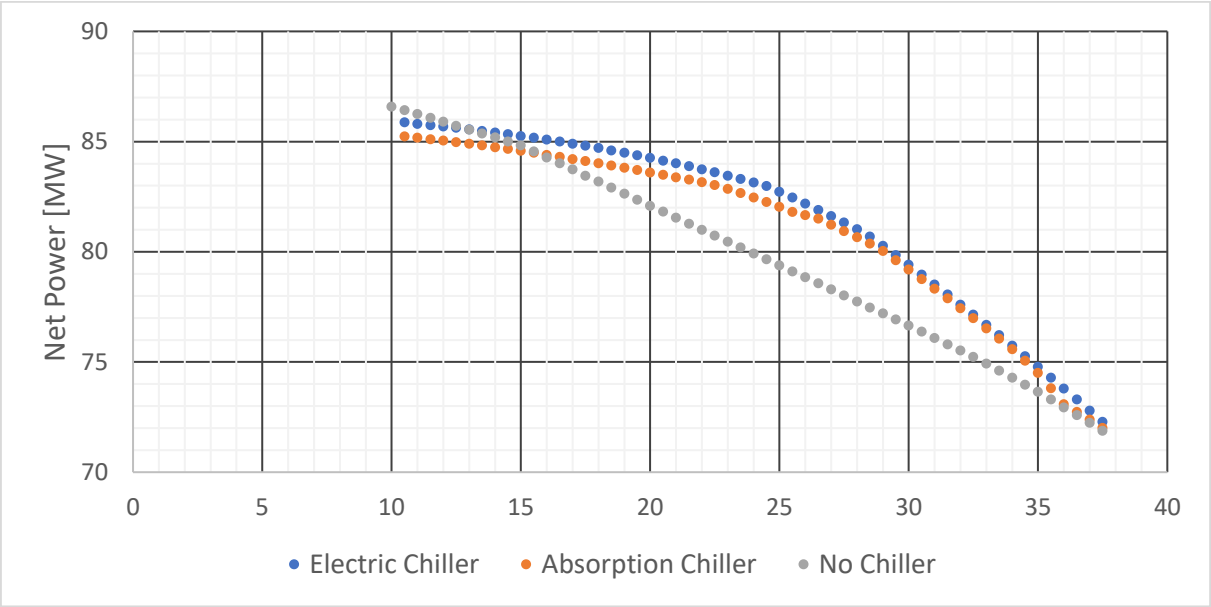

Figure B.15 Net power output of 2LP combined cycle operation at 100%RH.

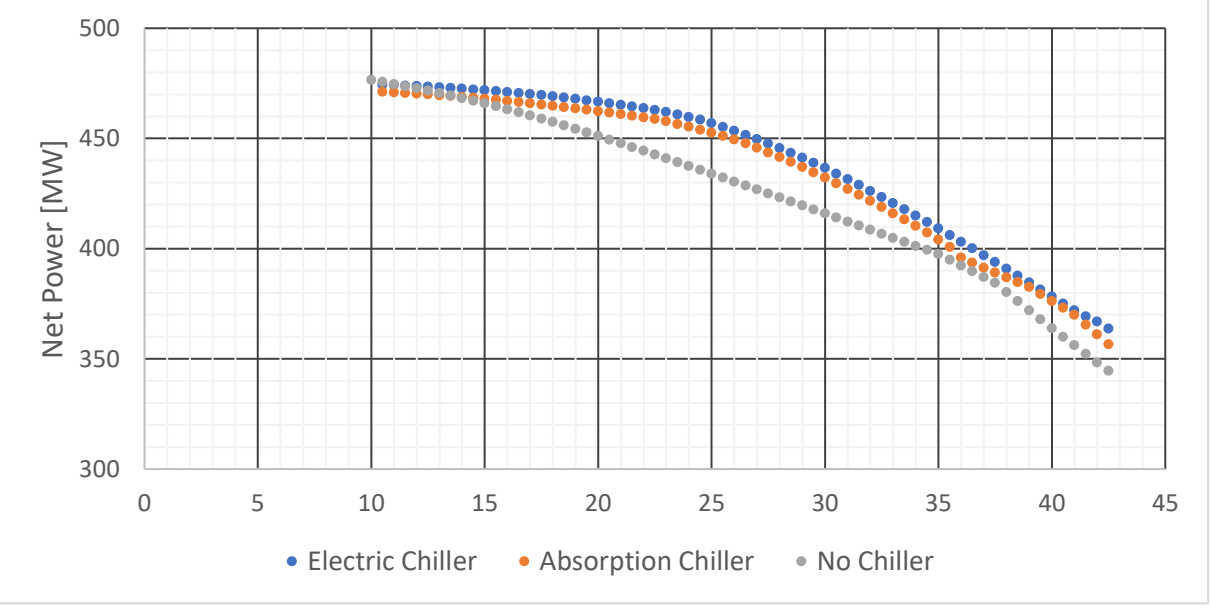

Figure B.16 Net power output of 2LP combined cycle operation at 100%RH.

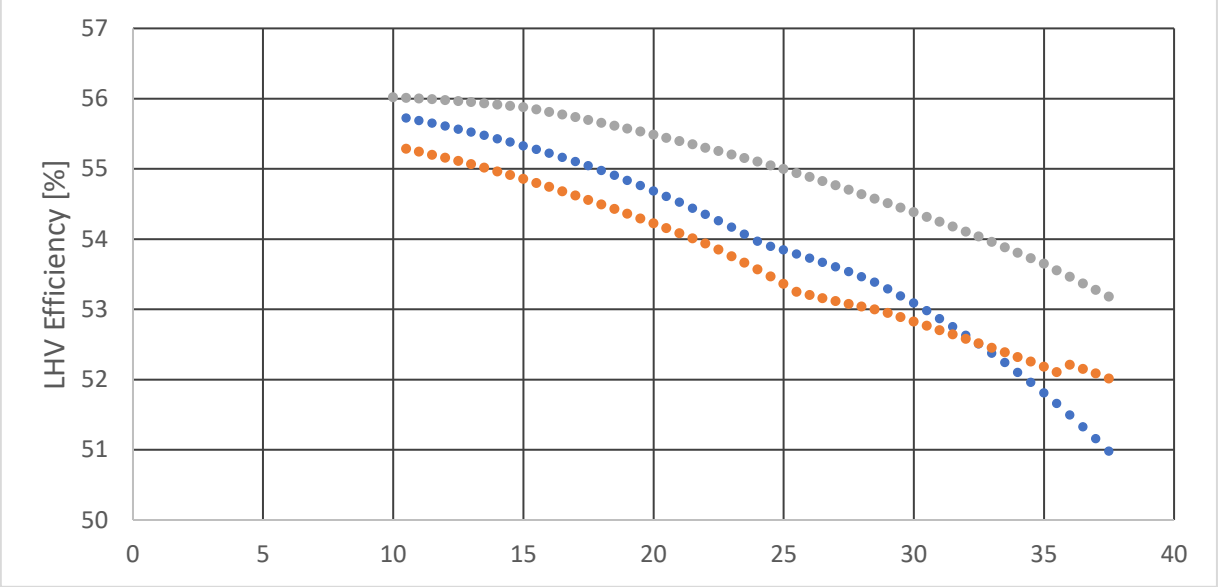

Figure B.17 LHV efficiency of the 2LP cycle at 100%RH.

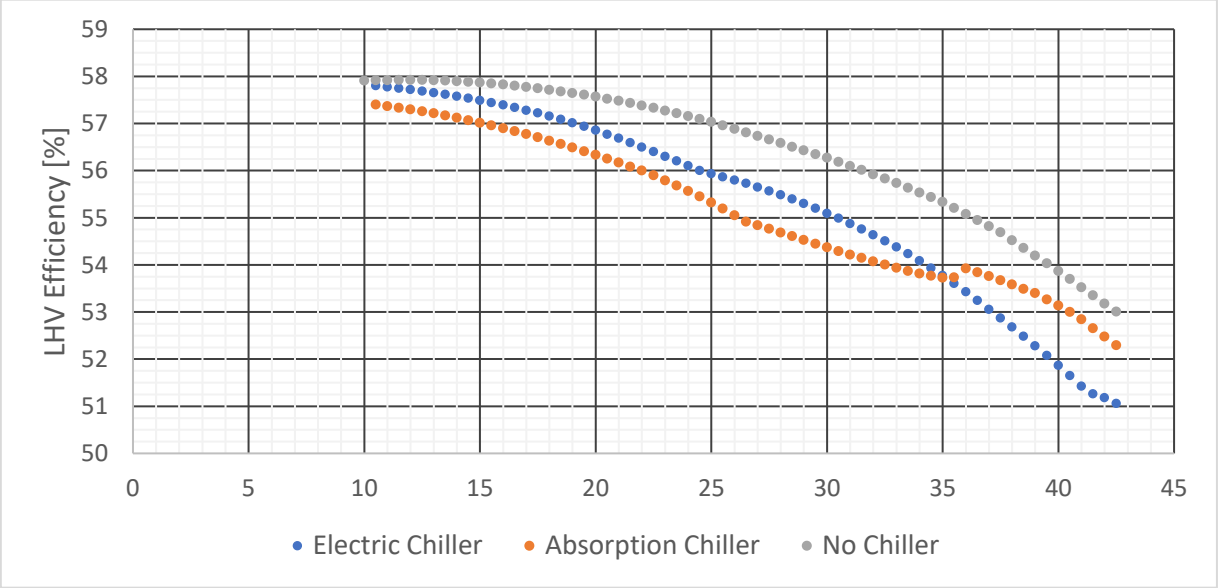

Figure B.18 LHV efficiency of the 3LP cycle at 100%RH.

The following information was obtained for 60%RH.

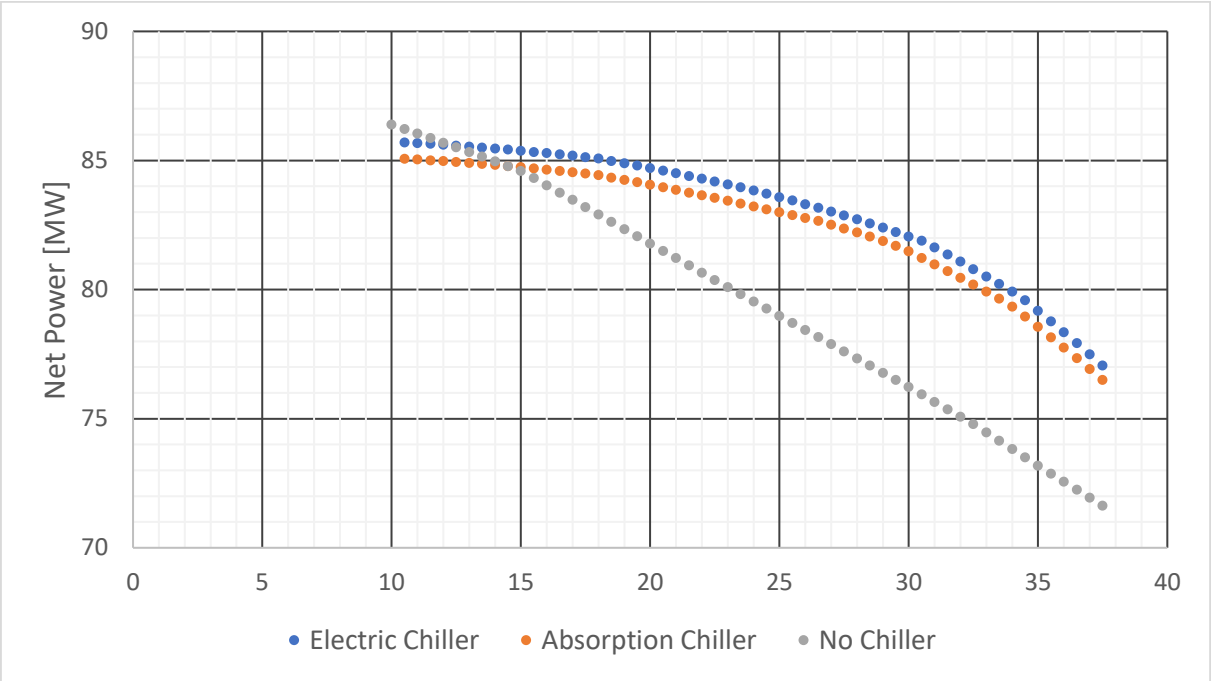

Figure B.19 Net power output of 2LP combined cycle operation at 60%RH.

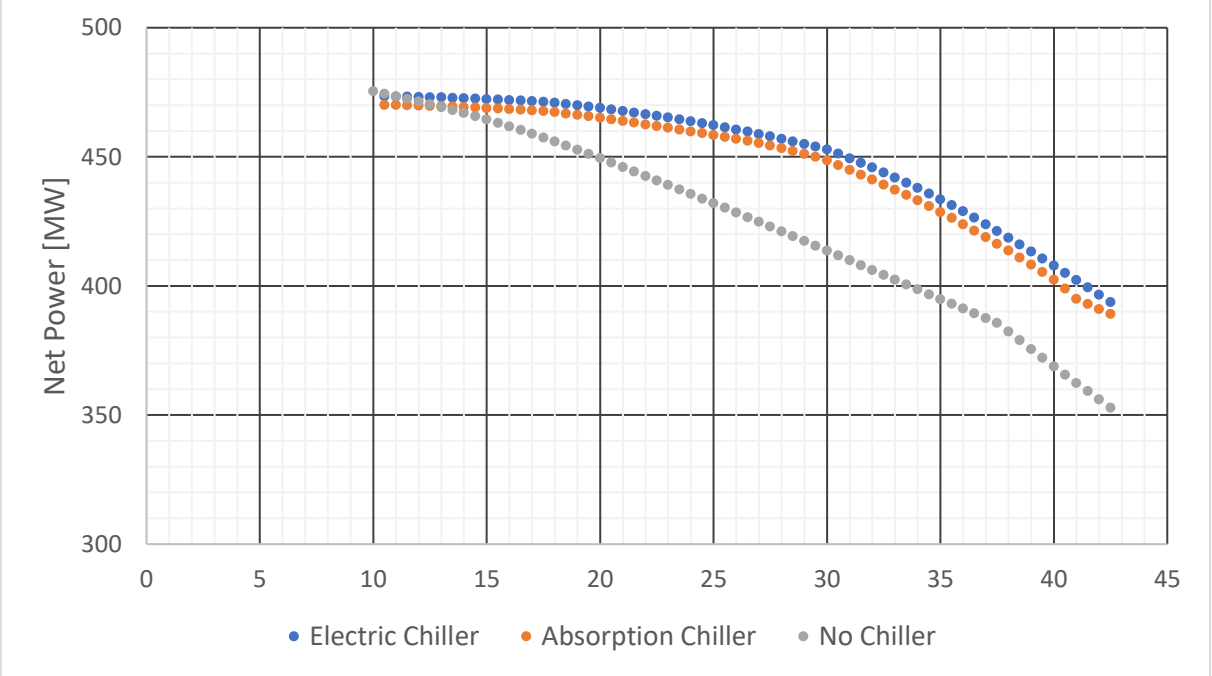

Figure B.20 Net power output of 3LP combined cycle operation at 60%RH.

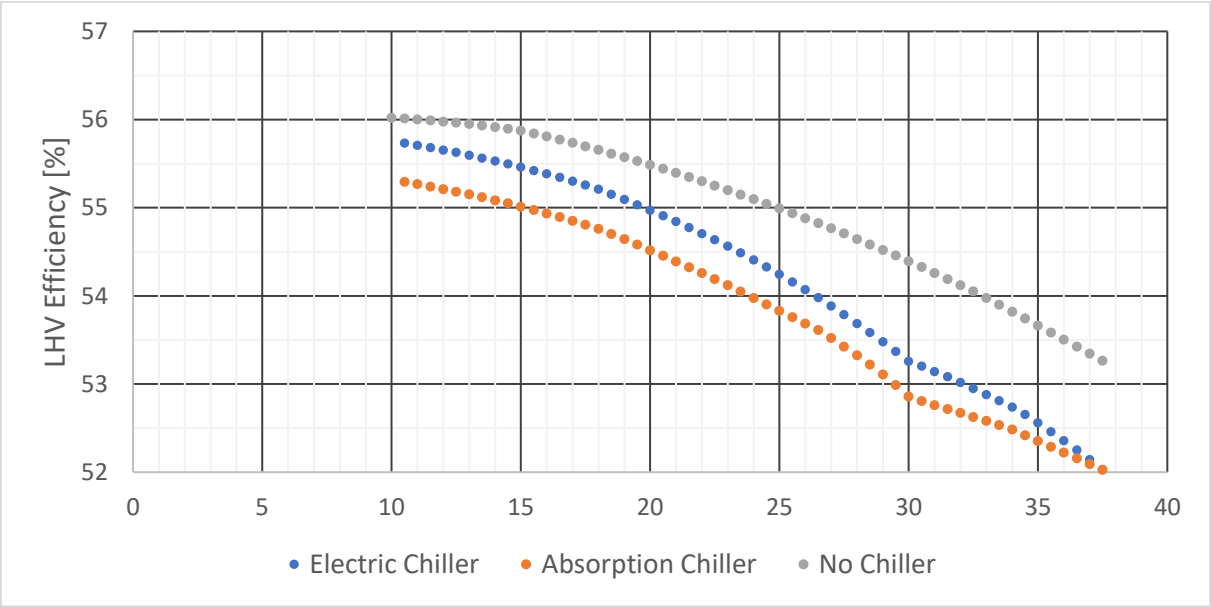

Figure B.21 LHV efficiency of the 2LP cycle at 100%RH.

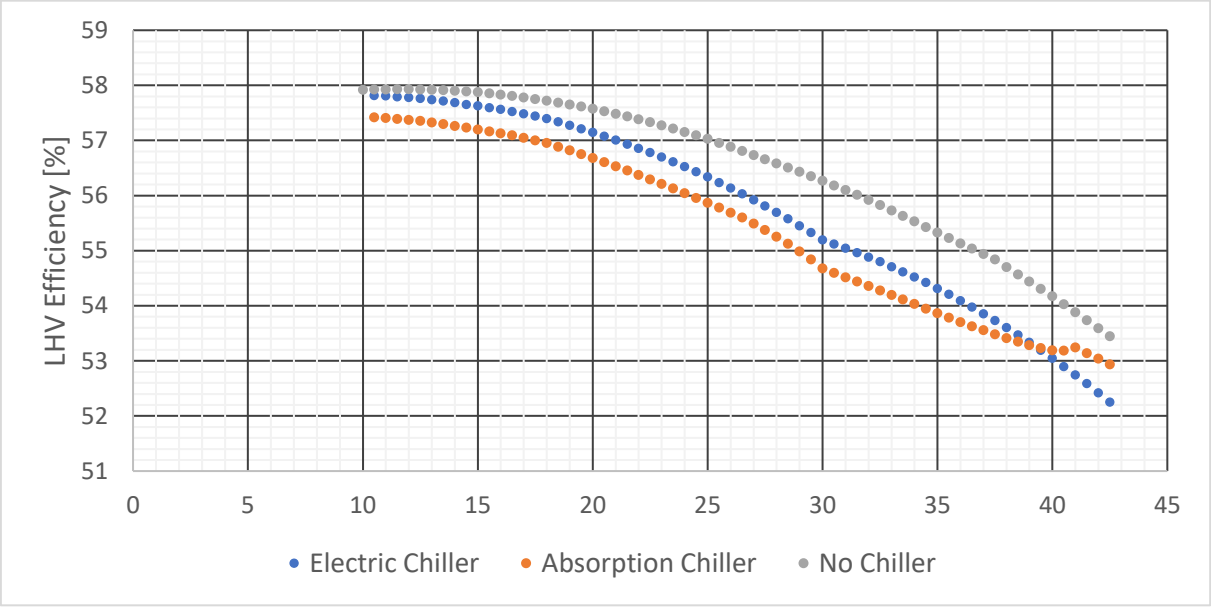

Figure B.22 LHV efficiency of the 3LP cycle at 100%RH.

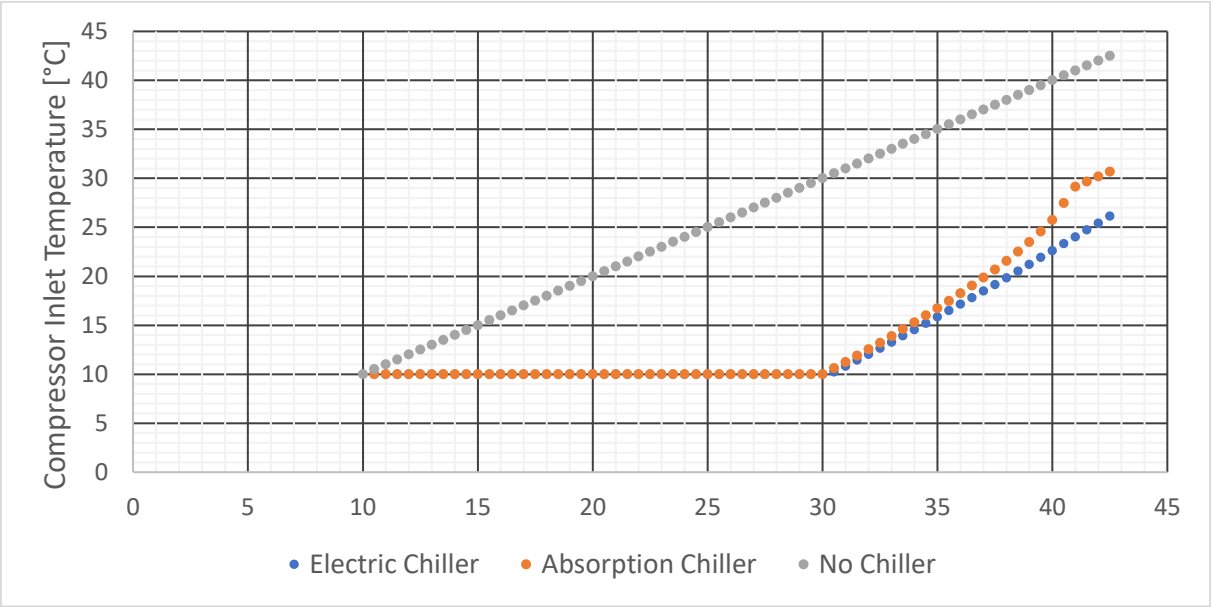

Figure B.23 Compressor inlet temperature of the 2LP cycle for 60%RH.

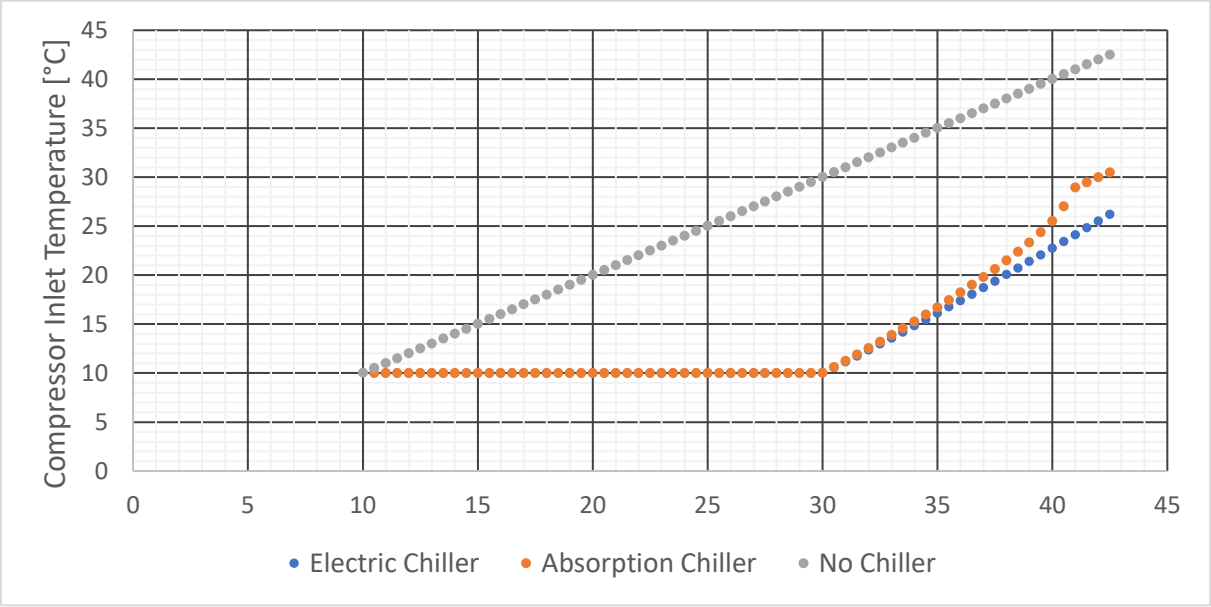

Figure B.24 Compressor inlet temperature of the 2LP cycle for 60%RH.

B.3.- Third Scenario.

The following information was obtained for 100%RH.

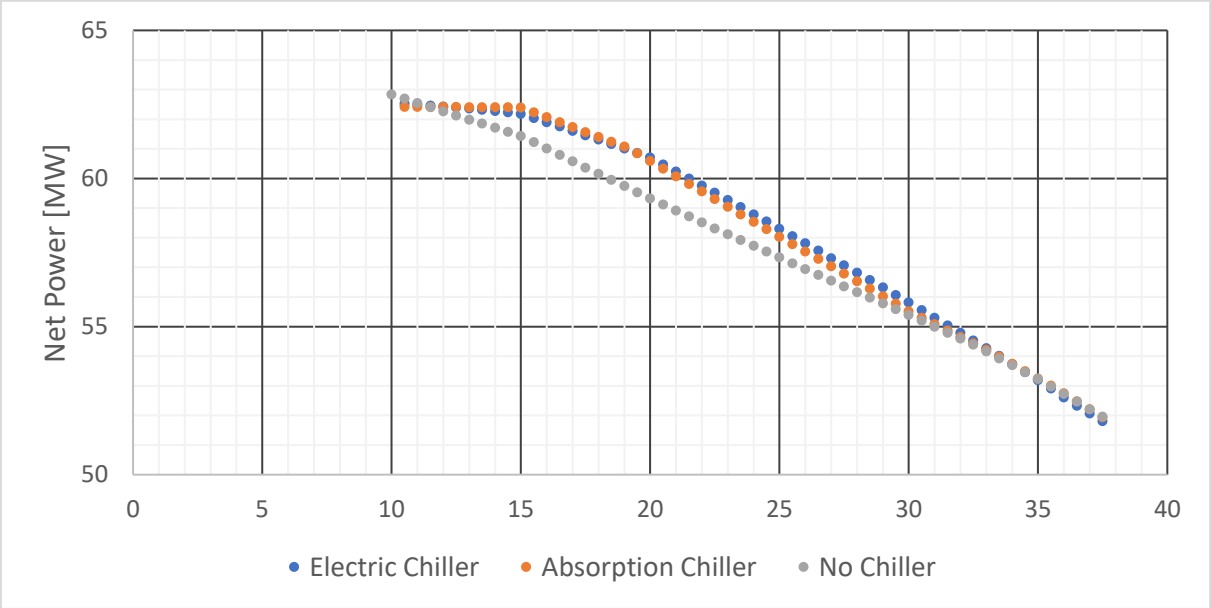

Figure B.25 Net power output of 2LP simple cycle operation at 100%RH.

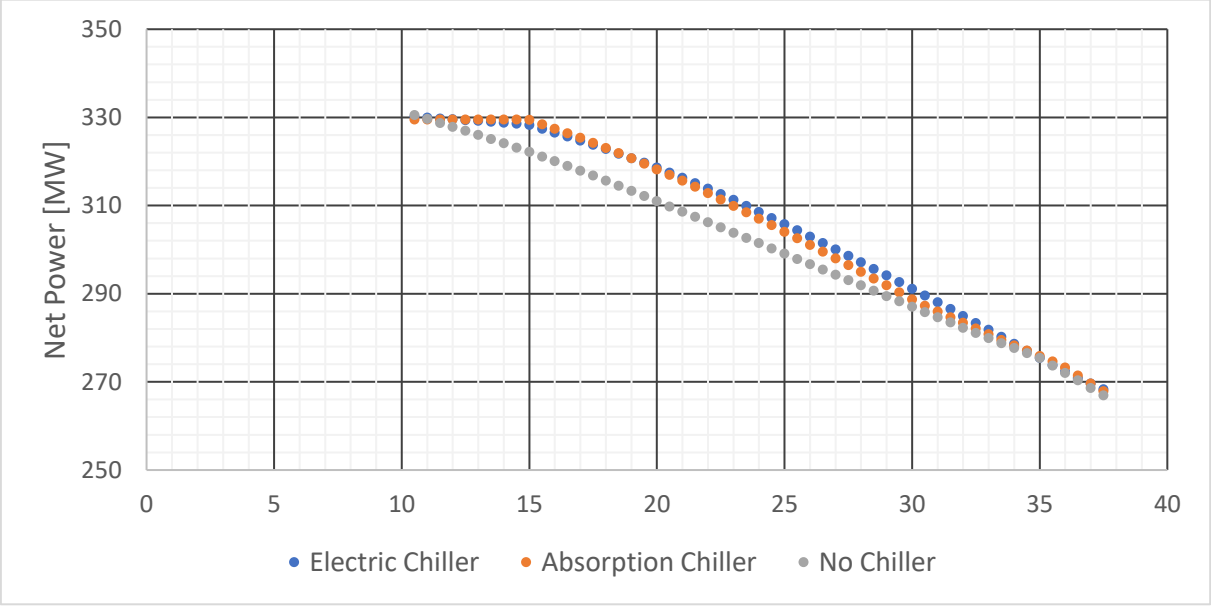

Figure B.26 Net power output of 3LP simple cycle operation at 100%RH.

The following information was obtained for 60%RH.

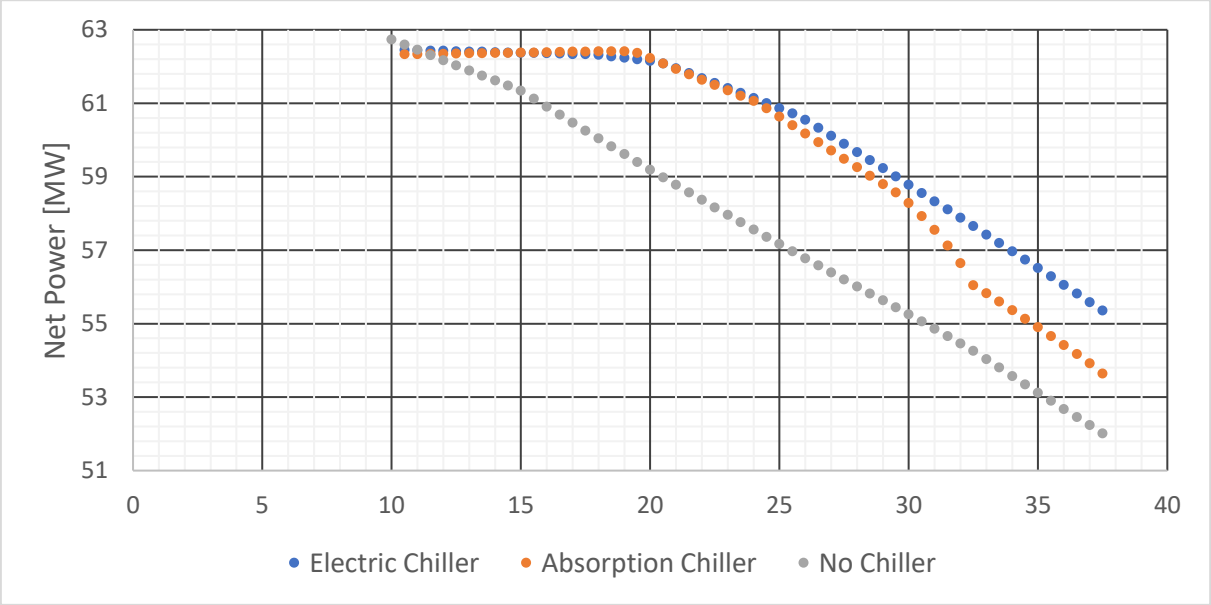

Figure B.27 Net power output of 2LP simple cycle operation at 60%RH.

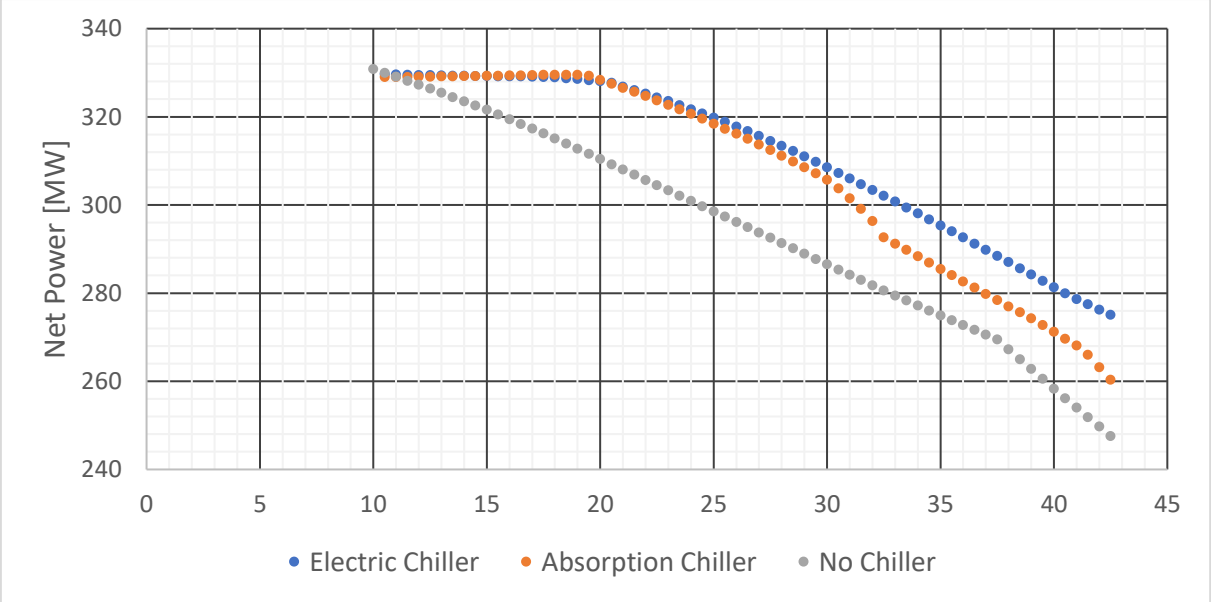

Figure B.28 Net power output of 3LP simple cycle operation at 60%RH.

B.4.- Fourth Scenario.

The following information was obtained for 100%RH.

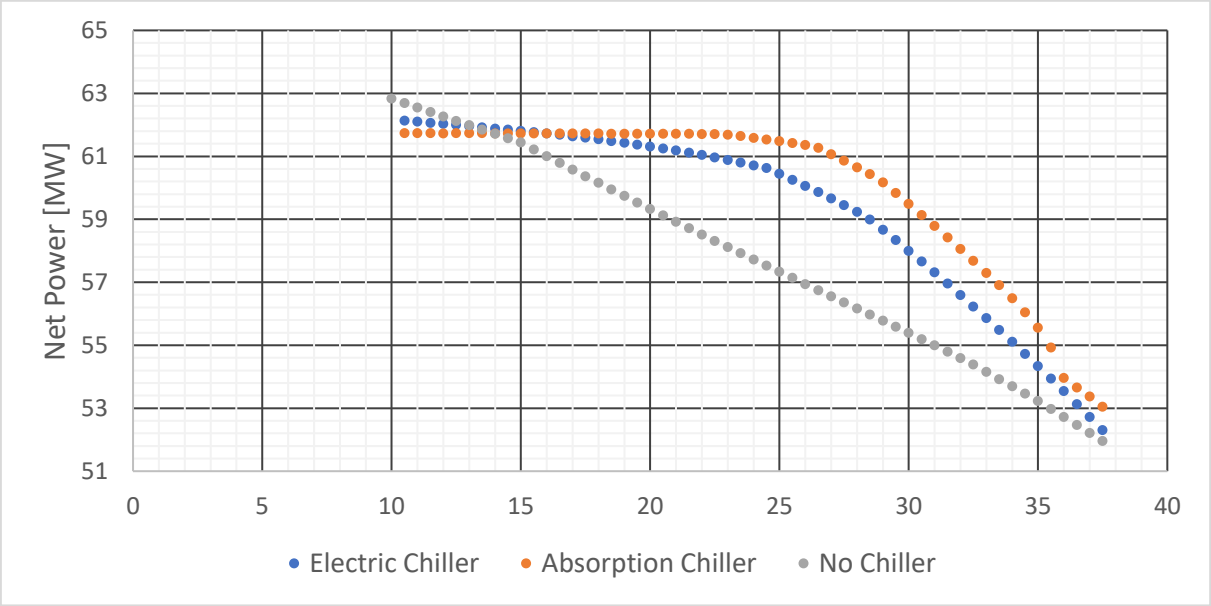

Figure B.29 Net power output of 2LP simple cycle operation at 100%RH.

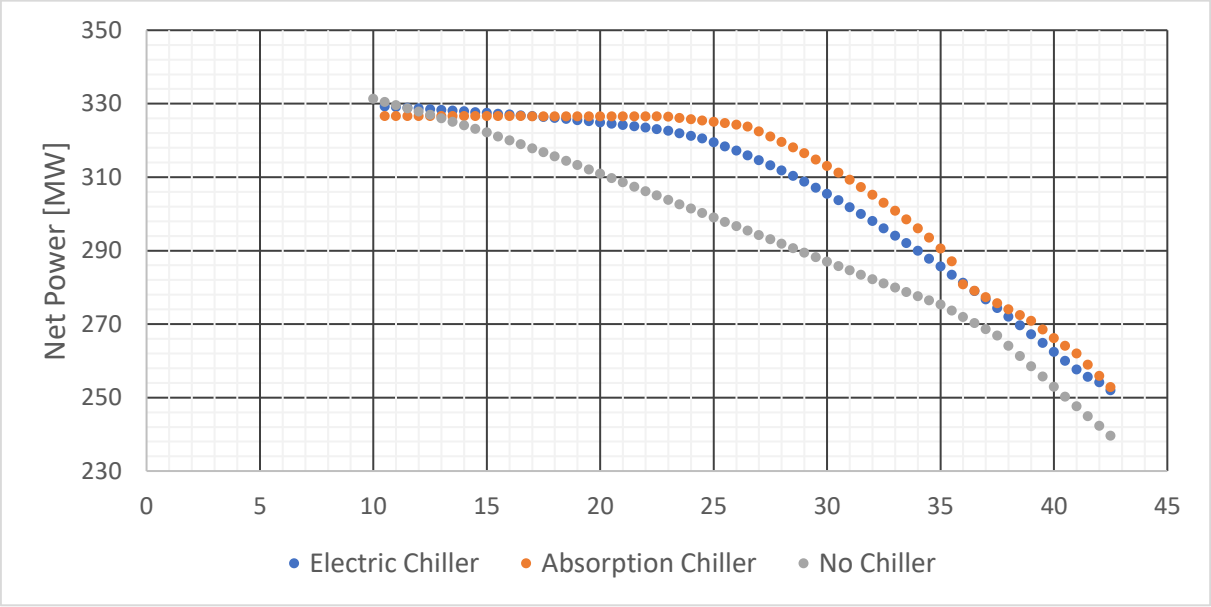

Figure B.30 Net power output of 3LP simple cycle operation at 100%RH.

The following information was obtained for 60%RH.

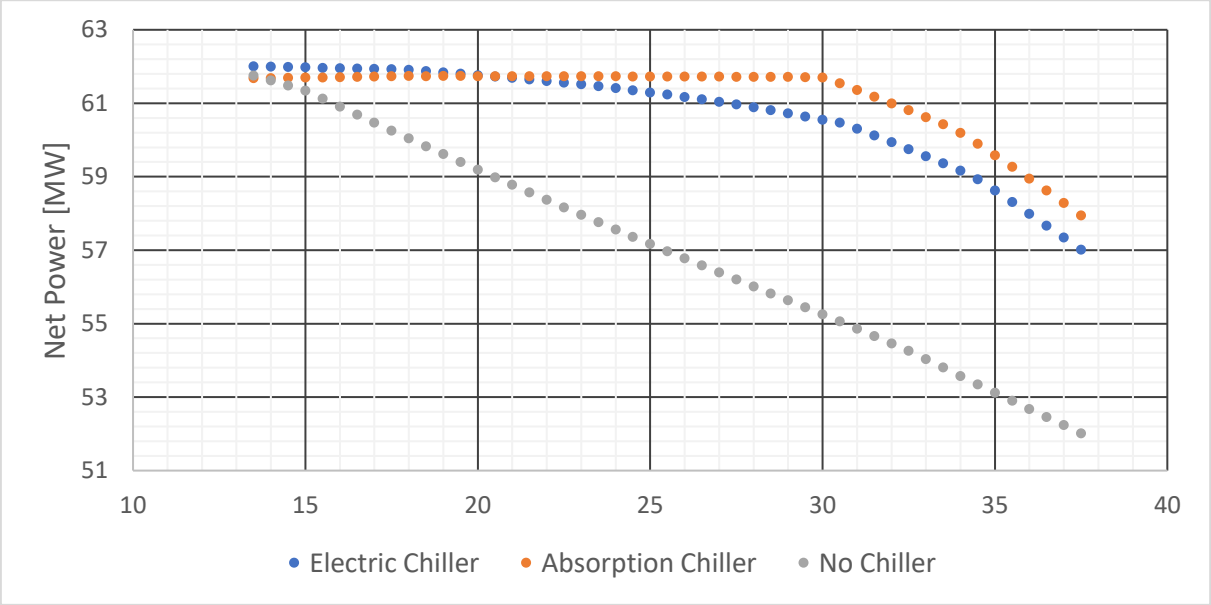

Figure B.31 Net power output of 2LP simple cycle operation at 60%RH.

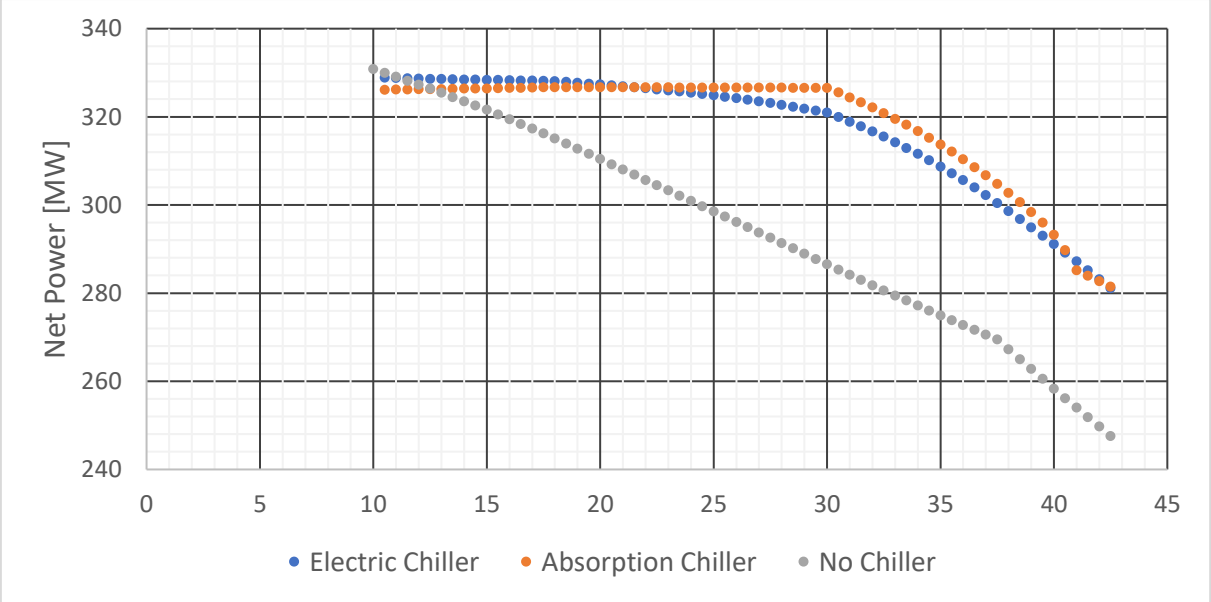

Figure B.32 Net power output of 3LP simple cycle operation at 60%RH.

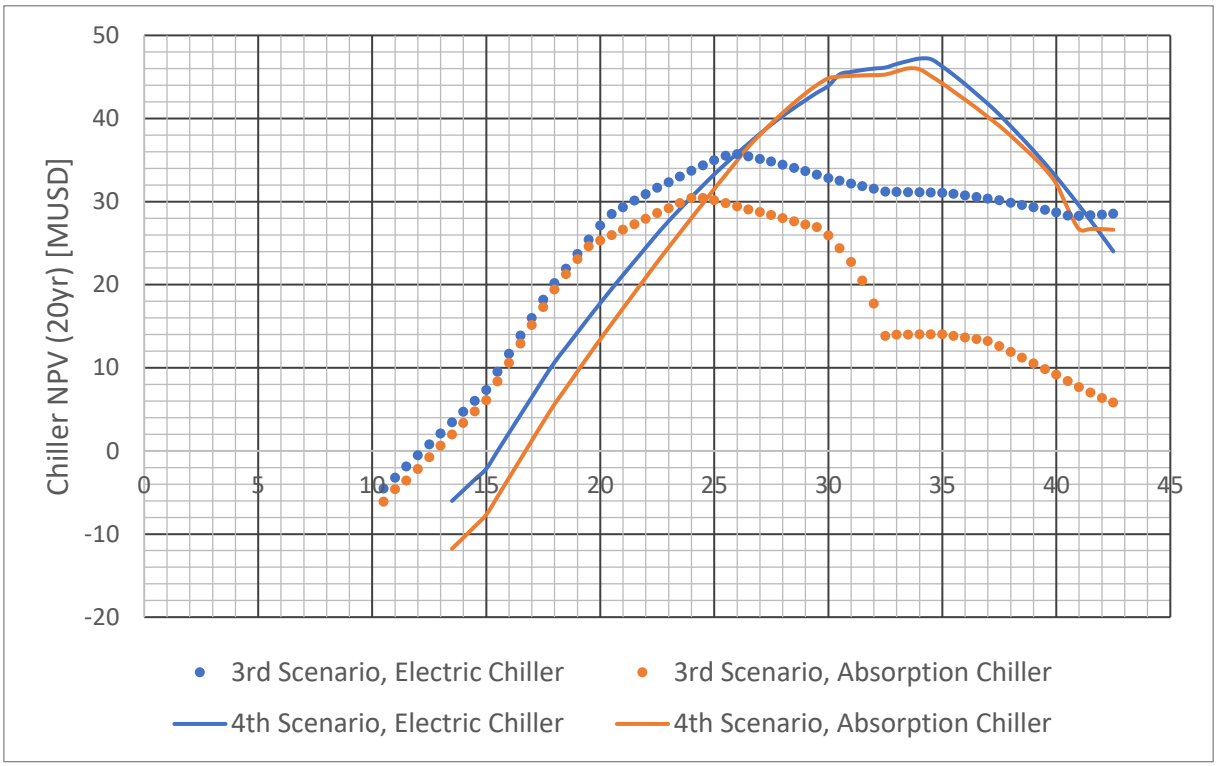

Figure B.33 NPV of using electric and absorption chillers of two different sizes, with respect to the simple 2LP cycle operation with no chiller.

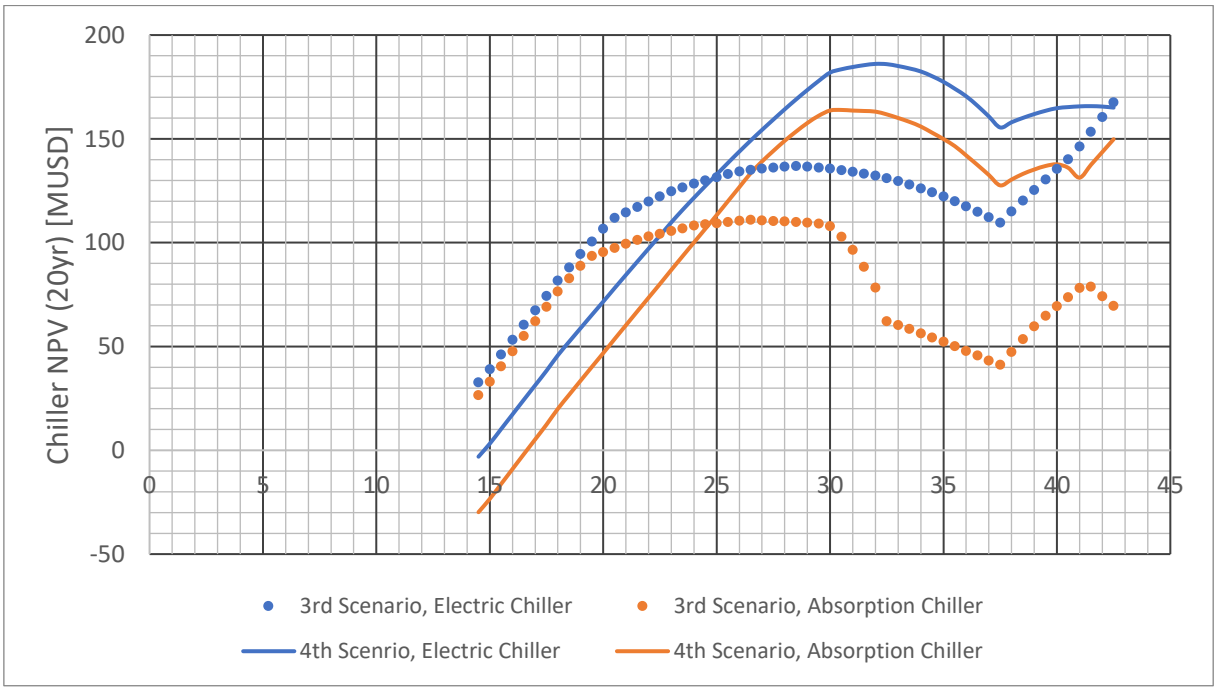

Figure B.34 NPV of using electric and absorption chillers of two different sizes, with respect to the simple 3LP cycle operation with no chiller.

Even though the output power in the absorption chiller is higher for some values of ambient temperature, the fuel demand also increases due to the use of an external boiler. The NPV is most of the time higher for the electric chiller despite the absorption having a higher output power.

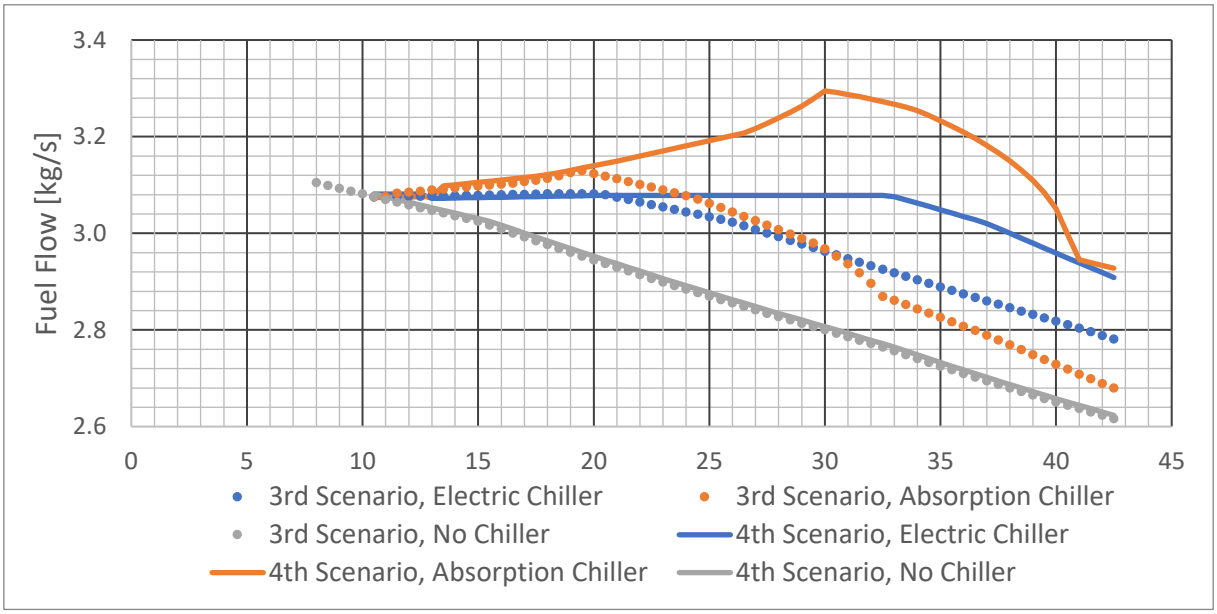

Figure B.35 Fuel flow for 2LP cycle, considering external boiler consumption.

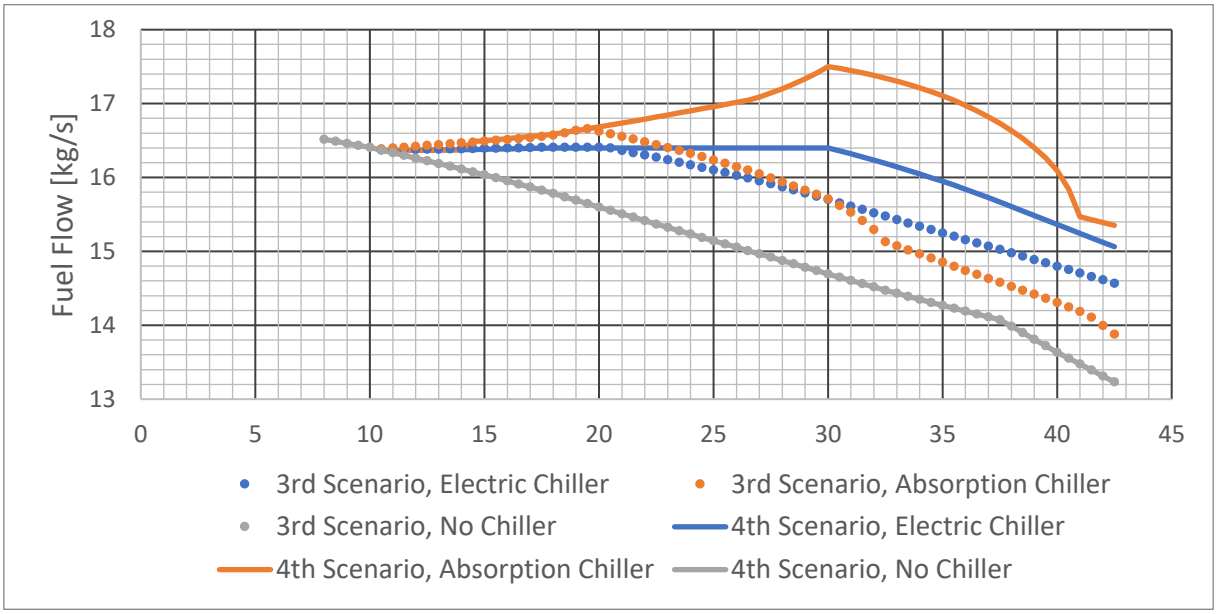

Figure B.36 Fuel flow for 3LP cycle, considering external boiler consumption.

B.5.- Blending.

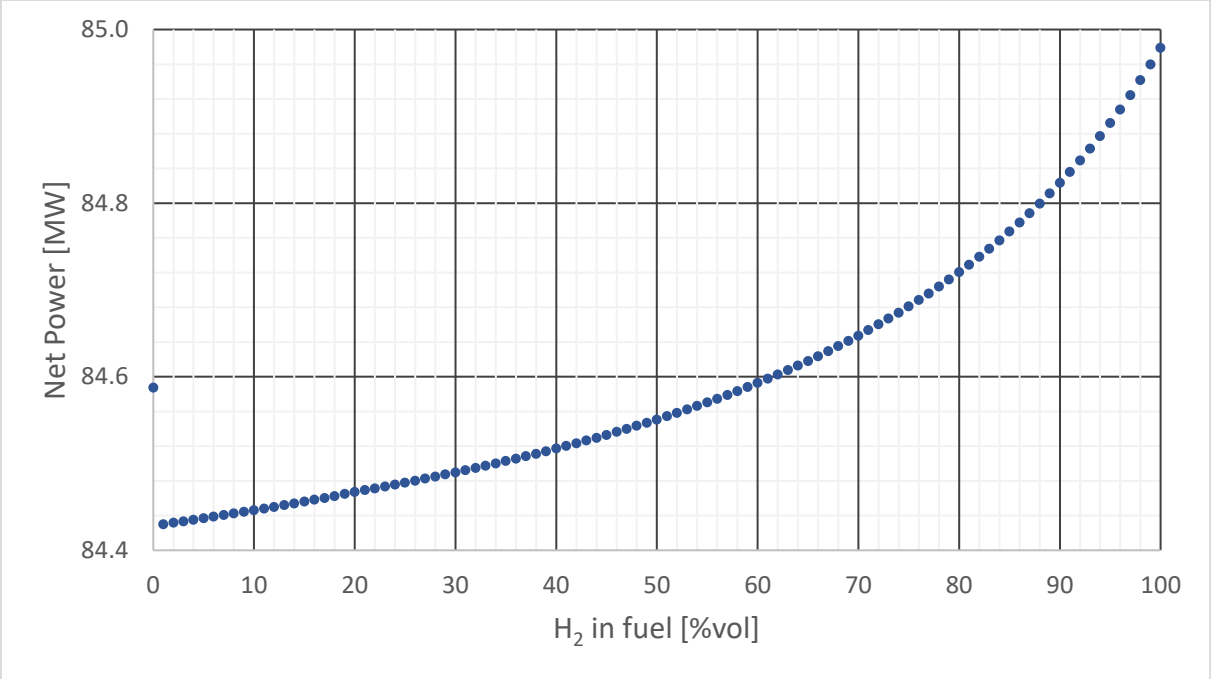

Figure B.37 Net power output depending on the amount of hydrogen used in the 2LP cycle.

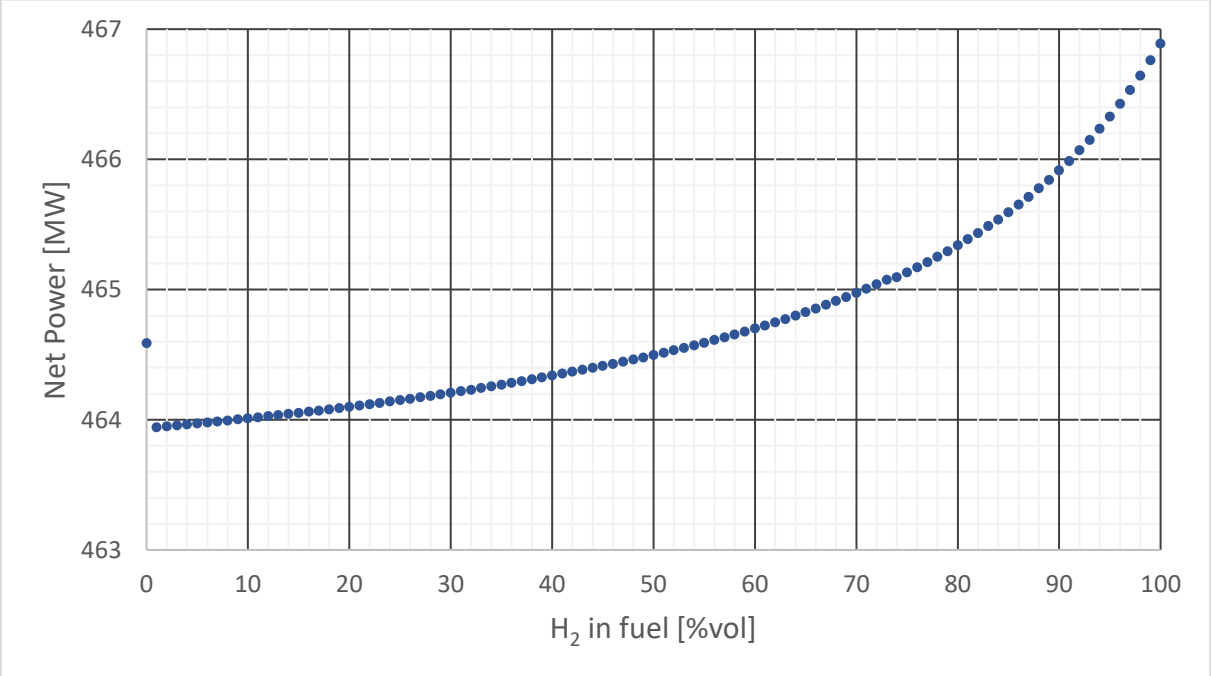

Figure B.38 Net power output depending on the amount of hydrogen used in the 3LP cycle.

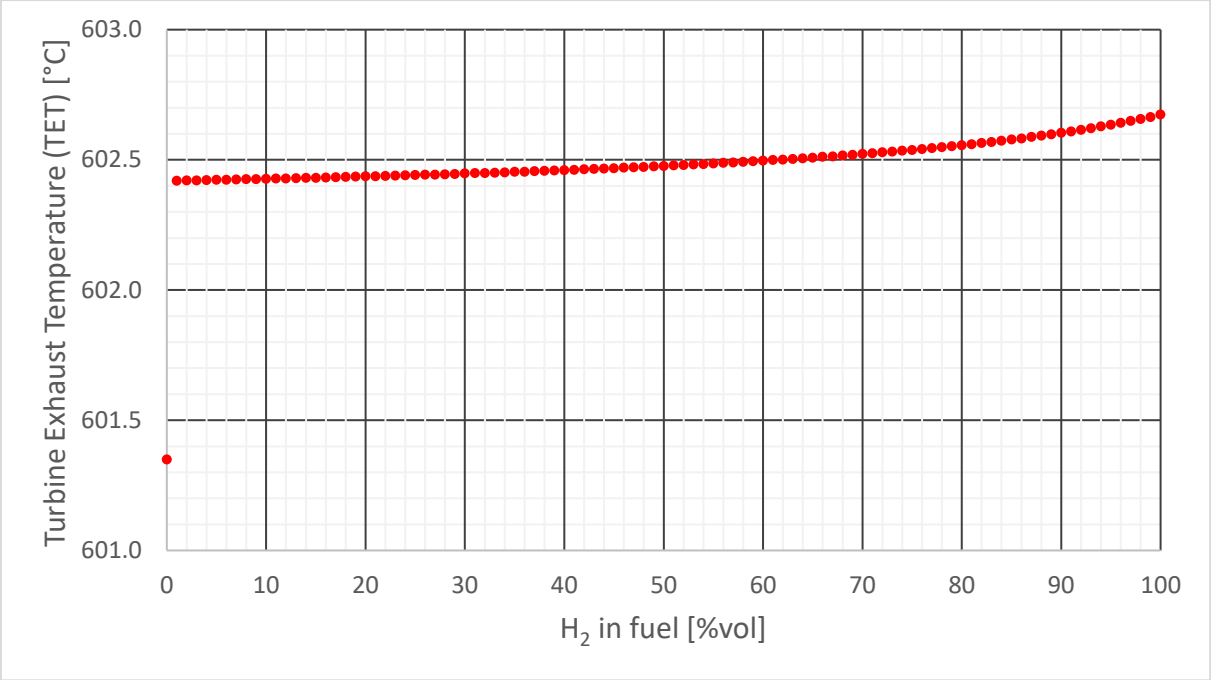

Figure B.39 TET depending on the amount of hydrogen used in the 2LP cycle.

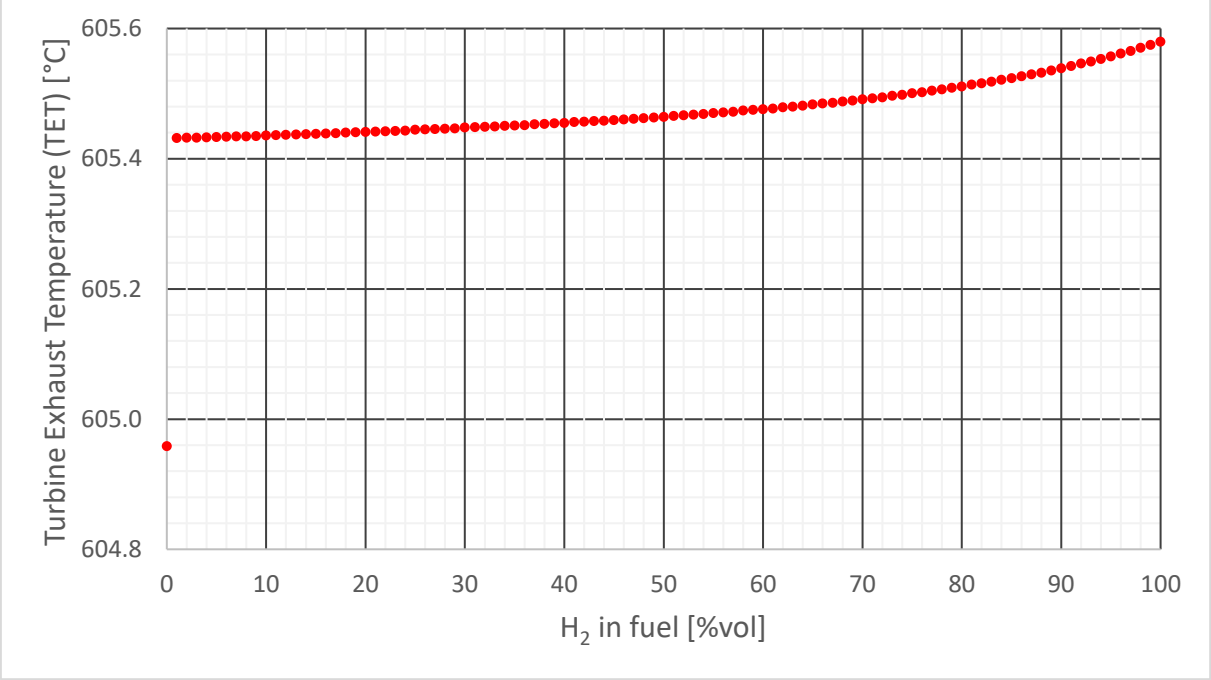

Figure B.40 TET depending on the amount of hydrogen used in the 3LP cycle.

Annex C. Blending considerations.

Hydrogen can be a carbon-free energy accumulator gas used to power machines, vehicles, and combined cycles. Although a lot of investment is made to use it, one must consider that its properties differ from other gases like methane.

Its higher volatility and flame velocity with respect to methane requires new control systems for fuel injection and a modification in the ventilation systems, using fuels with higher flame speeds could cause a flame propagation upstream into the premixer.

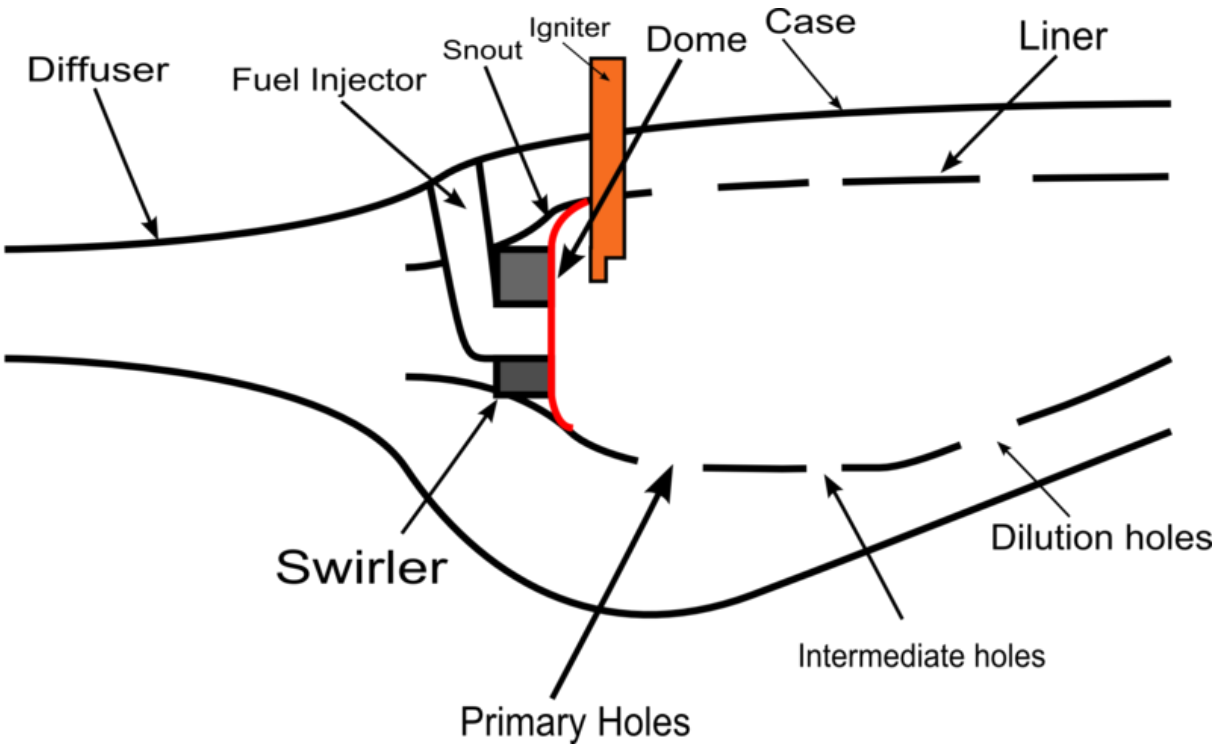

Figure C.1 Components of a gas turbine combustor. [36]

If the flame stays in the premixer it is called ‘flame holding’. If the flame does not stabilize, it goes downstream to the main combustion zone, and if this propagation moves between both chambers it is called ‘flashback’. Both behaviors are highly destructive for turbine components, applying unexpected thermal and mechanical stress on them.

Depending on the injector design, hydrogen can be used up to 80-95%, if it is designed for high flame speed.[37] The Lower Flammability Limit (LFL) is lower for hydrogen, which means that a concentration as low as 4% can lead to an explosion if an ignition source is present.[38]

Hydrogen, due to its small molecular size, can diffuse through materials otherwise considered as airtight or impermeable. This diffusion in metals also embrittles them, leading to premature brittle failure if no protection is applied.

Another consideration that must be evaluated is the increase of NO_X as a side effect of increasing combustion temperature. The magnitude of the increase in NO_X emissions increases exponentially with a higher percentage in volume of hydrogen. A 20% hydrogen mixture increases NO_X emissions by 10%; a 50% hydrogen mixture increases NO_X emissions by 35% and with 100% hydrogen, NO_X emissions double. However, solutions such as a larger or more efficient Selective Catalytic Reductor (SCR) are being used to limit the emission of this pollutant.

In the simulation, a higher pressure drop due to the use of a SCR has been considered. On top of all limitations on the percentage of hydrogen that can be injected, Siemens Energy, the turbine manufacturer, sets the maximum hydrogen in volume for the SGT-800 turbine (2LP) to 75% and for the SGT-4000F turbine (3LP), the maximum of 30% hydrogen. [39]

Its difference in volumetric energy density -energy per unit volume- and gravimetric energy density -energy per unit mass- can be obtained from the following cycle data:

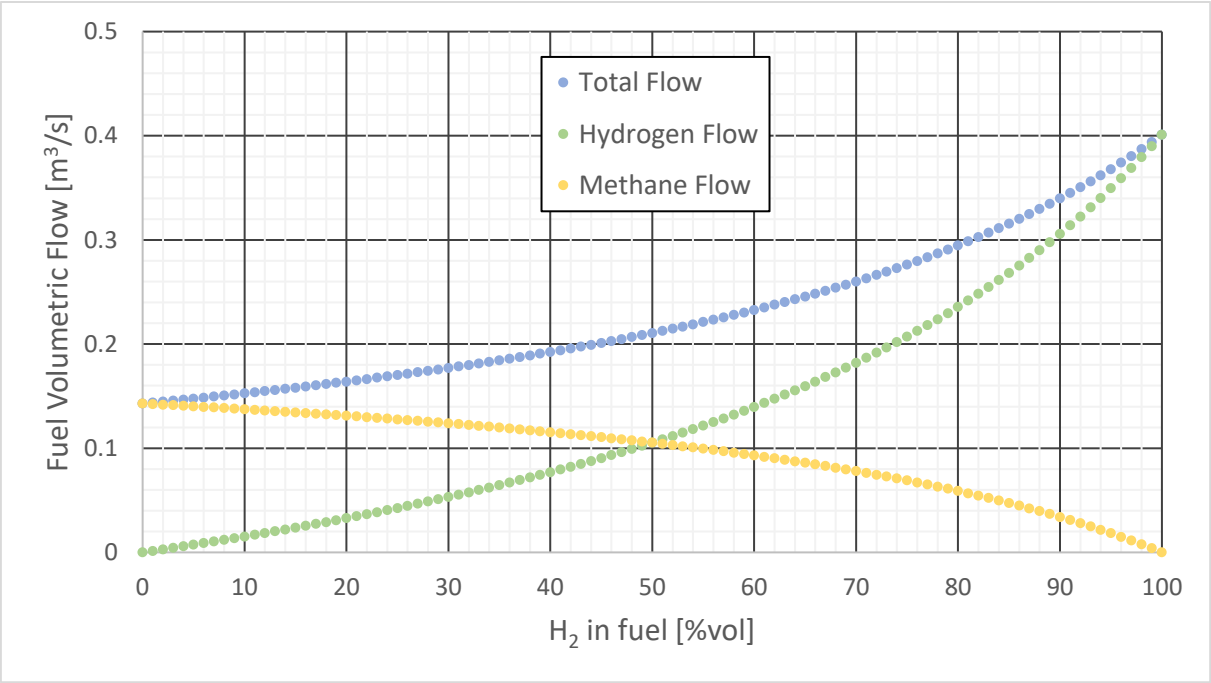

Figure C.2 Fuel volumetric flow of the 2LP cycle, depending on hydrogen volume percentage.

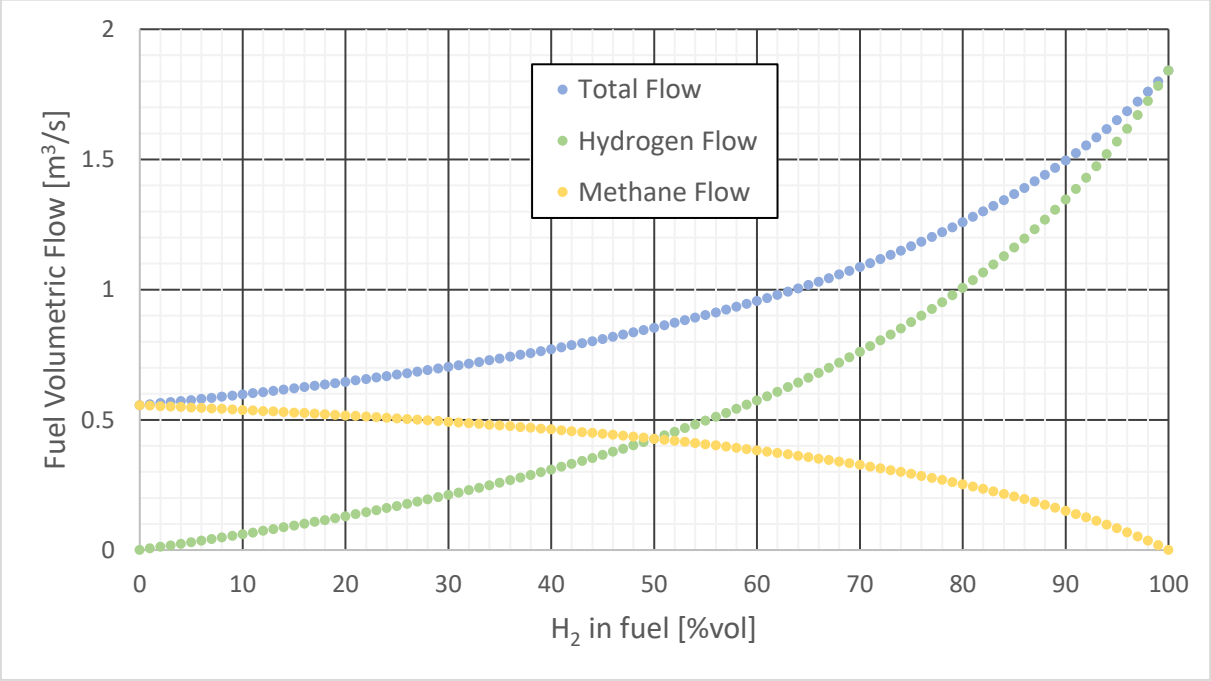

Figure C.3 Fuel volumetric flow of the 3LP cycle, depending on hydrogen volume percentage.

With the view to calculate the amount of natural gas and hydrogen used, the volume percentage has been converted into mass percentage. The densities of methane and hydrogen at Standard Temperature and Pressure (STP) are 0.657kg/m^3 and 0.0899kg/m^3 respectively. [40], [41]

Thermoflex gives the densities of methane and hydrogen at the turbine inlet, and they are 28.90 kg/m^3 and 3.63 kg/m^3, respectively.

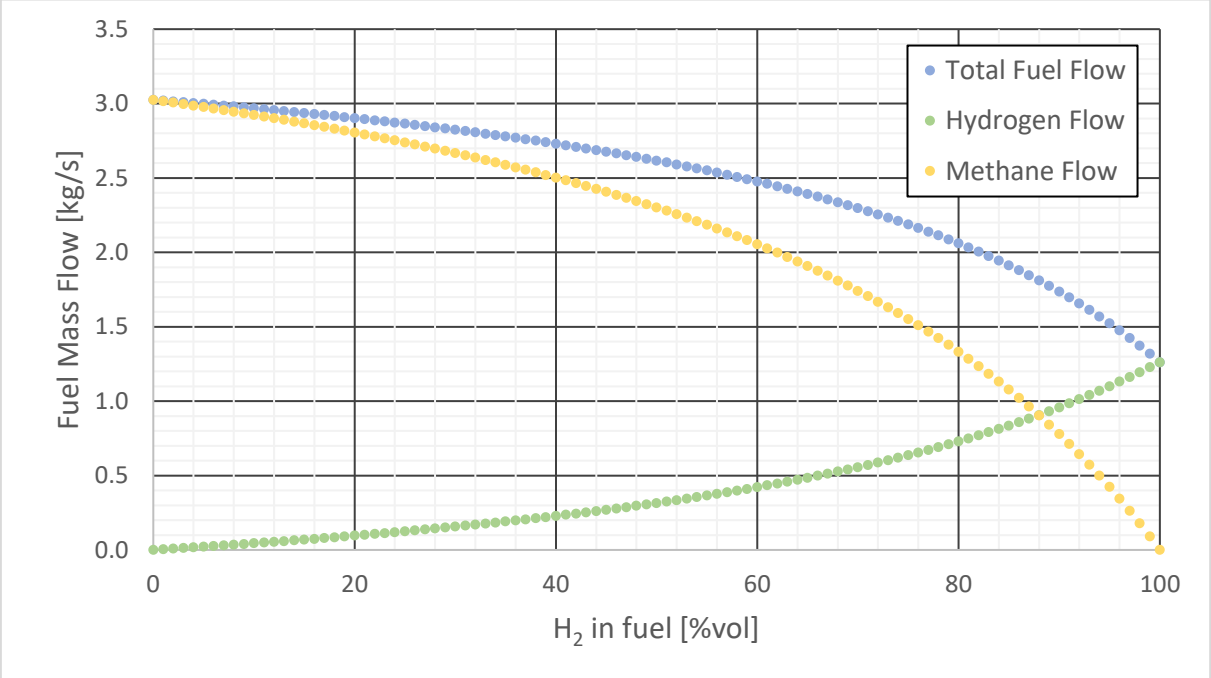

Figure C.4 Fuel mass flow of the 2LP cycle, depending on hydrogen volume percentage.

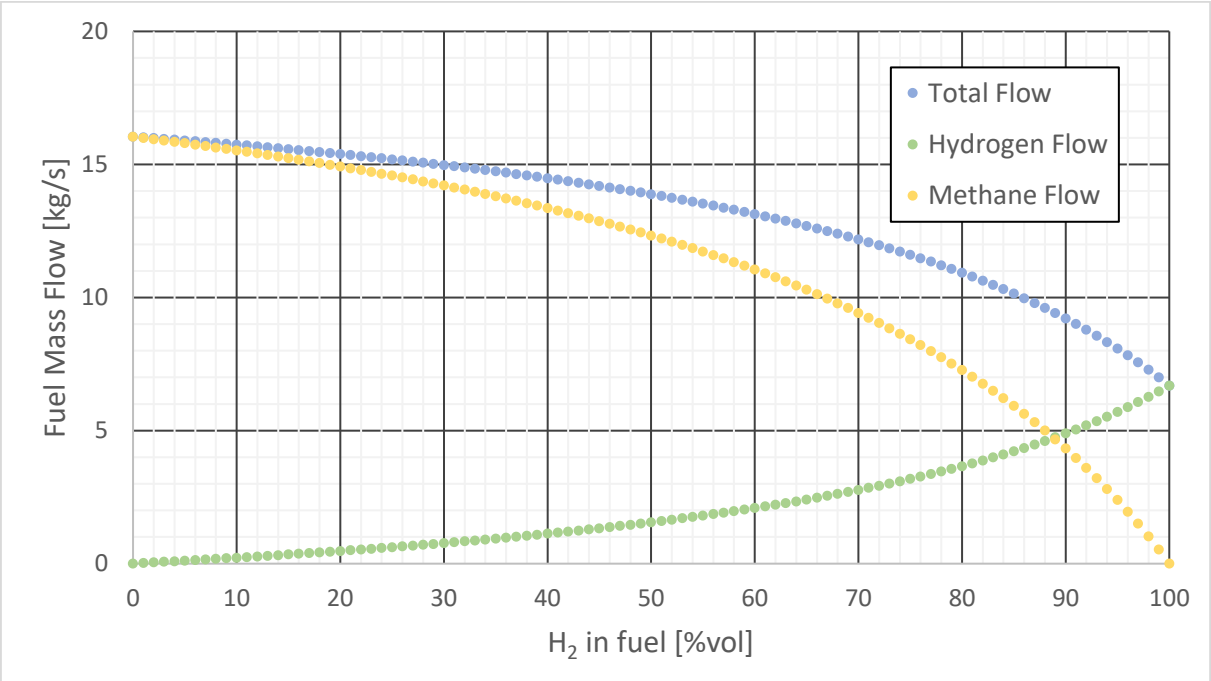

Figure C.5 Fuel mass flow of the 3LP cycle, depending on hydrogen volume percentage.

As the heating value of the fuel is approximately constant, it can be deduced that while hydrogen has more than double energy density with respect to mass, it has only a third with respect to volume, which is a big disadvantage in terms of transport and storage.

Annex D. Microsoft Excel Macros.

Two Microsoft Excel Macros have been used before obtaining access to EES software. They have been used to calculate the thermodynamic properties of humid air. For quick calculations, an interactive Psychrometric chart has been used. [42]

Humid air behavior is shown with the Psychrometric chart, and it is particularly useful to visualize the absolute and relative humidity with temperature.

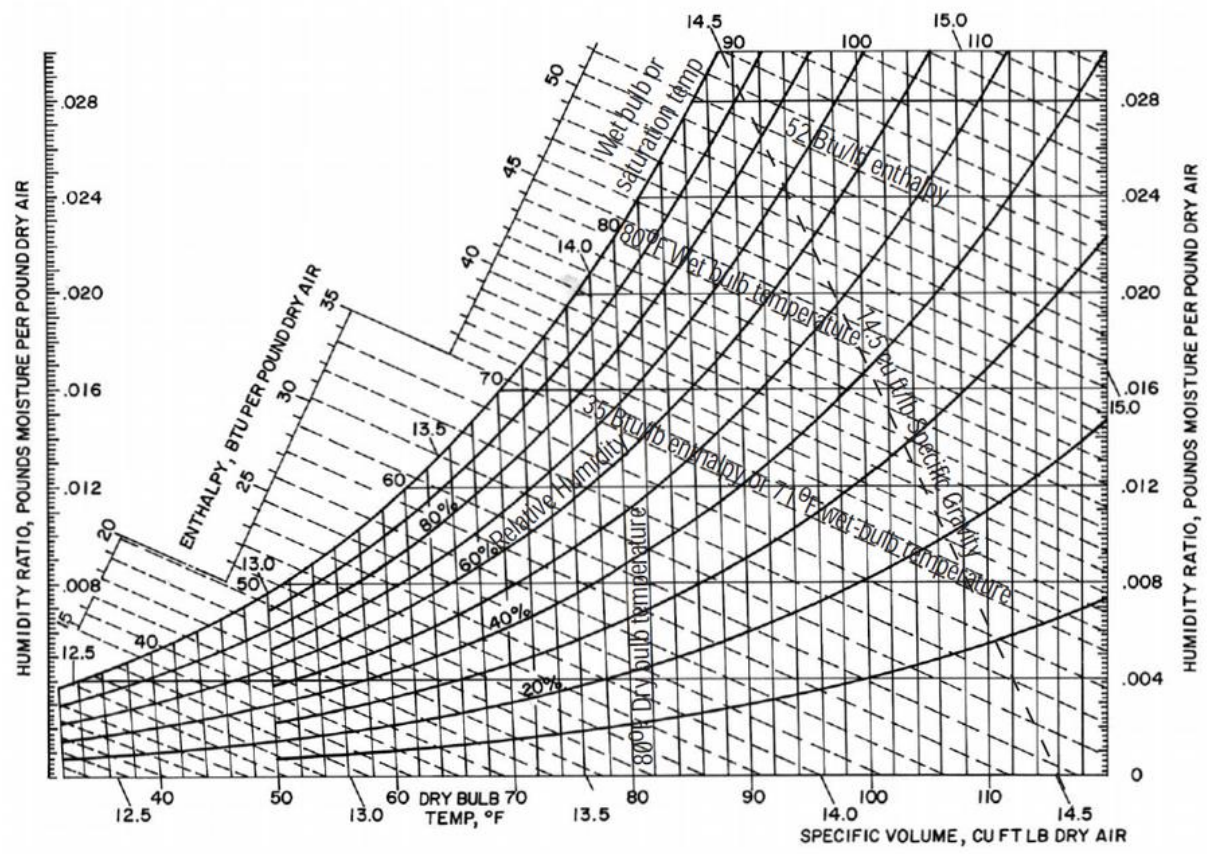

Figure D.1 Example of psychrometric chart. [43]

For more advanced calculations, the simple online calculator of the psychrometric chart was not enough, and the first macro “Psych” was downloaded and used. [44]

After adding it to an Excel module, it was available for the excel workbook. Although it was a useful tool, it had one main caveat: it required the air temperature, the barometric pressure and a third property as inputs, which made it impossible to calculate the temperature or pressure as they were defined as inputs.

Excel has a function called “GoalSeek” which incorporates the Newton-Raphson method, commonly used in calculus to find the solution of a function by iteration. [45] The function takes three input parameters:

1. VariableCell: the cell whose value is changed to modify the outcome.
2. GoalValue: the value desired in the GoalCell.
3. GoalCell: the cell whose value depends on VariableCell.

The goal is to obtain the value of VariableCell, using GoalValue and GoalCell as reference, as their difference is the absolute error that must be minimized. This is a fast workaround for the limitations of “Psych”, but its main disadvantage was that it worked by having a pop-up in the screen that had to be completed every run.

To fix this, the second excel macro was built. Excel only allows the use of GoalSeek for a single sheet of the workbook, and it has to be placed inside it to work properly unlike “Psych” which can be placed in a general module.

The following code was used to make a list of cells where the location of the first and third input parameters were entered. The second parameter was set to zero to make the use of the macro more intuitive.

```
Private Sub Worksheet_Change(ByVal Target As Range)
    Dim i As Integer
    Dim VariableCells() As String
    Dim GoalCells() As String
    Dim GoalValues As Double
    Dim VCellsInput As Range
    Dim cell As Range
    Dim cellCount As Integer
    Set VCellsInput = Me.Range("Y55:Y58") 'Definition of VariableCells
    Set GCellsInput = ThisWorkbook.Sheets("Comparative").Range("Z55:Z58") 'Definition of GoalCells
    cellCount = rng.Cells.Count


    ' Another way to input VariableCells
        'VariableCells(1) = "V48"
        'VariableCells(2) = "W44" ' More inputs can be added


    ReDim VariableCells(1 To cellCount)
    ReDim GoalCells(1 To cellCount)
        i = 1
    For Each cell In VCellsInput
        VariableCells(i) = CStr(cell.Value) ' Convert cell value to String
        i = i + 1
    Next cell

        i = 1
    For Each cell2 In GCellsInput
        GoalCells(i) = CStr(cell2.Value) ' Convertir cell value to String
        i = i + 1
    Next cell2

    ' Another way to input GoalCells
        'GoalCells(1) = "S42"
        'GoalCells(2) = "V46" ' More inputs can be added
        'GoalCells(3) = "Y42"

        GoalValues = 0 ' This can be changed to multiple values


    ' Execute GoalSeek if needed
    For i = 1 To cellCount
        If Not Intersect(Target, Me.Range(VariableCells(i))) Is Nothing Then
            Dim GoalCell As Range
            Dim GoalValue As Double
            Dim VariableCell As Range
            Set GoalCell = Me.Range(GoalCells(i))
            GoalValue = GoalValues
            Set VariableCell = Me.Range(VariableCells(i))

            ' Execute GoalSeek function
            On Error Resume Next
            GoalCell.GoalSeek Goal:=GoalValue, ChangingCell:=VariableCell
            On Error GoTo 0

            ' Opcional: Mensaje de confirmación
            If Abs(GoalCell.Value - GoalValue) < 0.01 Then
                MsgBox "The Goal Value has been obtained " & i
            Else
                MsgBox "The Goal Value could not be obtained " & i
            End If

            Exit For ' Switch to the next run
        End If
    Next i
End Sub
```

Figure D.2 Code used in the second macro to execute GoalSeek.

This might not be a definitive solution, but it allowed to check whether Thermoflex chiller calculations were correct and taking into account all types of heat or not.